

INFORMATION TO USERS

The most advanced technology has been used to photograph and reproduce this manuscript from the microfilm master. UMI films the text directly from the original or copy submitted. Thus, some thesis and dissertation copies are in typewriter face, while others may be from any type of computer printer.

The quality of this reproduction is dependent upon the quality of the copy submitted. Broken or indistinct print, colored or poor quality illustrations and photographs, print bleedthrough, substandard margins, and improper alignment can adversely affect reproduction.

In the unlikely event that the author did not send UMI a complete manuscript and there are missing pages, these will be noted. Also, if unauthorized copyright material had to be removed, a note will indicate the deletion.

Oversize materials (e.g., maps, drawings, charts) are reproduced by sectioning the original, beginning at the upper left-hand corner and continuing from left to right in equal sections with small overlaps. Each original is also photographed in one exposure and is included in reduced form at the back of the book.

Photographs included in the original manuscript have been reproduced xerographically in this copy. Higher quality 6" x 9" black and white photographic prints are available for any photographs or illustrations appearing in this copy for an additional charge. Contact UMI directly to order.

U·M·I

University Microfilms International
A Bell & Howell Information Company
300 North Zeeb Road, Ann Arbor, MI 48106-1346 USA
313/761-4700 800/521-0600

Order Number 9105498

The diffusion of muonic hydrogen atoms in hydrogen gas

Chen, Guo Fu, Ph.D.

The College of William and Mary, 1990

U·M·I
300 N. Zeeb Rd.
Ann Arbor, MI 48106

**The Diffusion of Muonic Hydrogen Atoms
in Hydrogen Gas**

**A Dissertation
Presented to**

**The Faculty of the Department of Physics
The College of William and Mary in Virginia**

**In Partial Fulfillment
of the Requirements for the Degree of
Doctor of Philosophy**

**By
Guo Fu Chen**

1990

**The Diffusion of Muonic Hydrogen Atoms
in Hydrogen Gas**

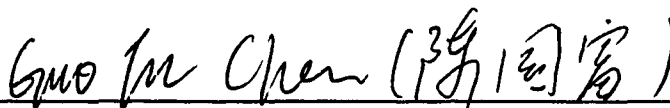
Guo Fu Chen

May 1990

APPROVAL SHEET

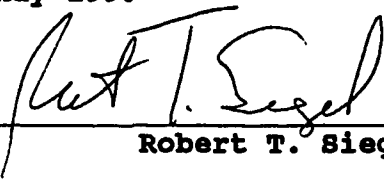
This dissertation is submitted in partial fulfillment of
the requirements for the degree of

Doctor of Philosophy

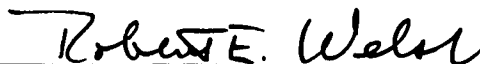


Guo Fu Chen

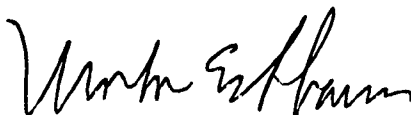
Approved, May 1990



Robert T. Siegel



Robert E. Welsh



Morton Eckhause



Richard L. Kiefer
Department of Chemistry



James J. Reidy
Department of Physics and Astronomy
University of Mississippi

TABLE OF CONTENTS

<u>CHAPTER</u>	<u>PAGE</u>
I. INTRODUCTION	2
General Remarks	2
The Purposes of The Experiment	8
The Design of The Experiment	10
II. THEORY	17
Scattering of (μ^-p) Atoms in Gaseous Hydrogen	17
Muon Moderation in Gaseous Hydrogen	23
Muonic Hydrogen Formation	26
III. DESCRIPTION OF THE EXPERIMENT	31
Outline of the Experiment	31
Detectors	36
IV. TECHNIQUES OF DATA ANALYSIS	44
The Energy Calibration and the Spectrum of Muonic X - rays and γ - rays of Au	44
Applications for Techniques of Data Analysis	51
V. EXPERIMENTAL DATA	101
Data Treatment Routines	101
The Final Data Sets of the Time Distributions Under Five Conditions	111
VI. DISCUSSIONS AND CONCLUSIONS	116
APPENDIX A.	129
APPENDIX B.	141

ACKNOWLEDGEMENTS

I would like to thank the many people who have made this work possible:

Dr. Robert Siegel, my advisor, for the countless hours put into the design, construction, and analysis phases of this experiment.

Dr. Robert Welsh, for his help during the experimental runs, helpful comments regarding the experiment, and for reading the manuscript.

Mr. William Vulcan, for all of his help during four years at William and Mary, and for his tireless efforts during the experimental runs and testing detectors before experimental runs.

Dr. Morton Eckhause, for his helpful comments, and for reading the manuscript.

Dr. James Reidy, for his many contributions to the experiment, his reading of the manuscript, and for being a pleasure to work with.

Dr. Peter Kammel, for his many valuable contributions to this experiment, especially during experiment runs.

Dr. Hannes Zmeskal, for the design, construction, and operation of the gas/vacuum system.

Dr. Joachim Hartmann, for his important contributions to this experiment, particularly his efforts to keep the experiment running smoothly.

Dr. Claude Petitjean, for his valuable comments and insights concerning this experiment.

Dr. Alex Zehnder, for his important comments and insights concerning this experiment.

Drs. Heather Wolverton, Dayle Hancock, and Donald Joyce for their valuable help during the experimental runs.

Dr. James Kraiman, for his help during experimental runs and for his contributions to the analysis.

Dr. Richard L. Kiefer, for reading the manuscript.

Ms. Dianne Fannin, Ms. Paula Spratley, and Ms. Sylvia Stout for the bountiful help they have provided me over the years, and for being so patient when answering my questions.

I would like to take this opportunity to thank the many people at the Paul Scherrer Institute for their hospitality.

This work was supported in part by the National Science Foundation.

ABSTRACT

This experiment measured the time distribution of muonic hydrogen atoms which were formed when negative muons were brought to rest in H₂ gas, containing Au target foils, at five pressures (750 mbar, 375 mbar, 188 mbar, 94 mbar and 47 mbar at 4.6 mm foil spacing). A Monte Carlo method is applied for deducing the initial velocity distribution, and preliminary results are obtained. The initial velocity distribution of μH atoms is reasonably well described as a 'Maxwellian' velocity distribution with a mean energy $E = 3.4$ eV. The corresponding muon mean capture energy is obtained: $E_c \approx 34$ eV for μH atom and $E_c \approx 68$ eV for μH_2 molecules. We also find the negative muon capture energy distribution is exponential.

In addition, a significant improvement of the negative muon mean life τ in Au is obtained in this experiment :

$$\tau_{\text{Au}} = 69.716 \pm 0.144 \text{ ns}$$

The "full decay curve fitting method" which we use in this experiment has an advantage over the previous method in three aspects :

- 1) We have measured the mean life and determined the time resolution $\sigma(E)$ of a detector at a particular energy level ;
- 2) We have determined the effective zero time of the decay curve;
- 3) We have provided a possible way to measure the mean life τ when τ is less than the time resolution $\sigma(E)$ of the detector ($\tau < \sigma(E)$).

THE DIFFUSION OF MUONIC HYDROGEN
ATOMS IN HYDROGEN GAS

Chapter I
INTRODUCTION

I. 1 General Remarks

A. Muon Decay

As is well known, a muon and an electron have very similar properties except for their differences in mass and stability :

$$(I-1) \quad m_\mu \approx 206 m_e$$

and

$$(I-2) \quad \tau_\mu \approx 2.2 \mu s, \tau_e \approx \infty$$

Muon decay is very similar to β decay :

$$(I-3) \quad \mu^- \rightarrow e^- + \bar{\nu}_e + \nu_\mu$$

$$(I-4) \quad \mu^+ \rightarrow e^+ + \nu_e + \bar{\nu}_\mu$$

and

$$(I-5) \quad p \rightarrow e^+ + n + \nu_e$$

$$(I-6) \quad n \rightarrow e^- + p + \bar{\nu}_e$$

According to the V - A theory of Feynman and Gell -- Mann [1], the invariant amplitude of muon decay is analogous to β decay :

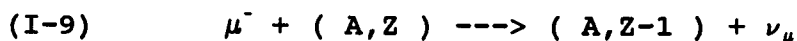
$$(I-7) \quad M = G_F / \sqrt{2} \bar{u}_2 \gamma_\lambda (1 - \gamma_5) u_\mu \bar{u}_e \gamma^\lambda (1 - \gamma_5) \nu_1$$

and the life-time of spontaneous μ decay [2] is :

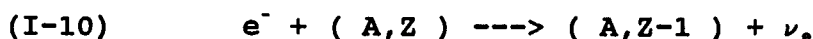
$$(I-8) \quad \begin{aligned} \tau_\mu &= 1/\Gamma = 192 \pi^3 / G_F^2 m_\mu^5 \\ &= 2.21 \cdot 10^{-6} \text{ s} \end{aligned}$$

B. Muon Absorption

Muon absorption in nuclei



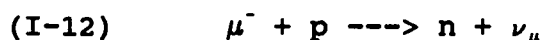
is analogous to orbital electron capture :



In the case of capture by a complex nucleus, the muon absorption rate increases rapidly with increasing Z , because the K orbit radius $a_\mu = (m_e/Zm_\mu) a_0$, where a_0 is the electron Bohr radius, implies that the muon is quite close to the nucleus. Basically, the capture rate is proportional to the probability of finding the muon in the nucleus (i.e., $|\psi_\mu(0)|^2$) and for a Bohr orbit $|\psi_\mu(0)|^2$ is proportional to Z^3 there being Z protons, so that [5]

$$(I-11) \quad \begin{aligned} \Lambda_{\mu c} &\propto Z |\psi_\mu(0)|^2 \\ &\propto Z^4 \end{aligned}$$

The calculation of the muon absorption rate involves matrix elements between the initial and all final nuclear states. There is a great deal of interest in the case for which a muon is captured in the simplest nucleus, a proton, because this is the only case in which the elementary semi-leptonic weak process (I-12) can be observed without nuclear structure complications



In order to perform a detailed calculation of the muon capture rate in hydrogen, the V - A theory of the leptonic interaction is applied to this fundamental semilepton process. The integrand of the matrix element is written below: [3] [4] [5]

$$(I-13) \quad H = V_{\alpha}^{+} (\bar{\phi}_{\nu} \gamma_{\alpha} \psi_{\mu}) + A_{\alpha}^{+} (\bar{\phi}_{\nu} i \gamma_{\alpha} \gamma_5 \psi_{\mu}) + h.c.$$

with

$$(I-14) \quad \phi_{\nu} = \frac{(1 + \gamma_5)}{\sqrt{2}} \psi_{\nu}$$

V_{α}^{+} and A_{α}^{+} are vector and axial vector currents :

$$(I-15) \quad V_{\alpha}^{+} = (\bar{\psi}_n [f_V \gamma_{\alpha} - i g_V \sigma_{\alpha\beta} p_{\beta} - i h_V p_{\alpha}] \psi_p)$$

$$(I-16) \quad A_{\alpha}^{+} = (\bar{\psi}_n [i f_A \gamma_{\alpha} \gamma_5 - g_A p_{\alpha} \gamma_5 + h_A \sigma_{\alpha\beta} \gamma_5 p_{\beta}] \psi_p)$$

with

$$(I-17) \quad p_{\beta} = [p^{(p)} - p^{(n)}] \text{ and } \sigma_{\alpha\beta} = (\gamma_{\alpha} \gamma_{\beta} - \gamma_{\beta} \gamma_{\alpha}) / 2$$

and with the limit of $p \rightarrow 0$

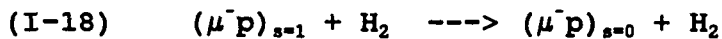
$$f_V(0) = c_V \quad \text{and} \quad f_A(0) = c_A$$

Here two important points are to be noted about the process (I-12):

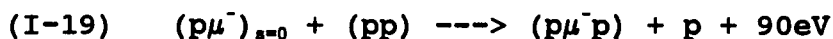
1) The capture rate of the muon in the hydrogen target depends strongly upon the spin S ($\hat{S} = \hat{S}_p + \hat{S}_{\mu}$) orientation of the proton and muon. When S_p and S_{μ} are anti-parallel (in the singlet hyperfine state $S = 0$), the reaction rate is roughly fifty times that of the rate when the spin S is in a parallel state ($S=1$) [6]. Therefore, independent measurements of the triplet (λ_t) and singlet

(λ_s) capture rates in hydrogen would provide an important test of the theory itself;

2) There are difficulties in obtaining a substantial population of muon - proton (μp) atoms in the triplet state. When the μp atom is in 1s state, the triplet ($S=1$) and the singlet ($S=0$) states are initially populated in proportions to their statistical weight; namely, 75 % in the triplet state and 25 % in the singlet state. In gaseous hydrogen, the population of the triplet μp state rapidly decreases with time because the muonic atoms collide with surrounding H_2 molecules, lose kinetic energy and deexcite from triplet to singlet until there is no longer a population of the triplet state :[4]



Therefore, the measurement of λ_t remains an open question [6]. The life-time of muonic atoms in the triplet state depends on the pressure of the gaseous hydrogen in the target vessel. When the pressure of the gaseous hydrogen target reaches about 10 atm, the life-time λ_T is only few a ns. Thus, after this short time all nuclear capture will take place on the singlet hyperfine state. On the other hand, in liquid hydrogen [4]



Here $p\mu^-p$ is a mesic-molecule ion. In this case, one must deal with $(p\mu^-p)$ as a "three-body" problem, so theoretical calculations become more difficult. [12]

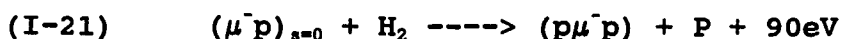
C. Mesic Atoms or Mesic - Molecular Ions Formed in a Hydrogen Target

Negative muons can be captured by protons in a hydrogen target and form mesic atoms (μ^-p) or mesic - molecular ions ($p\mu^-p$). At a low velocity the negative muon is trapped by the Coulombic field and cascades down to the lowest 1s atomic state. A neutral mesic atom will be formed once it is released from the molecular bond and it will start to migrate in the hydrogen medium. When the mesic atom is formed it is composed of both spin triplet ($S=1$) and spin singlet ($S=0$) hyperfine states in the proportion of their statistical weights of 3/4 and 1/4 respectively. The ratio of triplet to singlet in the mesic atoms does not remain constant in time but decreases due to the subsequent collisions. In high - pressure conditions the μ^-p atoms collide with surrounding H_2 molecules in the gaseous hydrogen target and the number of collisions depends on the mean free path of the μ^-p atoms ($1/\lambda = N\sigma$). The μ^-p atom will lose kinetic energy (K.E.) until the K. E. (in the center of mass system) falls below the hyperfine splitting of 0.183eV. After a short time ($\approx ns$) all the

muons in triplet states will be transformed into singlet states :



If the muon's capture occurs in liquid hydrogen, a further collision can continue

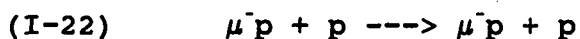


and a mesic - molecular ion complex will be formed. It is quite difficult theoretically to deal with the $(p\mu^-p)$ complex due to the fact that $(p\mu^-p)$ has to be treated as a three - body system.

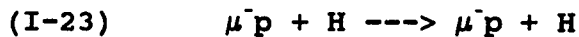
D. Muon scattering with nuclei and molecules

When μ^-p muonic atoms have been formed in a pure hydrogen target, they begin to migrate throughout the surrounding medium. There are roughly three levels of scattering reactions which are influenced by three different energy conditions :

1) At a high energy condition, the muonic hydrogen atom μ^-p is a neutral object whose size is about 200 times smaller than that of the usual atom [4]. In this sense, it looks like a neutron in many respects. The μ^-p atom scatters only with protons [7]. Thus, we can ignore the effects of atoms of hydrogen and molecules of hydrogen on the muonic atoms. Therefore, the scattering process is :



2) At low energy conditions the effects of electron screening play a significant role in the (μ^-p) scattering process in the hydrogen target [9]. So, the μ^-p scattering exists with the atom of hydrogen, i.e.



3) In the low energy region (0.01 -- 0.15 eV) we have to deal with the elastic scattering of μ^-p on the H_2 molecule [10] :



The interaction between the mesic atoms and nuclei of the H_2 molecule [11] and the scattering cross sections of μ^-p with H_2 at low energy ($\epsilon \geq 0.04$ eV) have been calculated and reported in the literature [11].

I. 2. The Purposes of the Experiment

The purposes of this diffusion experiment were as follows :

- 1) To determine the initial velocity distribution of the muonic hydrogen atoms when these μ^-p atoms are formed in a gaseous hydrogen target and have reached the 1s ground state;
- 2) To compare the time distribution data at different pressures with the theoretical predictions of time distributions which were dominated by the scattering cross sections of the diffusion process. This comparison enables us to test the

current theoretical calculation for μ^-p atom diffusion in gaseous hydrogen, and also to estimate the effects of electron screening and the H_2 molecular structure on the cross section;

3) To study the time behavior of the mixture of triplet state $(\mu^-p)_{1s}^T$ and $(\mu^-p)_{1s}^S$ singlet state in the various pressures of hydrogen gas, using the theoretical evaluation of the lifetime τ_T of the triplet state for $(\mu^-p)_{1s}$ atoms in hydrogen as a function of the hydrogen pressure;

4) To determine the muon mean life in Au and to compare that measurement with previous measurements.

With the data analysis, we should have more information about the formation of the μ^-p atom and the diffusion process of μ^-p in a hydrogen target. Therefore, this experiment will be a preparation for a subsequent experiment on muon absorption in hydrogen.

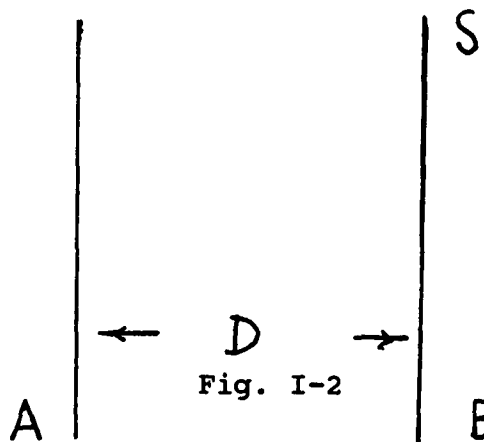
I. 3. The Design of The Experiment

In order to realize the above mentioned purposes of the experiment we carefully designed this experiment with reliability and flexibility. On the basis of wide investigation of previous experiments, reference to theoretical literature and discussion with collaborators, this experiment was assembled and performed in May 1987 in the μE_4 area of the Paul Scherrer Institute (PSI --- formerly the Swiss Institute for Nuclear Research (SIN) in Villigen, Switzerland).

The basic ideas for the design of this diffusion experiment were as follows :

A. Parallel Foils Separated at a Distance D in the Target Vessel

First of all, parallel foils were separated at a distance D in the target vessel (Fig. I-2),



where D was the distance between foils A and B, Au (100Å) or Al (2000Å) film were deposited on the surfaces of the foils, and S was the area of the foil.

The parallel foils had two functions as below :

1) The μ^-p atoms were formed in the gas between two foils, with an initial velocity distribution. The μ^-p atoms then scattered in the hydrogen or deuterium gas(or decayed);

2) The μ^-p atom drifted in the gas and eventually hit the Au or Al foils, The X ray or γ ray signals from the foil layers were detected with germanium detectors. The delayed signals of X ray or γ ray were a map of the initial velocity distribution of the muonic hydrogen atoms.

Using mathematical derivation (for more detail see Appendix A), we assumed that the μ^-p or μ^-d atoms formed uniformly in the gas gaps and that the initial velocity distribution was isotropic, i.e.

$$\begin{aligned} \rho(x,y,z) &= \rho \\ \text{(I-25)} \qquad \qquad \qquad &= 1/SD \end{aligned}$$

and

$$\text{(I-26)} \qquad \qquad \qquad f(\mathbf{v}) = f(v)$$

and also that there was an absence of scattering between μ^-p and the molecules of hydrogen gas.

Therefore, the relationship between the time distribution of the X ray (or γ ray) and the initial velocity distribution was :

$$\begin{aligned} P(t) &= 4\pi S \left\{ \int_0^{D/t} v^3 f(v) dv \int_0^1 \cos(\theta) d \cos(\theta) + \int_{D/t}^{\infty} v^3 f(v) dv \int_0^{D/vt} \cos(\theta) d \cos(\theta) \right\} \\ \text{(I-27)} \end{aligned}$$

and

$$(I-28) \quad P(t) = 2\pi/D \left\{ \int_0^{D/t} v^3 f(v) dv + \int_{D/t}^{\infty} \frac{D^2 v f(v)}{t^2} dv \right\},$$

where $P(t)$ was the probability that the μp atom was collected by foils at time t , and $f(v)$ was the initial velocity distribution of μp atoms. In principle, we could calculate the time distribution of the μp atoms as they hit the Au layer because we knew the initial velocity distribution $f(v)$ from eq. (I-27)

Next we considered several possible initial velocity distributions. We list them below using integral (I-28):

1) The initial velocity distribution may be a delta function :

$$(I-29) \quad f(v) = \frac{1}{4\pi v_0^2} \delta(v-v_0)$$

so the time distribution would be:

$$P(t) = \frac{1}{2v_0^2 D} \left\{ \int_0^{D/t} v^2 \delta(v-v_0) dv + \int_{D/t}^{\infty} \frac{D v \delta(v-v_0)}{t^2} dv \right\}$$

and

$$(I-30) \quad P(t) = \begin{cases} v_0/2D & , \quad t \leq D/v_0 \\ D/2v_0 t^2 & , \quad t \geq D/v_0 \end{cases}$$

2) The initial velocity distribution is a Maxwell distribution :

$$(I-31) \quad f(v) = (m/2\pi kT)^{3/2} \exp(-mv^2/2kT)$$

so, it follows that the time distribution is :

$$P(t) = 2\pi/D \left\{ \int_0^{D/t} v^3 f(v) dv + \int_{D/t}^{\infty} D^2/t^2 f(v) dv \right\}$$

and

$$(I-32) \quad P(t) = 2/D (2kT/\pi m)^{1/2} [1 - \exp(-mD^2/2kTt^2)]$$

3) If the initial velocity distribution is an exponential function :

$$(I-33) \quad f(v) = \beta e^{-\beta v}$$

thus the time distribution is :

$$P(t) = 2\pi/D \left\{ \int_0^{D/t} v^3 \beta e^{-\beta v} dv + \int_{D/t}^{\infty} D^2/t^2 v \beta e^{-\beta v} dv \right\}$$

and

$$(I-34) \quad P(t) = 12\pi/D\beta^2 [1 - e^{-\beta D/t} (\beta^2 D^2/3t^2 + D\beta/t + 1)]$$

B. Performing the Diffusion Experiment Under Various Conditions

This diffusion experiment was performed under various conditions which were chosen from many possible cases :

For d_2 gas we chose seven conditions : 750D, 750S, 375D, 375S, 188D, 188S and 94S (where the number indicates pressure in mbar, and D or S means double gaps or Single gaps in the target vessel) ;

For H_2 gas we chose five conditions : 750D, 375D, 188D, 94D and 47D. The main reasons for choosing these conditions are as follows :

1) According to theoretical predictions, the τ^T lifetime of the triplet state of μ^+p is strongly dependent upon the gas pressure. The relationship of τ^T and pressure is shown below in Fig. (I-3)

[6]

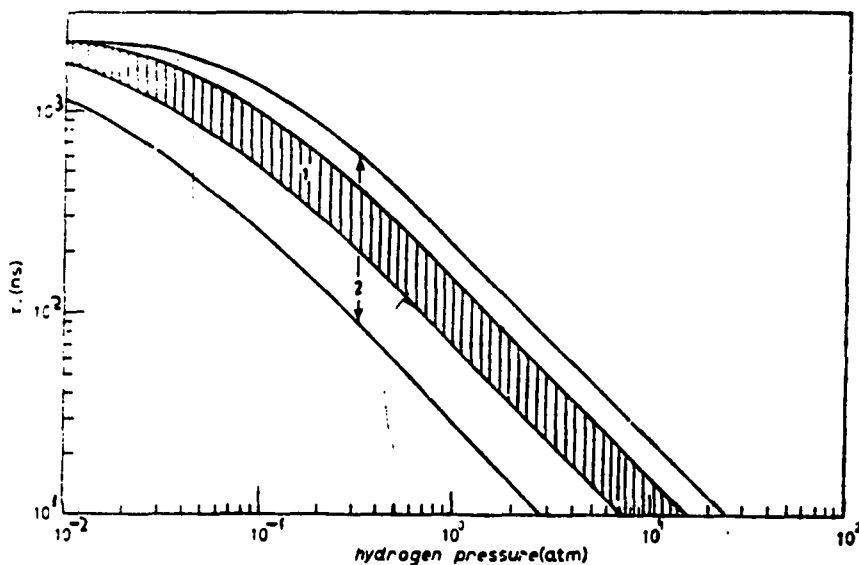


Fig. I-3

At a higher pressure, 750mbar, the life-time τ^T is thus predicted to be about 100 ns, but at a low pressure, 47mbar, the lifetime of a triplet state is expected to be about $\approx 2\mu\text{s}$. So in a high pressure condition we can ignore the triplet state because only the singlet state takes part in the scattering process. On the other hand, at lower pressure conditions we must take into account the ratio between the triplet state and the singlet state which is constant at all times.

In the condition between high and low pressure, the $\mu\bar{p}$ atoms are a mixture of triplet and singlet states, but also their ratio, $(\mu\bar{p})^T/(\mu\bar{p})^S$, decreases in time.

Therefore, we expect that the condition in which there will be an absence of scattering between $\mu\bar{p}$ and H_2 will be reached at lowest pressure. We are then able to apply the eq. (I-28) to the time distribution.

If this simplest case is reached, one may reconstruct the initial velocity distribution $f(v)$ from the experimental time distribution $P(t)$ by applying the integral (I-28).

In addition, it thus seems reasonable that this experiment was performed with deuterium gas first. The scattering probability for a (μp) atom in hydrogen is significantly larger than for a (μd) atom in deuterium gas. [7]

In order to establish the sensitivity of this experiment for each individual run, we pumped the gas out of the target vessel. Then the experiment was performed for an extended period. The data which accrued from the vacuum condition provide a frame of reference for other experimental data.

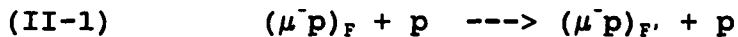
Chapter II

THEORY

II. 1. Scattering of a (μ^-p) Atom in Gaseous Hydrogen

A. A (μ^-p) Atom Scatters on a Proton

After a (μ^-p) atom is formed, the (μ^-p) atom starts scattering on a proton in gaseous hydrogen. The process is shown below :



where F, F' are the total spin of a muonic atom, respectively, before and after the scattering.

In the process (II-1) we have to deal with a three-body system. Generally speaking, for a description of the (II-1) process it is reasonable to use the adiabatic representation which consists of expanding the wave function of a three-body system over a complete set of the solutions of the two-center Coulomb problem. Consequently, this problem is reduced to the multichannel scattering problem with a great number of closed channels.

In order to reduce the difficulty of calculating the cross section of process (II-1) in multichannel scattering, we simplify the multichannel scattering to two-channel scattering with an accuracy of about 10 %.

By approximating the adiabatic method [7], we get the coupled equations :

$$\left(\frac{d^2}{dR^2} + k_1^2 - \frac{J(J+1)}{R^2} \right) x_1 = V_{11}x_1 + V_{12} x_2$$

(II-2)

$$\left(\frac{d^2}{dR^2} + k_2^2 - \frac{J(J+1)}{R^2} \right) x_2 = V_{21}x_1 + V_{22} x_2$$

or in matrix notation :

$$(II-3) \quad \Pi x = V x$$

where $\Pi_{ij} = (d^2/dR^2 + k_i^2 - J(J+1)/R^2) \delta_{ij}$, R is the distance between hydrogen nuclei, J is the total angular momentum of a three-body system and k_1, k_2 are the momenta in the respective reaction channel. k_1 and k_2 are expressed in the following way :

$$k_1^2 = 2M\epsilon/E_a \quad k_2^2 = 2M(\epsilon - \Delta)/E_a$$

$$M = m_\mu/m_p \quad \Xi^{-1} = (m_\mu + M_p)^{-1} + M_p^{-1}$$

$$m_p^{-1} = m_\mu^{-1} + M_p^{-1}$$

$$(II-4) \quad \Delta E = E_b - E_a = m_\mu/2 \left[(1+m_\mu/m_p)^{-1} - (1+m_\mu/m_p)^{-1} \right]$$

where m_μ is the muon mass, m_p is the proton mass, $\Delta E = \Delta E^{\text{hfs}}$ is the difference between two hyperfine state levels of $\mu\bar{p}$ atom and ϵ is the collision energy.

We apply the S matrix method to solve the coupled equations (II-2). As is well known, the S matrix is represented as follows [14] :

$$(II-5) \quad S = (1 + iT)(1 - iT)^{-1}$$

where [14]

$$T'(R) = -[u + T(R)V] V [u + V T(R)] \quad (\text{II-6})$$

and has the asymptotic behavior($T(\infty) = T$). u is the potential of the two-center problem, and V is the effective potential. The relationship between u and V is :

$$V = A u A^{-1}$$

where A is a matrix such that :

when J is even

$$A_{s=1/2} = \frac{1}{2} \begin{pmatrix} 1 & 1 & -\sqrt{3} \\ \sqrt{3} & 1 & 1 \end{pmatrix} \quad A_{s=3/2} = \begin{pmatrix} 0 & 0 \\ 0 & -1 \end{pmatrix} \quad \text{and}$$

when J is odd

$$A_{s=1/2} = \frac{1}{2} \begin{pmatrix} 1 & -\sqrt{3} & 1 \\ 1 & \sqrt{3} & 1 \end{pmatrix} \quad A_{s=3/2} = \begin{pmatrix} 0 & 0 \\ 1 & 0 \end{pmatrix}$$

When the collision energy $\epsilon > \Delta E$, the functions u and V are

$$(II-7) \quad u_1(R) = 1/\sqrt{k_1} j_J(k_1 \cdot R)$$

$$(II-8) \quad V_1(R) = -1/\sqrt{k_1} n_J(k_1 \cdot R)$$

and with asymptotic behavior :

$$(II-9) \quad u_1(R \rightarrow \infty) = 1/\sqrt{k_1} \sin(k_1 \cdot R - \pi J/2)$$

$$(II-10) \quad V_1(R \rightarrow \infty) = 1/\sqrt{k_1} \cos(k_1 \cdot R - \pi J/2)$$

where j_J and n_J are the Riccati-Bessel Spherical functions [20]

Then, the cross section is obtained :

$$(II-11) \quad \sigma_{ij}^S = \frac{4\pi}{k_i^2} \sum_J (2J+1) \frac{\delta_{ij} D_J^3 + (t_{ij}^J)^2}{(D_J-1)^2 + (t_{11}^J + t_{22}^J)^2}$$

where

$$(II-12) \quad D_J = t_{11}^J t_{22}^J - (t_{12}^J)^2$$

When the collision energy $\epsilon < \Delta E$, the functions u and V are :

$$(II-13) \quad u_1 = 1/\sqrt{k} j_J(kR), \quad V_1 = -1/\sqrt{k} n_J(kR)$$

$$(II-14) \quad u_2 = (-1)^{J+1}/\sqrt{2k} [j_J(ikR) - in_J(ikR)]$$

$$(II-15) \quad V_2 = (i)^{J+1}/\sqrt{2k} [j_J(ikR) + in_J(ikR)]$$

and with asymptotic behavior they are :

$$(II-16) \quad u_2(R=\infty) = 1/\sqrt{2k} e^{kR}$$

$$(II-17) \quad V_2(R=\infty) = 1/\sqrt{2k} e^{-kR}$$

The elastic scattering cross section is

$$(II-18) \quad \sigma_{ii}^S = \frac{4\pi}{k^2} \sum_J (2J+1) \frac{(t_{ii}^J)^2}{1 + (t_{ii}^J)^2}$$

Because of the conservation of the total spin s of the (μ^-p) and p (three body system), we take into account the statistical weights:

$$(II-19) \quad W_{FS} = \frac{2S + 1}{(2F+1) (2S+1)}$$

Therefore, the cross section of process (II-1) is

$$\sigma_{FF'} = \sum_S W_{FS} \sigma_{FF'}^S \quad (\text{II-20})$$

The equation (II-6) has been solved numerically [7]. We are therefore able to obtain the total cross sections. Notations are given below (with reference to Fig. II-1) :

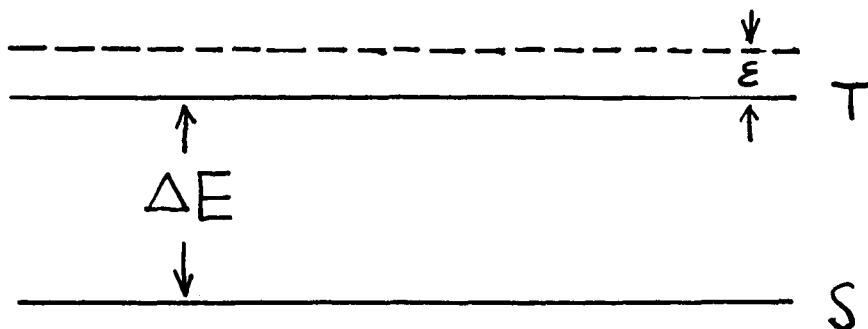


Fig. II -1

and

Initial state		Total cross section
S	$\epsilon < \Delta E_{hfs}$	σ_{SS}
S	$\epsilon \geq \Delta E_{hfs}$	$\sigma_{SS} + \sigma_{ST}$
T		$\sigma_{TT} + \sigma_{TS}$

where S is a singlet state and T is a triplet state.

The values of the energy-dependent total cross sections σ_{SS} , σ_{TT} and σ_{TS} are provided in Fig. (II-2), Fig.(II-3) and Fig.(II-4).

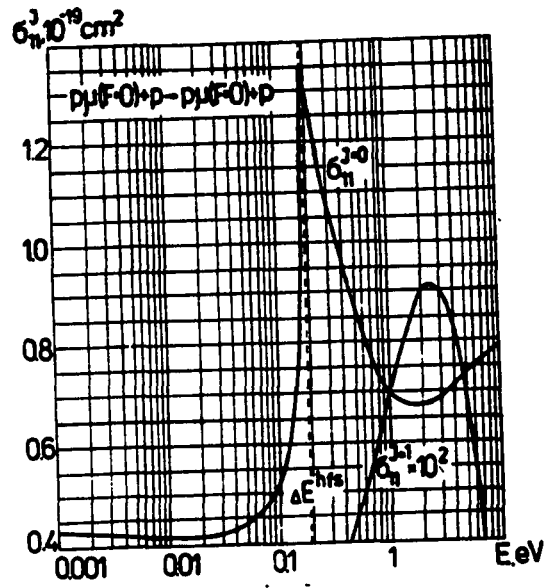


Fig. II-2

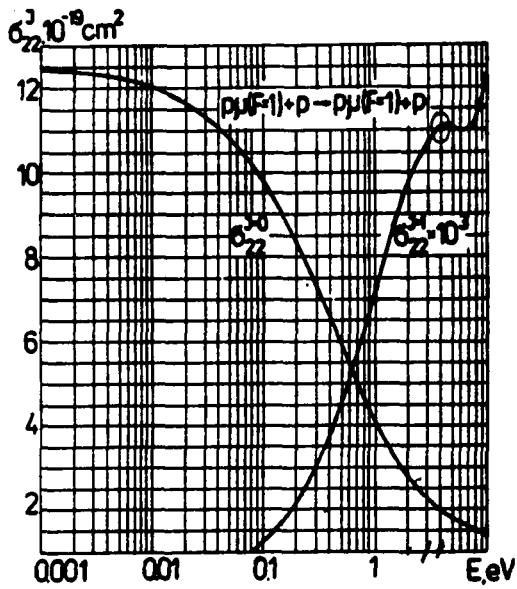


Fig. II-3

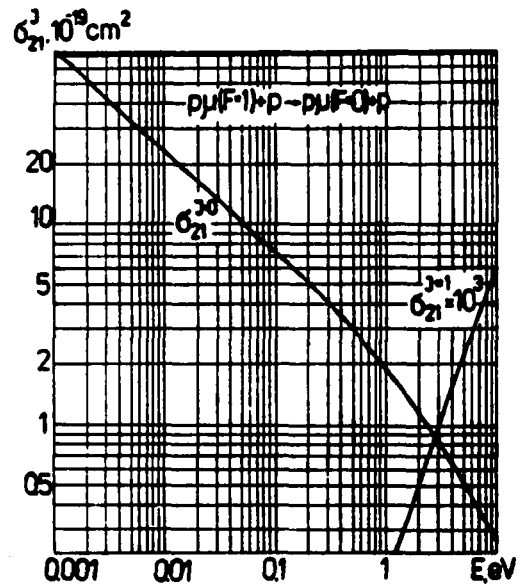


Fig. II-4

According to the principle of inverse reaction -detailed balance [21], the transition cross section σ_{ST} is

$$(II-21) \quad \sigma_{ST} = \frac{(2S_T + 1)}{(2S_S + 1)} \left(\frac{P_T}{P_S} \right)^2 \sigma_{TS}$$

where S_T, S_S represent the spin and P_T, P_S represent the momentum.

In the calculation of the $(\mu^-p) + p$ scattering cross section above, the effects of electron screening and molecular binding have been ignored completely.

Some authors recently took into account the influence of electron screening and molecular binding in low and extremely low energy regions. Their corrections are given in the published articles ([8],[10],[11],[9]).

II. 2. Muon Moderation in Gaseous Hydrogen.

A. Energy Loss of the Incident Muons due to Ionization

We consider the energy loss of the incident muons due to ionization. A charged particle moving through matter interacts with nuclei as well as with atomic electrons. The greatest part of the energy loss occurs during collisions with atomic electrons. The atomic electrons receive so much energy that they either become free or the atoms become excited. In either case, the energy comes from the kinetic energy of the incident particle, which will be thereby moderated.

The rate of energy loss of a particle with charge Ze as it progresses through a medium containing N electrons per cm^3 was calculated by Bloch-Bethe as follows [21] :

$$(II-22) \quad \frac{dE}{dx} = \frac{4\pi z^2 e^4 N_0 Z}{m_e v^2 A} \left[\log \frac{2m_e v^2}{I(1-\beta^2)} - \beta^2 \right]$$

where E is the kinetic energy of the muon, N is the number density of the stopping medium with Ze charge, m_e is the electron mass, I is the adjusted mean excitation energy, ($I \approx 20$ eV for H_2 , $I \approx 320$ eV for kynar ($\text{C}_2\text{H}_2\text{F}_2$) and $I \approx 1580$ eV for Au) and $\beta = v_\mu / c$.

Samples of stopping - power curves in Be, Cu and Pb are given in Fig. II-5.

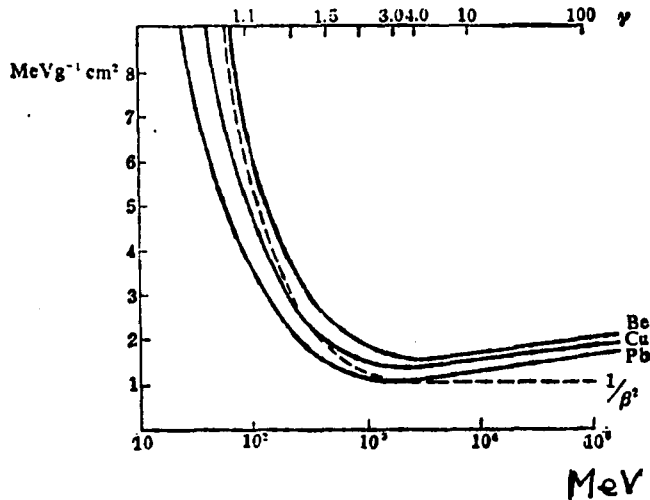


Fig. II-5

At high energy regions the curve will approach a plateau. The minimum energy loss $(dE/dx)_{\min}$ is about 1.2 Mev/gcm^{-2} in a medium of heavy elements and about 1.7 Mev/gcm^{-2} in a medium of light elements.

A muon passing through hydrogen gas not only ionizes the atoms above the ionization limit but also excites the atoms below the ionization limit. So a sizeable fraction of kinetic energy is imparted to the atoms and some of it can then be transformed into scintillation light.

In addition, we considered the radiation loss of a fast muon in a medium with N_0, Z, A . As is well known, the radiation loss of a fast electron is given in eq. (II-23)

$$\frac{dE}{Edx} = \frac{4 r_0^2 N_0 Z^2}{137A} [\ln (183/Z^{1/3} + 1/18)] \quad (\text{II-23})$$

where $r_0 = e^2/m_e c^2$.

We notice that the energy loss dE/dx is inversely proportional to m^2 . Thus the radiation energy loss of a muon will be at a relative rate of $(m_e/m_\mu)^2$ for an electron. This relative rate is about $2.5 \cdot 10^{-5}$. Therefore, in most cases we ignore the radiation loss for muons.

II. 3. Muonic Hydrogen Formation

A. The (μ^-p) Atoms Formed in Gaseous Hydrogen by Atomic Capture

The process in which a proton atomically captures a muon in gaseous hydrogen is complicated. The process has been studied for quite a long time. There is a great deal of interest among both theorists and experimental physicists in the energy level at which a muon will be captured by a proton.

Theoretical predictions for the capture energy vary from near thermal [27], $\approx 0.038\text{eV}$, up to the X ray energy, several keV [23].

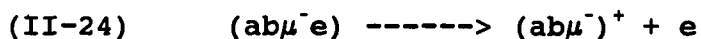
Various models yield various capture energies. A brief summary of these different theories is given below :

1) The Bohr Model

Briefly, in the Bohr model atomic capture will occur when the energy of the muon is equal to the energy of a K - shell electron, i.e., muonic capture energy is equal to about 13.6 eV. This means the capture occurs in the $n_\mu \approx 14$ orbit of a muonic atom.

2) The Auger Transition Model [13]

Atomic capture of a muon proceeds via excitation of an electron, i.e. Auger transition :



where a or b = { p, d, t } - the hydrogen nuclei, $a\mu^-$ - the hydrogen muonic atom in the ground state (1s).

As a result, this model predicts that atomic capture will occur near thermal energies with orbital quantum numbers < 14 [22], namely, the capture energies will vary from 0.038 eV to less than 13.6 eV.

3) Haff and Tombrello Model [24]

Atomic capture will occur on isolated atoms. An important result of this model is that half of the muons will be captured by hydrogen atoms when their energies are above 75 eV.

4) Korenman and Rogovaya Model [25]

In this model that the maximum capture probability energy distribution occurred at a muon energy of about 50 eV [25].

5) The Adiabatic Model [26]

According to the adiabatic model, capture occurs at energies greater than 50 eV [27].

Obviously, these theoretical predictions give muon energies at the time of capture which vary widely.

B. The Standard Model of Muonic Hydrogen Formation

The usual model of muonic hydrogen formation is as shown below

:



One assumes that the kinetic energy and the momentum of the muon at the time of capture are $1/2 m_\mu v^2$ and $m_\mu v$ respectively, and the kinetic energy and momentum of the $\mu\bar{p}$ atom formed in hydrogen are $1/2 MV^2$ and MV respectively.

In first order approximation, we ignore the hydrogen atom thermal kinetic energy (≈ 0.038 eV, at room temperature). According to momentum conservation,

$$(II-25) \quad m_\mu v_\mu = M V$$

$$(II-26) \quad T_\mu = \frac{1}{2} m_\mu v_\mu^2 \quad T_{M^*} = \frac{1}{2} MV^2$$

where M is the mass of one molecule in μH , μH_2 , μD , or μD_2 . Therefore, the ratio of the kinetic energy of a muon to the kinetic energy of the formed atom or molecule of isotopic hydrogen is

$$(II-27) \quad T_\mu / T_{M^*} = M / m_\mu$$

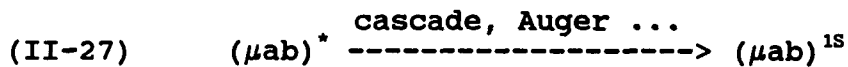
We list those ratios T_μ / T_{M^*} in the table (II-1) :

TABLE II-1

Formation	Mass M^*	Ratio T_μ / T_{M^*}
μH	1038 MeV	≈ 10
μH_2	1976 MeV	≈ 20
μD	1976 MeV	≈ 20
μD_2	3852 MeV	≈ 39

Thus T_μ is the energy of the muon at the time of capture, T_μ is defined as the muon capture energy, and T_M^* is the kinetic energy of the $(\mu ab)^*$ when $(\mu ab)^*$ is formed.

General speaking, when the muonic hydrogen atom was formed, the formed atom is in an excited state, and deexcites through cascade and Auger processes down to the 1S ground state :



We note that all these deexciting processes are internal. Thus, the kinetic energy of the formed hydrogen atom is conserved. Namely

$$T_M^* = T_M$$

As previously defined, the initial velocity of the formed hydrogen atom is

$$(II-28) \quad \begin{aligned} V &= (2MT_M^{1S})^{1/2} \\ &= v^* \end{aligned}$$

in other words, the velocity of the formed atom stays constant during the deexciting process.

We should consider the recoil of the muonic atom when an X ray is emitted in the deexcitation. According to momentum balance :

$$(II-29) \quad MV' + p_x = MV$$

where M is the mass of a formed atom or molecule, $p_x = h\nu/c$ is the momentum of the X ray emitted and MV, MV' are the momenta of the

formed molecule, respectively, before and after emitting an X ray.

So

$$\Delta V \approx p_x/M$$

and

$$(II-30) \quad \Delta V/V \approx [(h\nu)^2/2TMc^2]^{1/2}$$

For a (μ p) atom, $h\nu \leq 2.6$ keV, $Mc^2 = 1038$ MeV and $T \approx 50$ eV.

Thus

$$(II-31) \quad \Delta V/V < 0.008$$

The measurement of velocities in this experiment has a precision of about 10%. Comparing this with expression (II-31), we are confident that we could ignore the effects of the recoil of a formed atom.

Chapter III
Description of the Experiment

III. 1. The Outline of The Experiment

A. Muon Beams

The experiment was performed in the μE_4 area at the Paul Scherrer Institute.

The main ring of the cyclotron produced a 590 Mev proton beam [28] which was extracted and directed towards a target which was a 12 cm long, 6mm thick block of Be. The proton beam produced pions in the Be target, and then muons, generated from pion decay, were collected by a 5 m long superconducting 5 Tesla solenoid and transported to the experimental area (Fig. III-1)

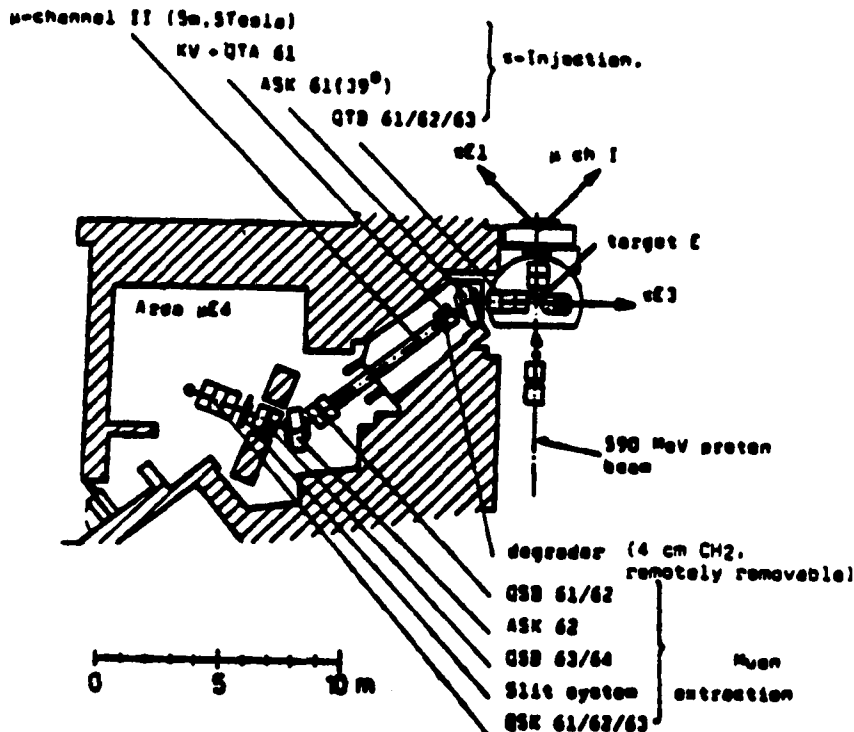


Fig. III-1

Varying the muon momentum enabled us to optimizing muon stopping rate in the foil stack. The optimal muon momenta would be 35 MeV/c for a single gap stack, 34 MeV/c for a double gap stack and 39 MeV/c for a 0.25 mm steel window on the target. The appropriate magnet settings are listed in the Table III-1.

Table III -1

Magnet	$P_\mu = 34 \text{ MeV/c}$	$P_\mu = 35 \text{ MeV/c}$	$P_\mu = 39.6 \text{ MeV/c}$
QTB 61	+2192	+2214	+2377
QTB 62	-1840	-1858	-1994
QTb 63	+1080	+1090	+1170
ASK 61	-1140	-1151	-1236
QSB 61	+635	+654	+739
QSB 62	-350	-360	-407
QSB 63	-302	-311	-351
QSB 64	+514	+529	+599
ASK 62	-506	-521	-589
QTA 61	-1485	-1500	-1600
QSK 61	+558	+574	+650
QSK 62	-595	-612	-694
QSK 63	+505	+520	+588

Slit Settings (volts)

Left	2.3	2.3	2.3
Right	2.3	2.3	2.3
Top	2.3	2.3	2.3
Bottom	2.3	2.3	2.3

Typical single scaler rates for the various beam conditions are shown in Table III-2 (refer to Fig. III-2 for designations and Table III-3 for descriptions of counters)

Table III-2

Rates (s^{-1})

Scaler	$P_{\mu} = 34 \text{ MeV/c}$	$P_{\mu} = 35 \text{ MeV/c}$	$P_{\mu} = 39.6 \text{ MeV/c}$
2/10	54450	54220	55500
2*3/10	27891	27772	31800
2*3a/10	19151	18889	18200
2*3* $\overline{3a}$	27664	27540	31400
$\overline{\mu DT}/10$	16139	14209	15600
3a	36205	33275	27800
μPD	137988	121397	134000
lifetime	61 %	53 %	52 %
Master	10792	13401	13810
Proton Beam	191 μA	188 μA	155 μA

B. Target, Window and Gas System

The target consisted of a set of plastic foils which was constructed of 9 μm thick kynar ($\text{C}_2\text{H}_2\text{F}_2$) foil, with 100 \AA thick layers of Au deposited on each surface, and was placed inside an aluminum pressure vessel. Because the plastic kynar has low vapor pressure, it was chosen as the major component of the stack. In the single gap case, the distance between the two foils was 2.3 mm and the whole assembly had 50 foils. In double gap case, the distance between two foils was 4.6 mm and the whole assembly had 30 foils.

Three different target windows were used in the experiment, as given below :

<u>TARGET</u>	<u>WINDOW</u>	<u>CONDITION</u>
0.25 mm	steel window	high pressure
0.1 mm	Al window	low pressure Au target
0.1 mm	Ti window	low pressure Al target

The gas and vacuum system is shown in Fig. C. Briefly, it consists of a forepump, a turbomolecular pump, a gas input, a gas output and a Pd filter. The presence of impurities in the gas was monitored by a quadrupole mass spectrometer. The H_2 or D_2 gas was at 300 K and was continuously circulated through a Pd purifier during data acquisition.

The experimental setup for the H_2 diffusion experiment is illustrated in Fig. III-2.

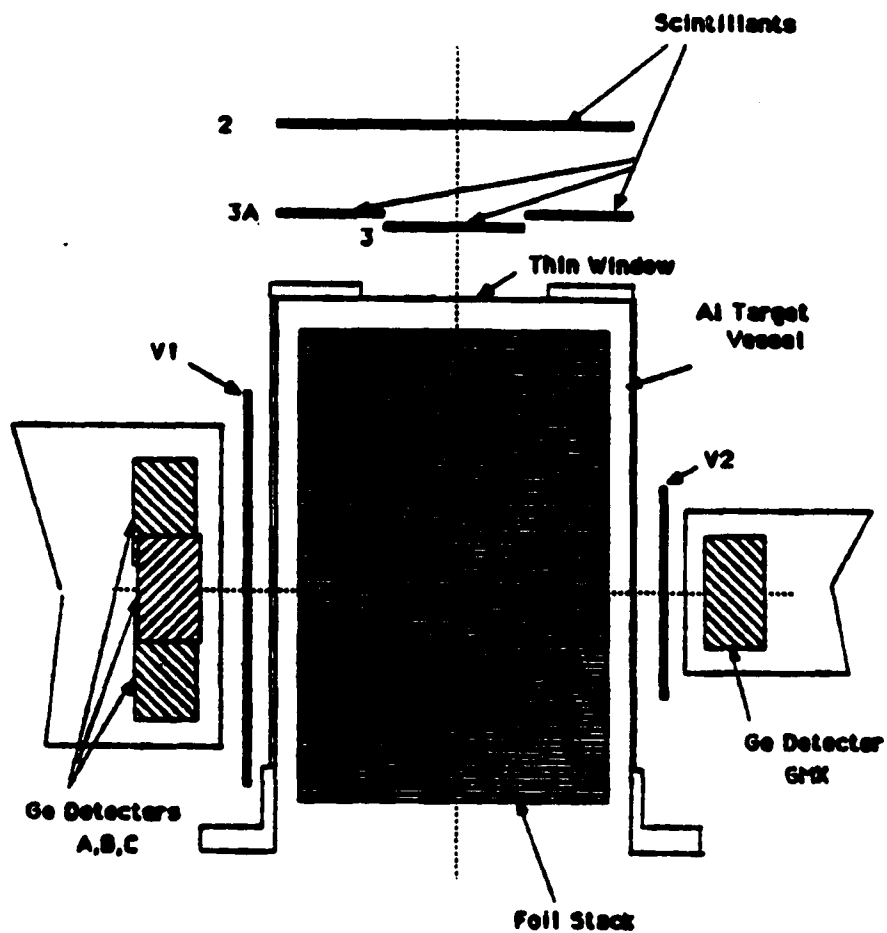


Fig. III-2 -- Plan View of Apparatus

III. 2. Detectors

A. Counters

Six scintillation counters were used in the experiment. Their sizes are given in Table III-3 :

Table III-3
Scintillation Counters

Counter	Dimensions (cm)	Discriminator Setting (mV)
2	20x20x0.06	200
3	5.5 diameter x 0.05	130
3a	18x14x0.5 with 5 cm aperture	50
v1	14 diameter x 0.2	40
v2	8 x 8 x 0.3	80
v3	8 x 8 x 0.3	50

The scintillator telescope was comprised of counters 2, 3 and 3a. The number of muons entering the target vessel were indicated by the coincidence of $2 \cdot 3 \cdot \overline{3a}$. The counters V1, V2 and V3, which were located in front of TU germanium detector (located above the apparatus in Fig. II-2), vetoed the charged particles, such as muon-decay electrons.

B. Germanium Detectors

1) Ge Detector Characteristics

The semiconductor γ ray detectors consist of a piece of ultrapure germanium in which electrons and holes are produced when a γ ray is absorbed. These electrons and holes are then collected by an electric field [32].

When γ rays enter a detector, any of three primary interactions may take place between the γ rays and electrons: a photoelectric interaction, a Compton collision or a pair production event ($\gamma \rightarrow e^+ + e^-$). Whereas a photoelectric event produces an amount of ionization corresponding directly to the γ ray energy, Compton events produce a variable amount of ionization. As a result of the Compton process a general Compton background will be produced in the γ ray spectra.

The average energy that is required to produce a hole-electron pair is expressed in terms of the parameter ϵ . However, for a given energy absorbed in the primary interaction, the total number of hole-electron pairs created is subject to statistical fluctuations due to the random energy loss. Any process that consumes energy without producing ionization is lost from the point of a view of electrical signal production.

If the average number of charged carriers produced is E/ϵ , where E is the energy absorbed in the detector, the standard deviation is [30]:

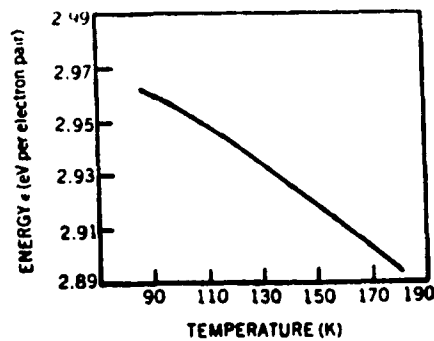
$$\sigma = (F E/\epsilon)^{1/2}$$

or

$$(III-1) \quad FWHM = 2.355 (FE/\epsilon)^{1/2} ,$$

with F a smoothing factor (the Fano Factor). If the total absorbed energy were to be used in producing ionization, and no statistical fluctuations would occur in the signal, this Fano Factor would be zero. Generally, the Fano Factor ranges between 0 and 1.

The dependence of the energy band gap on temperature is reflected in the change in ϵ with temperature. this dependence is illustrated below in Fig. III-3. [29]



Variation of ϵ , the average energy required to produce a hole-electron pair, with temperature for germanium.

Fig. III-3

Possible trapping centers exist in crystals due to their impurities and imperfections. If the average time in which a carrier remains trapped before being released by thermal excitation is very short compared with the pulse - shaping time used in the amplifier, trapped carriers will be released quickly enough to contribute to the total signal and will not be lost. On the other hand, if the time is comparable to, or larger than, the pulse-shapping times, trapped carriers will be partially or completely lost. Since the amount of charge lost by trapping is almost proportional to the total charge produced, the trapping effect on the spectral line width increases as the γ ray energy increases (see Table III-3) : [31]

Table III-3

Detector A

E (keV)	FWHM (keV)
1332.89	2.47
1173.87	1.71
661.42	1.64
383.77	1.17
355.85	1.14
302.69	1.13
276.25	1.10
136.35	0.88

2) The Analytic Approximation of the Peaks Obtained From Ge Detectors

The following is a brief summary of Ge detector characteristics mentioned above :

i) Due to incomplete charge collection, trapping effects, and pulse in the amplifier pile-up, the standard Gaussian shape may be distorted in the low-energy region and has an exponential tail.

ii) A smooth background is generated by the electronic noise of the detection system associated with detector, the detector leakage current, trapping centers in the crystal, impurities and imperfections of the crystal. Thus the background can be represented by a polynomial of a suitable order, and this regular part of the background is independent of the photopeaks.

iii) The Compton background can be represented by a step function which rides on a polynomial background, and this part of the background is related to the photopeaks.

Therefore, an analytic approximation of the peaks obtained from Ge detector is found to be :

$$F(x,P) = \text{regular background} + \sum_i \{ \text{compton background} + \text{pure}$$

Gaussian + exponential tail at low energy side of photopeak }

where $F(x,P)$ is an analytic expression of the photopeaks, and the terms in the { } are dependent on photopeaks.

For simplicity, we consider only a single photopeak. Thus, the $F(x,P)$ is found to be :

$$F(x,P) = \sum_{k=1}^{m+1} a_k x^{k-1} + Ag \exp[-(x-x_i)^2/2\sigma^2] + \text{Compton background} \\ + \text{exponential tail at low energy side of a peak)}$$

(III-2)

where m is the order of a polynomial, usually $m \leq 2$. Ordinarily, we can consider the background to be linear.

The Compton background can be expressed as a step function :

$$(III-3) \quad h \operatorname{erfc}[(x-x_i)/\sigma_g]$$

where h is the height of the step, σ_g is the resolution of the Ge detector, and erfc is defined as

$$(III-4) \quad \operatorname{erfc}(x) = 1/2 - 1/\sqrt{2\pi} \int_{-\infty}^x \exp(-t^2/2) dt$$

The tail effects of the trapping centers and pile-up can be described by folding the exponential function into the Gaussian distribution [30], i.e.,

$$(III-5) \quad F_{\text{tail}} = D \int_{-\infty}^{x_0} \exp[B(\tau-x_0)] \exp[-(x-\tau)^2/\sigma_e^2] d\tau$$

Performing the integration, we obtain

$$F_{\text{tail}} = D / \sqrt{2\pi} \sigma_e \exp[B(x-x_0) + B^2\sigma_e^2] \operatorname{erfc}[(x-x_0)/\sigma_e + B\sigma_e.]$$

(III-6)

where D is a constant describing the normalization amplitude, B determines the exponential decaying part of the integral. In an approximation we obtain [30]

$$(III-7) \quad \text{erf}(x) = \{ 1 - \exp[-(x-x_0)^2/2\sigma_t^2] \} \delta$$

Thus, the tailing function is considered to be

$$(III-8) \quad F_{\text{tail}} = A_t \exp[B(x-x_0)] \{ 1 - \exp[-(x-x_0)^2/2\sigma_t^2] \} \delta$$

in place of eq. (III-6), where

$$(III-9) \quad A_t = D \sqrt{2\pi} \sigma_0 \exp(B^2 \sigma_0^2),$$

$$\delta = 1 \quad \text{for } x < Cx_0$$

$$(III-10) \quad \delta = 0 \quad \text{for } x \geq Cx_0$$

and

$$(III-11) \quad \sigma_t = \frac{B\sigma_0^2}{1.175 - \sqrt{\ln [\text{erfc}(-B\sigma_0)]^{-2}}}$$

$$(III-12) \quad C = \frac{(B\sigma_0^2/x_0) \sqrt{\ln [\text{erfc}(-B\sigma_0)]^{-2}}}{1.175 - \sqrt{\ln [\text{erfc}(-B\sigma_0)]^{-2}}} + 1$$

The three parts above which contributed to an analytic approximation of the function of form of a photopeak are illustrated in Fig. (III-4).

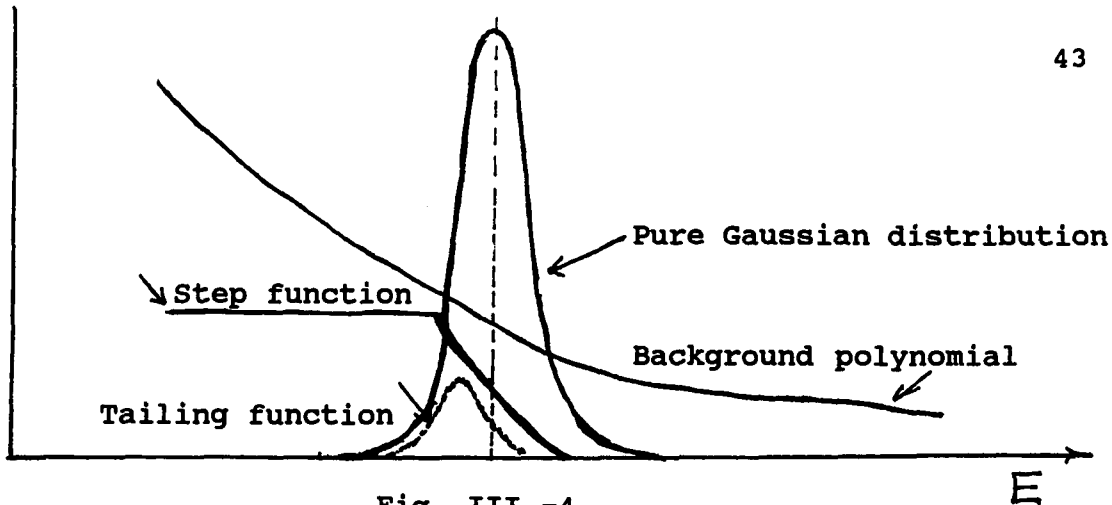


Fig. III -4

Thus, the functional form representing a j th photopeak $F(x,p)$ Eq.(III-2) is now found to be :

$$F(x,P) = \sum_{k=1}^{m+1} a_k x^{k-1} + h_j \operatorname{erfc}[(x-x_j)/\sigma_g] + A_{g,j} \exp[-(x-x_j)^2/2\sigma_g^2] \\ + A_{t,j} \exp\{ 1 - \exp[-(x-cx_j)^2/2\sigma_t^2] \} \delta$$

(III-13)

When there were several photopeaks in a region of interest, we assumed that the width parameters of the Gaussians within a peak group were equal. So an analytic approximation to the peaks in this region, was obtained by summing the peak-related parts in eq.(III-13) :

$$F(x,P) = \sum_{k=1}^{m+1} a_k x^{k-1} + \sum_{j=1}^n h_j \operatorname{erfc}[(x-x_j)/\sigma_g] + A_{g,j} \exp[-(x-x_j)^2/2\sigma_g^2] \\ + A_{t,j} \exp\{ 1 - \exp[-(x-cx_j)^2/2\sigma_t^2] \} \delta$$

(III-14)

Based on the eq. (III-14), physicists have developed the relevant programs (such as FITA, developed at T.U. Munchen), to evaluate the relevant parameters.

Chapter IV
Technique of Data Analysis

IV 1. The Energy Calibration and the Spectrum of Muonic X Rays and γ Rays of Au

A. Energy Calibration

The energy calibration was performed for each detector by using the radioactive sources of ^{137}Cs , ^{57}Co , and ^{133}Ba . Accepted values of the characteristic energies of these radioactive sources are given in from the Table of Isotopes [42].

We assume that the centroids of peaks in the spectrum have a polynomial relationship with the energies of the corresponding lines from the radioactive sources. That is,

$$(IV-1) \quad E_i = a_0 + a_1 x_i + a_2 x_i^2 + \dots + a_n x_i^n$$

where a_0, a_1, \dots, a_n are the coefficients of an n order polynomial. x is a channel number, and E_i is one of the characteristic line energies of the radioactive sources. Usually we limit the order n to be less than 4, because the physical property of Ge detectors basically should be linear. On the other hand, due to various reasons which caused a distortion of linearity of the detectors, such as impurities, crystal imperfections, leakage current, incomplete charge collection and electronic effects, the responses of the Ge detectors are not perfectly linear, so we always choose the square term and cubic term as correction terms of linearity.

As an example, we apply the program FITA [41] to fit energies to order n for Tape 59 and detector C. The coefficients of the least chi-square n order polynomial fit were obtained as shown below :

Order	Coefficients of N-Order Polynomial				Chi-Square
	a_0	a_1	a_2	a_3	
N					χ^2
1	12.18923	$8.55417 \cdot 10^{-2}$			0.01924
2	12.18923	$8.55625 \cdot 10^{-2}$	$-4.639373 \cdot 10^{-8}$		0.02432
3	11.93671	$8.612249 \cdot 10^{-2}$	$-4.188593 \cdot 10^{-7}$	$7.675229 \cdot 10^{-11}$	0.03529

If the difference of the same coefficient among the various orders is relatively small, that is evidence for stability of the fitting (One also need to check the reduced chi-square).

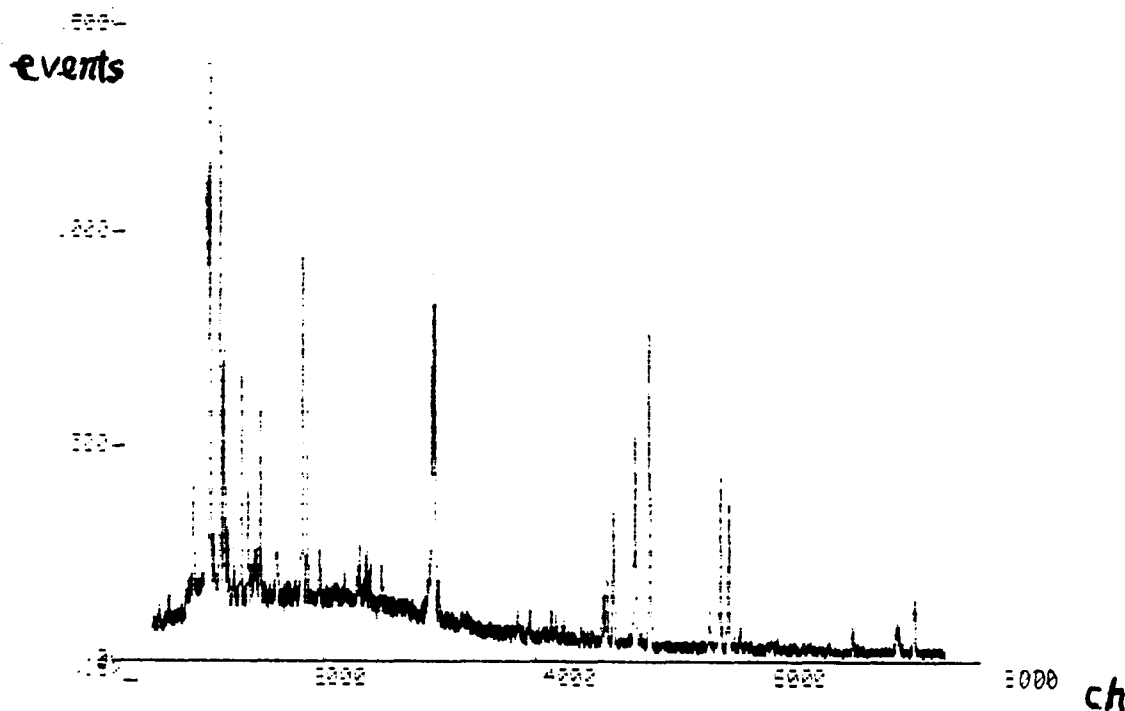
In most cases the Ge detector is not perfectly linear over a wide (several hundred keV) energy interval. In the case above, the linear fit χ^2 is a little smaller than it is for the second or third order fit, but according to experience, the second or third order polynomial is better than the first order polynomial in fitting the widest energy spectrum. So we use the third order polynomial.

IV 1.

B. The spectrum of muonic X rays and γ rays of Au

After calibration of each detector, the energy of any photopeak in the spectrum could be determined and then compared to tabulated values in tables of muonic X rays [39], [72]. Thus, most of the photopeaks in the spectrum could be readily identified. Since the identification of photopeaks which were directly related to the delay events was of major interest, a solid Au target of 520 mg/cm^2 and $\approx 4 \text{ cm}$ diameter was used to get high statistics signals of Au related photopeaks. In this way, we established a master energy table for each detector, and identified several of the most useful photopeaks in the analysis from the spectrum of Au.

A spectrum of μAu in B detector in the Run of May of 1987 is shown below :



MASTER ENERGY TABLE

TAPE 44 AU TARGET B DETECTOR MAY 87 RUN

NO.	CH	AREA events	ENERGY+-ERROR		FWHM keV	NOMINAL keV	ID
			keV	keV			
1	0.7571718E+04	2805.0	521.316+-	0.034	1.50	521.400	PT196
2	0.7415283E+04	2415.0	511.083+-	0.074	2.57	511.004	E+E-
3	0.6987292E+04	877.0	483.008+-	0.081	1.43	482.86	PT194
4	0.6761937E+04	241.0	468.178+-	0.223	1.38	468.03	AU192
5	0.6579952E+04	150.0	456.177+-	0.375	1.52	456.031	AL 7-1
6	0.6525028E+04	186.0	452.551+-	0.304	1.52	452.541	AL 6-1
7	0.6436439E+04	499.0	446.697+-	0.125	1.52	446.720	AL 5-1
8	0.6275183E+04	445.0	436.026+-	0.146	1.31	436.062	AL 4-1
9	0.6217663E+04	414.0	432.215+-	0.162	1.31	432.000	PT196
10	0.6027121E+04	310.0	419.574+-	0.238	1.67	420.900	PT196
11	0.5980764E+04	557.0	416.494+-	0.141	1.67	416.300	AU192
12	0.5927330E+04	1223.0	412.942+-	0.071	1.67	412.906	AL 3-1
13	0.5816917E+04	6765.0	405.595+-	0.020	1.34	405.591	AU 5-4
14	0.5734292E+04	8557.0	400.090+-	0.017	1.34	400.093	AU 5-4
15	0.5634208E+04	1838.0	393.415+-	0.039	1.18	393.500	PT196
16	0.5071020E+04	13375.0	355.695+-	0.016	1.27	355.650	PT196
17	0.4938447E+04	11952.0	346.775+-	0.020	1.28	346.740	AL 2-1
18	0.4732687E+04	5357.0	332.899+-	0.025	1.35	332.900	PT196
19	0.4665990E+04	3491.0	328.392+-	0.036	1.35	328.450	PT194
20	0.4633342E+04	2151.0	326.184+-	0.053	1.35	326.200	PT196
21	0.4538460E+04	372.0	319.763+-	0.162	1.24	321.620	OS193 ??
22	0.4487957E+04	667.0	316.342+-	0.095	1.24	316.490	AU192
23	0.4435257E+04	418.0	312.769+-	0.148	1.25	312.946	AU10-6
24	0.4257001E+04	668.0	300.663+-	0.075	0.99	300.740	PT194
25	0.4192615E+04	412.0	296.282+-	0.118	0.99	295.980	AU192
26	0.4150355E+04	814.0	293.405+-	0.064	0.99	293.540	PT194
27	0.3939004E+04	963.0	278.987+-	0.104	1.48	??????	
28	0.3830768E+04	1118.0	271.585+-	0.095	1.48	271.351	AU 3-8
29	0.3088669E+04	1085.0	220.490+-	0.089	1.07	220.4	AU6-5, *.5F7-
30	0.3048503E+04	11324.0	217.707+-	0.033	1.04	217.701	AU 6-5

MASTER ENERGY TABLE (continued)

31	0.3027122E+04	12454.0	216.224+-	0.035	1.04	216.392	AU 6-5
32	0.2997395E+04	2724.0	214.162+-	0.045	1.07	214.152	AU 3-6
33	0.2956402E+04	1052.0	211.317+-	0.094	1.07	211.025	F 4-1
34	0.2547412E+04	1620.0	182.823+-	0.074	1.31	182.842	AU 10-7
35	0.2380415E+04	593.0	171.130+-	0.137	0.90	171.138	O 5-1
36	0.2343925E+04	1914.0	168.570+-	0.050	0.90	168.463	F 2-1
37	0.2324084E+04	739.0	167.177+-	0.121	0.90	167.114	O 4-1
38	0.2199894E+04	1103.0	158.450+-	0.081	1.11	158.411	O 3-1
39	0.2111965E+04	722.0	152.258+-	0.122	1.11	151.485	AU 12-8
40	0.1963734E+04	2984.0	141.799+-	0.035	1.11	141.870	AU 9-7
41	0.1847402E+04	5627.0	133.570+-	0.039	1.16	133.531	O 2-1
42	0.1802401E+04	14327.0	130.382+-	0.021	1.16	130.452	AU 7-6
43	0.1562237E+04	1726.0	113.322+-	0.047	0.79	112.52	PT193 ?
44	0.1453631E+04	345.0	105.582+-	0.045	0.80	105.534	AL 6-2
45	0.1410110E+04	5108.0	102.475+-	0.019	0.79	102.413	N 2-1
46	0.1373139E+04	1050.0	99.835+-	0.075	0.79	99.799	AL 5-2
47	0.1357080E+04	1222.0	98.687+-	0.066	0.79	98.625	AL 5-2
48	0.1325416E+04	961.0	96.423+-	0.085	0.79	96.351	C 5-1
49	0.1293701E+04	3277.0	94.154+-	0.028	0.87	94.090	C 4-1
50	0.1224959E+04	8088.0	89.231+-	0.014	0.87	89.295	C 3-1
51	0.1157138E+04	2023.0	84.367+-	0.043	0.88	84.295	AU 8-7
52	0.1099255E+04	1972.0	80.212+-	0.044	0.88	80.2	AUKB2, 77.9KB1
53	0.1067244E+04	7825.0	77.911+-	0.016	0.88	77.9	PT KB2
54	0.1031121E+04	15001.0	75.313+-	0.018	0.86	75.256	C2-1, 75.7PT
55	0.9744950E+03	1371.0	71.238+-	0.117	0.86	???????	
56	0.9406420E+03	14143.0	68.799+-	0.019	0.86	68.804	AUKR1
57	0.9143370E+03	15763.0	66.903+-	0.023	0.86	66.832	PTKR1, AUK
58	0.8998640E+03	11575.0	65.859+-	0.030	0.86	66.005	AL3-2, PTKR
59	0.7855690E+03	3393.0	57.606+-	0.052	0.86	57.563	AU8-8
60	0.5567890E+03	417.0	41.028+-	0.091	0.74	41.117	O 7-2
61	0.5362160E+03	536.0	39.534+-	0.072	0.74	39.513	AL 6-3
62	0.4547480E+03	295.0	33.609+-	0.121	0.74	33.586	O 4-2

During the cascade process in the Au atom a muon which captured on a Au atom at a highly excited state de-excited to the 1s ground state with emission of several " circular " ($\Delta n=-1, \Delta l=-1$) X rays. We were able to observe this cascade process by correlating peaks in the Master Energy Tables with known μAu energies. An example of the results is in the tables below :

<u>Transition</u>	<u>Energy [45,46]</u> (keV)		<u>Observed Energy</u> (keV)	<u>Area</u> (events)
9K _{17/2} - 8J _{15/2}	57.513			
		--->	57.606	3393.
9K _{15/2} - 8J _{13/2}	57.606			
8J _{15/2} - 8I _{13/2}	83.880			
		--->	84.367	2023.
8J _{13/2} - 8I _{11/2}	84.081			
7I _{13/2} - 6H _{11/2}	130.452			
		--->	130.382	14327.
7I _{11/2} - 6H _{9/2}	130.961			
6H _{11/2} - 5G _{9/2}	216.226		216.224	12454.
6H _{9/2} - 5G _{7/2}	217.701		217.707	11324.
5G _{9/2} - 4G _{7/2}	400.093		400.090	8557.
5G _{7/2} - 4F _{5/2}	405.591		405.595	6765.

The energy of the other circular transitions(4--> 3 $\approx 890\text{keV}$, 3-->2 $\approx 2400\text{keV}$, 2-->1 $\approx 5700\text{keV}$ [45]) is outside of the energy region scanned by the detectors (Ge A,B,C detector range up to 500 keV).

After a muon has reached the 1s ground state of the μAu atom, the muon may be absorbed by the Au nucleus ($Z=79$), which can leave the nucleus in an excited state. Deexcitation then occurs with the emission of one or more neutrons followed by γ ray emission from Pt ($Z=78$). Since nuclear γ rays are also related to the muon diffusion process, we have a great deal of interest in them as well. We list observed γ rays below from a Master Energy Table for Detector B:

<u>Isotope</u>	<u>Nominal Energy [46]</u> (kev)	<u>Determined Energy</u> (kev)	<u>Area</u> (events)
^{196}Pt	521.400	521.310	2805.
^{194}Pt	482.860	483.008	877.
^{196}Pt	432.000	432.215	414.
^{196}Pt	420.900	419.574	310.
^{196}Pt	393.500	393.415	1838.
^{196}Pt	355.650	355.695	13375.
^{196}Pt	346.740	346.775	11952.
^{196}Pt	332.900	332.899	5357.
^{194}Pt	328.450	328.392	3491.
^{196}Pt	326.200	326.184	2151.
^{194}Pt	300.740	300.663	668.
^{194}Pt	293.540	293.405	814.

IV 2. Applications for Techniques of Data Analysis

A. Simplest Examples Correlated in Our Experiment

Before one can make a meaningful comparison between a theoretical velocity distribution and the observed time distribution, the theoretical model will have to be modified to include the (non-zero) time resolution effects in the detectors.

First, we investigated the resolution function for each detector. The data which we get from the detectors are subject to observation errors, i.e. due to the uncertainty in the measurements, a variable whose true time is t may be observed at some different value t' . Because of the uncertainties inherent in the measuring systems one can even observe events where ideally there should be none, e.g., at negative times.

A function $\Delta(t, t')$ which describes the distribution of the measurable quantity t' for a given true value t is defined as the measured resolution for variable t . According to a general rule if the true probability density function (PDF) is $f(t; \lambda)$, the probability density function for t' is given by [18] [19] [43]

$$(IV-2) \quad F(t'; \lambda) = \int_{-\infty}^{\infty} f(t; \lambda) \Delta(t, t') dt$$

In eq. (IV-2) the true variable t is integrated over and replaced by the observable t' . In most cases, the theoretical distribution $f(t, \lambda)$ is "smeared out" by the experimental resolution function

into its observation function $F(t)$. If the experiments were performed with detectors such that the effective resolution function $\Delta(t,t')$ could be represented by a delta function $\delta(t,t')$, the integral (IV-2) would give a PDF the same as the original theoretical function. So integral (IV-2) becomes

$$(IV-3) \quad F(t';\lambda) = \int_{-\infty}^{\infty} f(t;\lambda) \delta(t,t') dt \\ = f(t;\lambda)$$

In most experiments, it is reasonable to assume that repeated measurements with a detector on the value t would lead to observations t' which are normally distributed about t . Hence, the resolution function of the detectors can be taken as

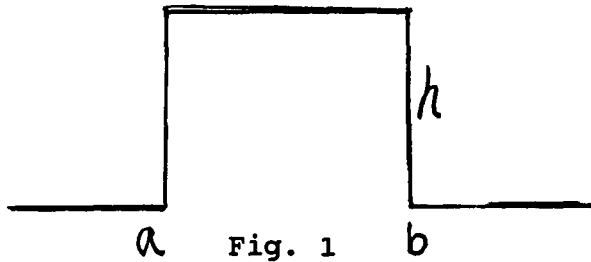
$$(IV-4) \quad \Delta(t,t') = 1/\sqrt{2\pi} * \exp(-(t'-t)^2/2\sigma^2)$$

where the standard deviation σ measures the experimental uncertainty (2.35σ is called the full width at half-maximum)

In many cases it is not possible to perform the integration (IV-2) algebraically. A numerical procedure, such as the Monte Carlo method, then has to be used

Because of the importance of the resolution transform (IV-2) with regard to the normal distribution in experiments, we study some very simple examples to help understand the effects of resolution of detectors on observed curves.

EXAMPLE I Suppose the theoretical function $g(t)$ is uniform in the interval a and b , as Fig. 1



$$g(t) = \begin{cases} h & a \leq t \leq b \\ 0 & t < a, t > b \end{cases}$$

$$= h\theta(t-a)\theta(b-t)$$

Using eq. (IV-2) and substituting $v=(t-t')/\sigma$, we obtain

$$(IV-5) \quad F(t') = h/\sqrt{2\pi} \int_a^b \exp[-(t-t')^2/2\sigma^2] dt$$

$$= h\{ \Psi [(b-t')/\sigma] - \Psi [(a-t')/\sigma] \}$$

Here, the function Ψ is defined as follows

$$(IV-6) \quad \Psi(t) = 1/\sqrt{2\pi} \int_{-\infty}^t \exp[-v^2/2\sigma^2] dv$$

We can calculate the function $f(t')$ numerically, The feature of $f(t')$ is shown in fig 2.

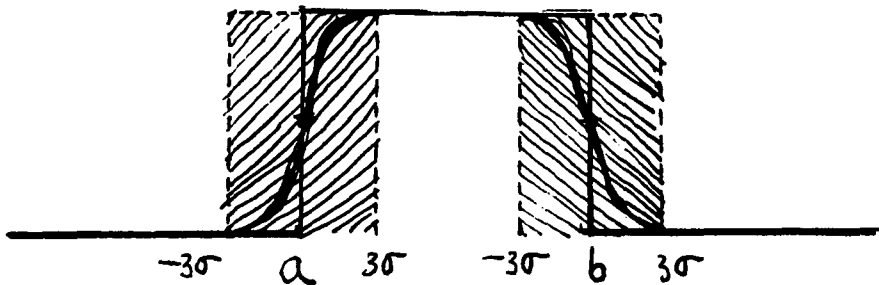


Fig.2

It is interesting to note that the theoretical function $f(t)$ was different from the experiment only at the leading edge ($\approx 3\sigma$) and the back edge ($\approx 3\sigma$). We divide the observation curve (Fig. 2.) into parts I,II,III. In regions I and III the observational curve was " smeared out " from the original curve. Region II is nearly unchanged. When $t'=b$, from eq.(IV-5), we obtain

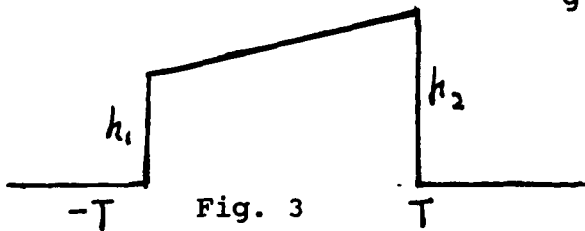
$$(IV-7) \quad F(b)=h\{ \Psi (0) - \Psi [(a-b)/\sigma] \}$$

Here $\Psi (0)=1/2$, $\Psi [(a-b)/\sigma]=0$, if $\| (a-b)/\sigma \| \geq 3$, So

$$(IV-8) \quad F(b)=h/2.$$

When $t'=a$, $f(a)=h/2$ as well. Therefore, we are able to determine the starting point t_a and stop point t_b from the "smeared out" region I and III .

EXAMPLE II Suppose the theoretical function $g(t)$ is linear in the interval $-T$ and T , as Fig.3



$$g(t)=\begin{cases} at + b & -T \leq t \leq T \\ 0 & t < -T, t > T \end{cases}$$

$$=(at + b)\theta(t+T)\theta(T-t) \quad (IV-9)$$

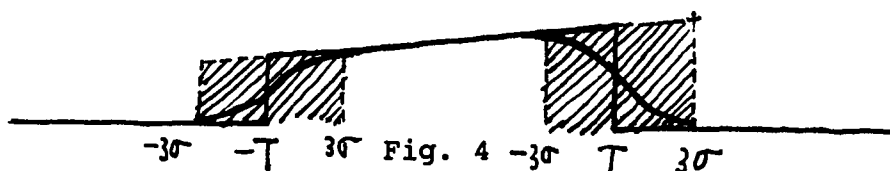
Using eq.(IV-2), (IV-4) and substituting $v=(t-t')/\sigma$, we obtain

$$(IV-10) \quad \begin{aligned} F(t') &= \int_{-\infty}^{\infty} g(t) \Delta(t-t') dt \\ &= \int_{-T}^T (at'+b)/\sigma \sqrt{2\pi} \{ \exp[-(t-t')^2/2\sigma^2] \} dt \\ &= (at'+b) \{ \Psi [(t'+T)/\sigma] - \Psi [(t'-T)/\sigma] \} \\ &\quad + \sigma a \int v/\sqrt{2\pi} \{ \exp[-v^2/2] \} dv \end{aligned}$$

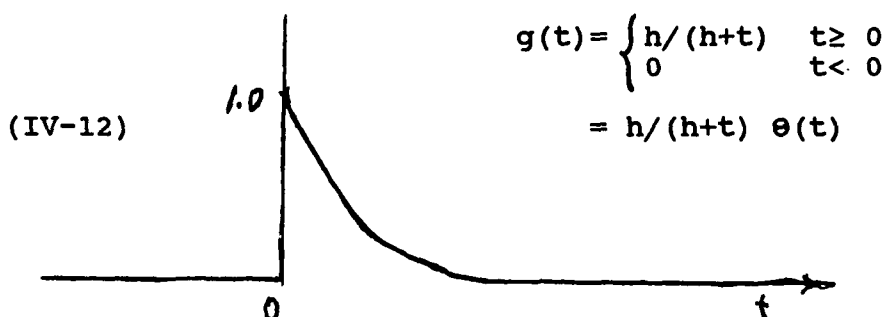
the second term vanished because of the odd function $[v \exp(v^2/2)]$,
So

$$(IV-11) \quad F(t') = (at' + b) \{ \Psi [(t'+T)/\sigma] - \Psi [(t'-T)/\sigma] \}$$

We are able to calculate the eq.(IV-11) numerically. The feature of $F(t')$ is as in Fig 4.



EXAMPLE III Suppose the original function $g(t)$ is a decreasing function of t in the interval $0 \rightarrow \infty$, as Fig 5.



$$g(t) = \begin{cases} h/(h+t) & t \geq 0 \\ 0 & t < 0 \end{cases} \\ = h/(h+t) \theta(t)$$

Fig. 5

In this case $g(t)$ differs from the cases which we have discussed before. In the preceding cases we can separate variables from the eq.(IV-2), and thus easily get eq.(IV-6) and eq.(IV-11). Now we cannot apply the separated variables method for eq.(IV-2).

According to eq. (IV-2), We obtain

$$(IV-13) \quad F(t) = \int_{-\infty}^{\infty} h / [(h+t') \sigma \sqrt{2\pi} \exp[-(t-t')^2 / 2\sigma^2]] dt' \\ = \int_0^{\infty} h / [(h+t') \sigma \sqrt{2\pi} \exp[-(t-t')^2 / 2\sigma^2]] dt'$$

There are two ways to solve eq. (IV-13) in principle:

- (i) directly evaluate the integral (IV-13) numerically;
(ii) Monte Carlo method [see appendix A] .

In most cases method(i) does not work. We have not found a universal way to integrate eq.(IV-2) numerically. On other hand, method (ii) always works. But it is unacceptably inefficient for certain common integrands and requires various analytic formulae in addition to the integrand. It is fortunate that in this specific case in which the $g(t)$ is a decreasing function that we can work out the integral (IV-13) : either method(i) or method (ii).

Consider the integral

$$(IV-14) \quad I = \int_{-\infty}^{\infty} \int_{-\infty}^{\infty} \int_{-\infty}^{\infty} f(x, y, z) dx dy dz$$

The Monte Carlo method is based on the following equation :

$$(IV-15) \quad \frac{\text{vol}(s)}{N} \sum_{i=1}^n f(x_i) = \int_s f + - \sqrt{\frac{\text{var}(f)}{N}}$$

where each x_i is a randomly and uniformly chosen point in the spaces. The 'plus-or-minus' term in (IV-15) is a one standard deviation error estimate for the integral (IV-15). and

$$(IV-16) \quad \text{var}(f) = \langle f^2 \rangle - \langle f \rangle^2 \quad [34]$$

Here the angle brackets denote taking the arithmetic mean over the N sample points, [34]

$$(IV-17) \quad \langle f \rangle = \frac{1}{N} \sum_{i=1}^n f(x_i) \quad \langle f^2 \rangle = \frac{1}{N} \sum_{i=1}^n f^2(x_i).$$

We applied numerical integration of eq.(IV-13) using Simpson's 3/8 rule : [34]

$$\int_{x_1}^{x_4} f(x) dx = h [3/8 * f_1 + 9/8 * f_2 + 9/8 * f_3 + 3/8 * f_4]$$

We fixed the parameters $h=10$ and $\sigma=2$ in the decreasing function (IV-12), and chose the increment $\Delta t=1$ from $t=-10$ to $t=10$, $\Delta t=5$ from $t=10$ to 105. Therefore we obtained the numerical values of integral (IV-13) which was calculated numerically both by method(i) and method (ii) as shown in table I. [36]

TABLE I

* H =10. $\sigma=2.$, MONTE CARLO EVENTS=100k

t	THEORETICAL $g(t)=h/(h+t)$	INTEGRATION $\epsilon < 10^{-5}$	MONTE CARLO	$\sigma(t)$
-0.100000E+02	0.000000E+00	0.276661E-06	0.000000E+00	
-0.900000E+01	0.000000E+00	0.326868E-05	0.000000E+00	
-0.800000E+01	0.000000E+00	0.303524E-04	0.198658E-04	0.140472E-04
-0.700000E+01	0.000000E+00	0.221920E-03	0.230680E-03	0.470873E-04
-0.600000E+01	0.000000E+00	0.128057E-02	0.123982E-02	0.108740E-03
-0.500000E+01	0.000000E+00	0.585007E-02	0.608215E-02	0.238930E-03
-0.400000E+01	0.000000E+00	0.212473E-01	0.219893E-01	0.453605E-03
-0.300000E+01	0.000000E+00	0.617044E-01	0.621045E-01	0.757485E-03
-0.200000E+01	0.000000E+00	0.144438E+00	0.144258E+00	0.114592E-02
-0.100000E+01	0.000000E+00	0.275603E+00	0.275427E+00	0.156837E-02
0.000000E+00	0.100000E+01	0.435528E+00	0.435682E+00	0.447214E-03
0.100000E+01	0.909091E+00	0.582649E+00	0.582661E+00	0.314286E-03
0.200000E+01	0.833333E+00	0.679346E+00	0.679133E+00	0.239449E-03
0.300000E+01	0.769231E+00	0.715062E+00	0.715084E+00	0.193698E-03
0.400000E+01	0.714286E+00	0.705125E+00	0.705028E+00	0.163215E-03
0.500000E+01	0.666667E+00	0.672546E+00	0.672266E+00	0.141002E-03
0.600000E+01	0.625000E+00	0.633828E+00	0.633966E+00	0.123603E-03
0.700000E+01	0.588235E+00	0.596496E+00	0.596634E+00	0.109426E-03
0.800000E+01	0.555556E+00	0.562653E+00	0.562604E+00	0.976070E-04
0.900000E+01	0.526316E+00	0.532350E+00	0.532338E+00	0.875977E-04
0.100000E+02	0.500000E+00	0.505157E+00	0.505134E+00	0.790569E-04
0.150000E+02	0.400000E+00	0.402611E+00	0.402614E+00	0.505964E-04
0.200000E+02	0.333333E+00	0.334835E+00	0.334824E+00	0.351364E-04
0.250000E+02	0.285714E+00	0.286657E+00	0.286657E+00	0.258145E-04
0.300000E+02	0.250000E+00	0.250630E+00	0.250628E+00	0.197642E-04
0.350000E+02	0.222222E+00	0.222664E+00	0.222665E+00	0.156162E-04
0.400000E+02	0.200000E+00	0.200322E+00	0.200323E+00	0.126491E-04
0.450000E+02	0.181818E+00	0.182060E+00	0.182060E+00	0.104538E-04
0.500000E+02	0.166667E+00	0.166853E+00	0.166853E+00	0.878410E-05
0.550000E+02	0.153846E+00	0.153992E+00	0.153994E+00	0.748468E-05
0.600000E+02	0.142857E+00	0.142974E+00	0.142975E+00	0.645363E-05
0.650000E+02	0.133333E+00	0.133428E+00	0.133428E+00	0.562183E-05
0.700000E+02	0.125000E+00	0.125078E+00	0.125078E+00	0.494106E-05
0.750000E+02	0.117647E+00	0.117712E+00	0.117712E+00	0.437686E-05
0.800000E+02	0.111111E+00	0.111166E+00	0.111167E+00	0.390405E-05
0.850000E+02	0.105263E+00	0.105310E+00	0.105309E+00	0.350391E-05
0.900000E+02	0.100000E+00	0.100040E+00	0.100040E+00	0.316228E-05
0.950000E+02	0.952381E-01	0.952727E-01	0.952721E-01	0.286828E-05
0.100000E+03	0.909091E-01	0.909392E-01	0.909398E-01	0.261345E-05
0.105000E+03	0.869565E-01	0.869329E-01	0.869824E-01	0.239114E-05

We compare the values in Table I calculated by Monte Carlo and numerical integration with the theoretical values. The data obtained by three independent ways are consistent with each other.

We see from the table that points which in the original curve (IV-12) were smeared out were not only at the edge of the original curve but also at the inside area of the original curve. This effect did not exist in the examples I and II. It is somewhat unexpected. For instance , at point $t=8$ (which is 4σ away from the edge), the theoretical value = 0.555556 and Monte Carlo value = 0.562604. The 'smeared out' effect is 0.007 about 1.5% . This effect of smearing in the integration (IV-13) was caused by the nonlinear feature of the original function in the neighborhood of points t from -4σ to 4σ . The reasons are as following :

As is well known, the Gaussian distribution function $\Delta(t-t';\sigma)$ is a short range function, i.e. Its significant value only ranges from -4σ to 4σ about the center. But it is also symmetric from right to left. So if the theoretical function is locally nonlinear at t from $t-4\sigma$ to $t+4\sigma$, the value of integral (IV-13) at t will be smeared out. i.e. the contributions to integral (IV-13) from the right and left sides do not balance. This is sketched in Fig. 6 .

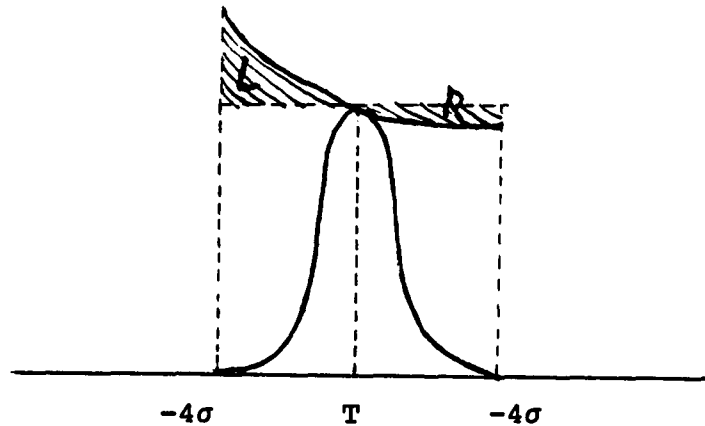


Fig. 6

In Fig. 6 ,the shaded area L corresponds to the contribution from the left side and the shaded area R corresponds to the contribution from the right side. The dotted lines indicate the shaded regions of a Gaussian probability distribution which corresponds to probability $(1-10^{-4})$.

Thus, if the original function at the neighborhood of t is linear, the smeared out feature will not exist. That is why in examples I and II, the area II was not smeared out at all. We can discover this from table (I) also. For instance , we obtained the value $F =0.833333$ at $t=8-3\sigma$, $F =0.416666$ at $t=8+3\sigma$, and $F =0.555556$ at $t=8$. Therefore the difference at the right side is $\Delta Fr=0.277777$, and at the left side is $\Delta Fl=0.138889$; so $\Delta Fr > \Delta Fl$ and the value at this point will be smeared out by integral

(IV-13). On the other hand, we easily find in the table (I) that for large t , the original function satisfies the local linear condition and no smearing occurs.

We conclude, as discussed in the preceding three examples, that the effects of a Gaussian resolution of detectors on the observed curves presented two aspects. First, it is strongly affected by both edges of the original distribution function. This is sketched in Fig. 7;

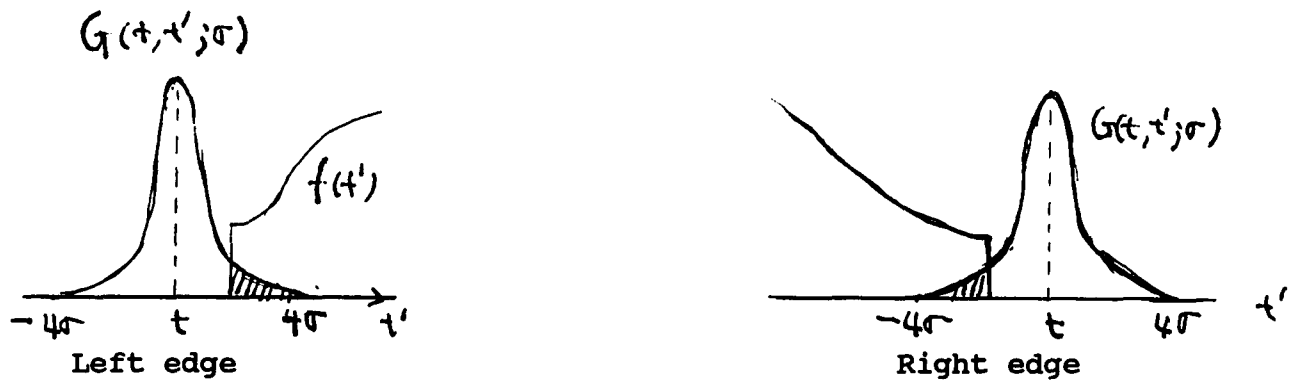


Fig. 7

Second, it is also strongly dependent on the feature of the inside part of the original distribution function. As a result of smearing effects, the observed curve may be quite different from the original one in certain cases (especially as σ was quite large). Hence, it is very important that the eq. (IV-2) be solved before a meaningful comparison with experimental data can be made. Besides this, each detector individually imposed 'smeared out' effects on the observed curves. For precise measurements, this case also needed to be dealt with carefully.

IV. 2

B. The Measurement of the Mean Life τ of Muon in Au and Determination of the Precise " Zero" Time of the Decay Curve

(A) DECAY SIGNALS

When the solid gold target was placed in the muon beam, muons were captured by Au nuclei. In the first step of the capture process the muon removed one or more electrons from the Au muonic atom by the Auger effect. After emission of the X rays in the cascade process, the muon reaches the 1S state of the μAu atom. Most muons were absorbed by the Au nucleus ($Z=79$), often leaving the nucleus in an excited state. Then deexcitation occurred with the emission of one or more neutrons followed by γ -ray emission from Pt ($Z=78$). Such nuclear γ rays are not emitted promptly (as are muonic X rays). Instead, they are emitted with a time delay which corresponds to the muon mean life in gold. A series of nuclear γ rays emitted by Pt ($Z=78$) has been observed with the Ge detectors. The prominent nuclear γ rays from Pt are listed in Table II as follows [45] [46].

TABLE II
(NUCLEAR GAMMA RAYS FROM PT)

Isotope	Energy (kev)	Yield[39]
¹⁹⁶ Pt	355.65	0.36 +- 0.05
¹⁹⁶ Pt	332.90	0.11 +- 0.02
¹⁹⁴ Pt	328.45	≈ 0.10

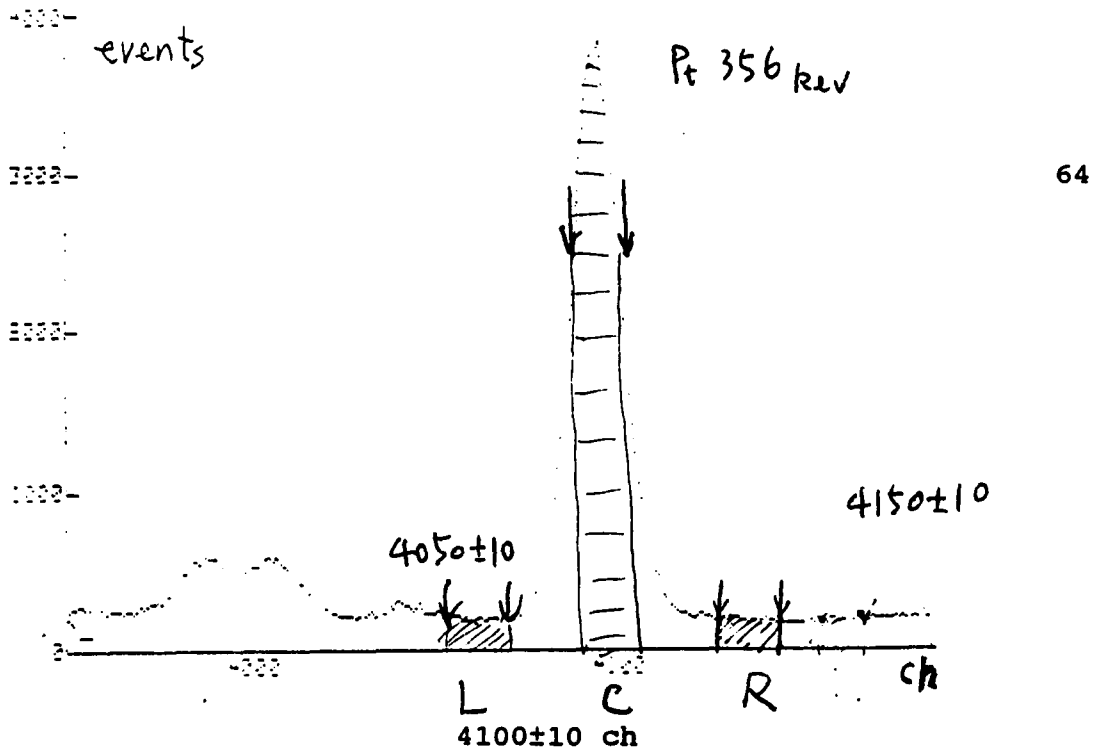
We focus attention on the photopeak ¹⁹⁶Pt³⁵⁶ which has a large yield. In the experiment of the summer 1987 we had four Ge detectors (A. B. C. JR) and in the summer of 1988 five Ge detectors (A. B. C. JR. TU).

In the analysis of the data sets, we were primarily concerned with the time distribution of the decay events. To obtain the time distributions we generated two-dimensional energy versus time spectra on magnetic tape. The analyzed time region included times from 900ns up to 1.3μs. and data sets from tapes with identical conditions (solid Au target) were summed. The intensities of the peaks of interest were determined as a function of time(or of energy). We projected the two-dimensional data sets on the energy axis or time axis. Thus, we obtain the intensities of the peaks as

a function of time or as a function of energy. Fig. 8 is a sketch of the peak of ^{196}Pt 356keV as a function of energy for Ge detector A. The raw data for the ^{196}Pt (356keV) γ ray must be corrected for events which were background. The center of the Pt 356 γ ray photopeak was located at channel 4100 (in the Ge detector A, see Fig.8). We chose the energy width from -10 ch to 10 ch at the center(for high signal/noise ratio), then projected the spectra on time axis. We then got the raw data from Pt 356 photopeak(as shown in Fig. 9). Therefore we obtained the backgrounds which contributed to a plateau on the right side and left side of the Pt 356 photopeak(see Fig. 8).

The raw signal and the backgrounds from the left side and from the right side are shown respectively in Fig. 9 ,Fig. 10 and Fig.11.

In order to extract the time distribution of the decay events, we subtracted the average of the background on the right side and on the left side from the raw signal, and eventually we obtain the net signal which was the time evolution of the $^{196}\text{Pt}^{356}$ peak.



64

Fig.8 -- The time distribution of photopeak Pt 356. In Fig.8, the shaded region C was the contribution of γ ray Pt 356 (signal/noise > 10), The shaded regions L and R were the background contribution respectively from the left plateau and the right plateau in the spectrum of Pt 356.

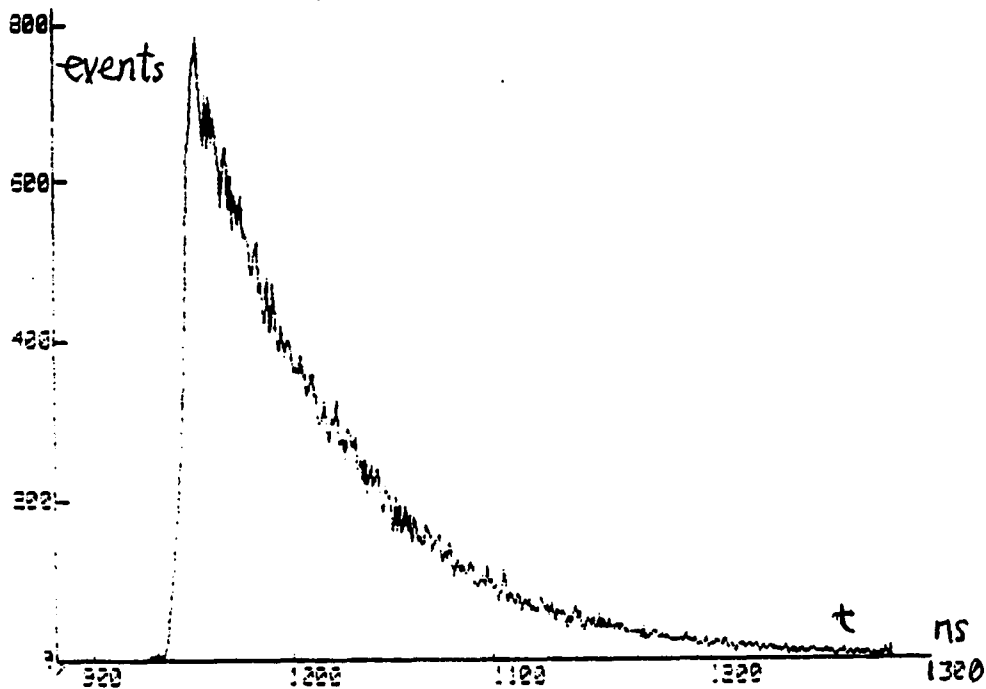


Fig.9 -- The time distribution of photopeak Pt 356.

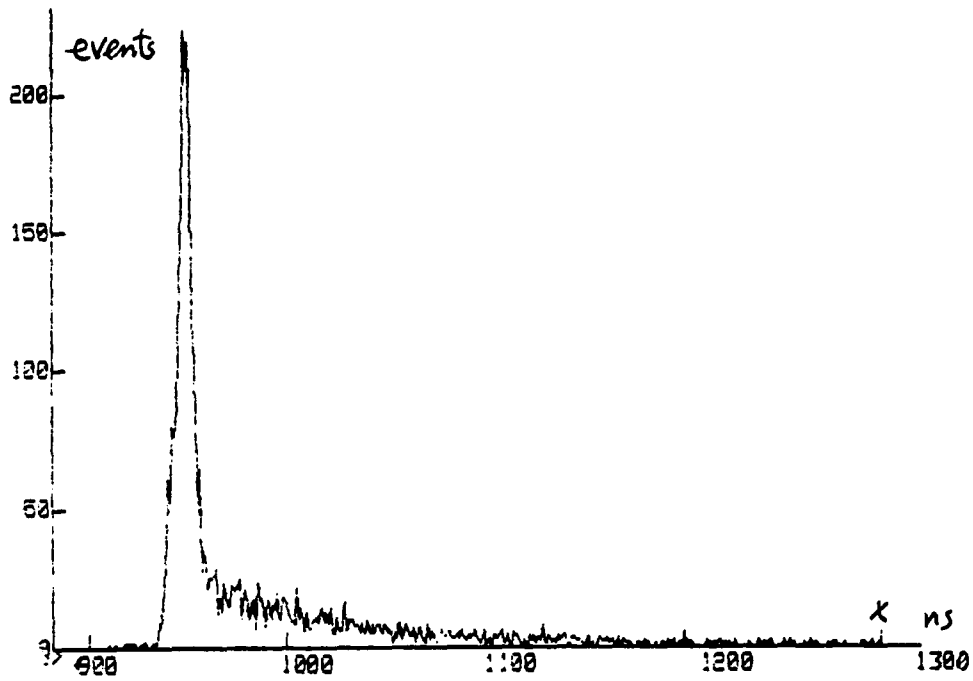


Fig. 10 -- The time distribution of background from a right plateau of Pt 356

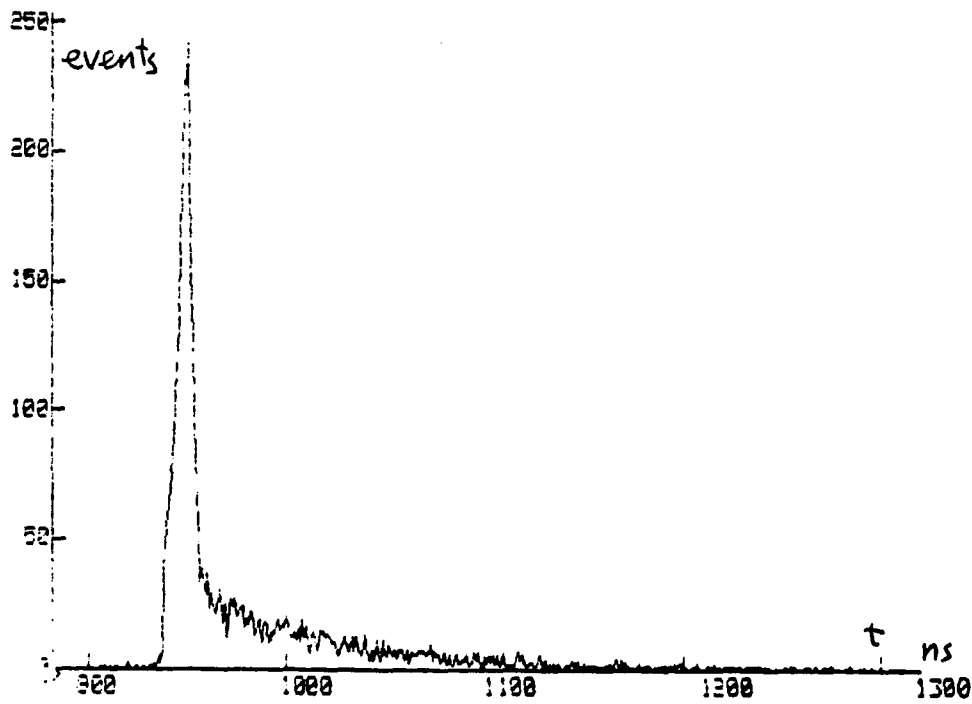


Fig. 11 -- The time distribution of background from a left plateau of Pt 356.

(B) ANALYSIS OF DECAY EVENTS

As is well known, the decay events obey the exponential rule.

The distribution function is given below:

$$(IV-18) \quad g(t) = \begin{cases} A \exp(-t/\tau) & t \geq 0 \\ 0 & t < 0 \end{cases}$$

$$= A \exp(-t/\tau) \theta(t).$$

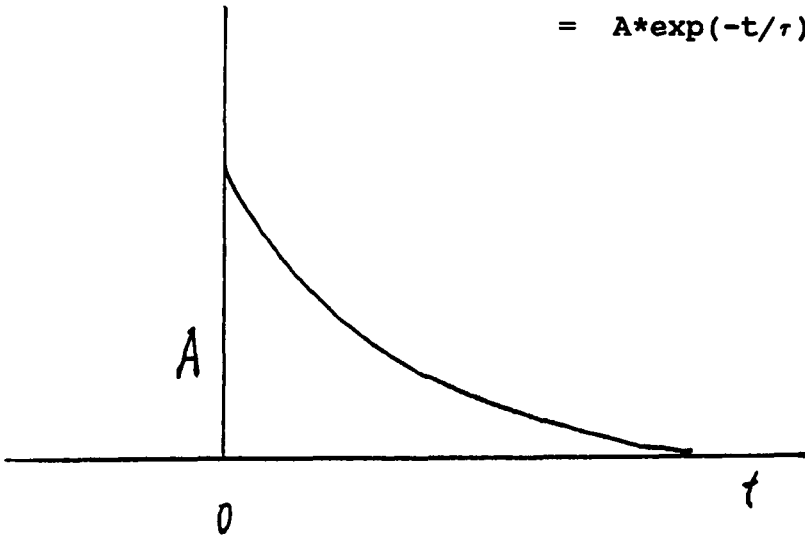


Fig. 12

According to eq.(IV-2), the observed curve will transform as

$$(IV-19) \quad F(t') = \int_{-\infty}^{\infty} g(t) \Delta(t-t') dt \\ = A \exp(-t/\tau) * \exp\{[(t-t')/\sigma]^2/2\} / \sigma \sqrt{2\pi}$$

The time resolution functions of the Ge detectors used in the experiment were Gaussian distributions tested before experiment. The parameters σ corresponding to the Ge detectors were determined. Generally, the σ is a function of energy. As the energy decreases, the deviation $\sigma(E)$ increases. This is shown in table III

TABLE III

		Detector A				
Photopeak	Energy(kev)	FWHM(ns)	Error(ns)	$\sigma(E)$ (ns)	error(ns)	
Au 6-4	621.7	7.90	0.29	3.36	0.12	
Au 14-5	615.5	8.17	0.27	3.48	0.12	
Au 5-4	405.6	8.95	0.20	3.81	0.09	
Au 5-4	400.1	9.00	0.19	3.83	0.08	
Al 2-1	346.7	9.84	0.23	4.19	0.09	
Au 6-5	217.7	12.35	0.16	5.26	0.07	
Au 10-7	182.8	14.06	0.26	5.98	0.11	
O 2-1	133.5	17.48	0.31	7.44	0.13	
N 2-1	102.4	21.78	0.42	9.26	0.18	

We apply the separate variables method to the integral (IV-19). and rewrite the exponent

$$-t'/\tau - [(t-t')^2 / 2\sigma^2] = -t'/\tau + \sigma^2/2\tau^2 - 1/2\sigma^2 (t' - t + \sigma^2/\tau)^2$$

Substituting $u = (t - t' + \sigma^2/\tau)/\sigma$, we obtain

$$\begin{aligned} \text{(IV-20)} \quad F(t') &= A \exp(-t/\tau + \sigma^2/2\tau^2) \int_{-\infty}^{t-\sigma^2/\tau} \exp(-u^2/2) / \sqrt{2\pi} du \\ &= A \exp(-t/\tau + \sigma^2/2\tau^2) \Psi(t/\sigma - \sigma/\tau) \end{aligned}$$

The original exponential distribution is shown in the Fig.12 and the observed distribution in Fig.13.

In the D area the $F(t')$ was smeared out (shown in Fig.13); in the other region the difference is a constant factor $\exp(\sigma^2/2\tau^2)$. It is interesting that except for the D region, $F(t')$ is still an exponential function with the same rate $1/\tau$ and amplitude A.

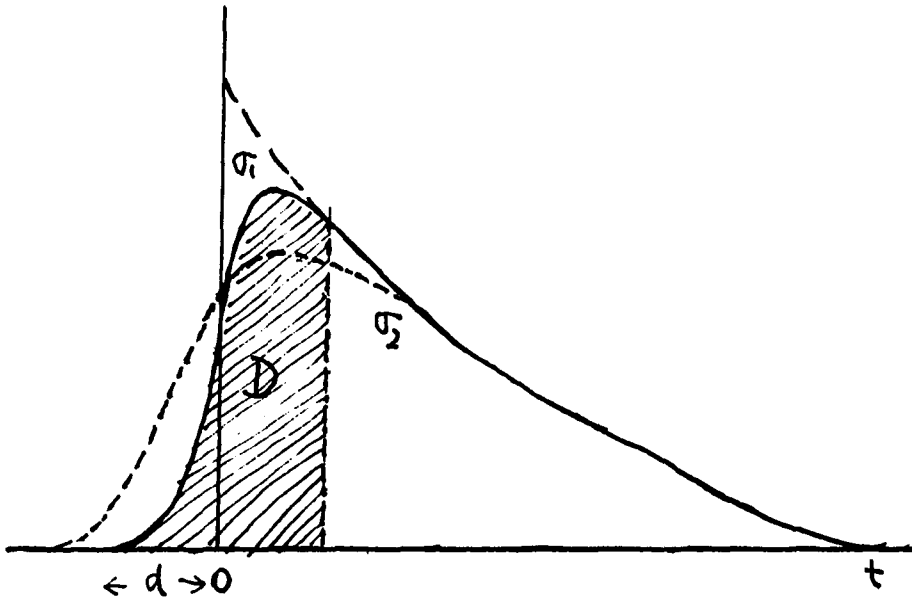


Fig. 13

In Fig.13, the shaded region is determined by the standard deviation σ_1 of detector; the dotted line corresponds to the standard deviation σ_2 ($\sigma_2 \gg \sigma_1$)

IV. 2

(C) method (I): Cut the leading edge from the observed curve

If we cut the D region away from the observed curve, the remaining part of the observed curve will be approximately exponential with two parameters (mean life τ and amplitude A). Then we use the least-squares method to fit the curve. The parameters τ and A will be determined with the least $\chi^2/(n-m)$, where n is the number of degrees of freedom, and m is the number of the parameters.

The numerical minimization procedures are quite complicated in general. 'MINUIT' of the CERN Program Library is a flexible minimization program, and is available for use

on the VAX 11/750. So we directly applied 'MINUIT' to fit the exponential mean life time curve which has the leading edge cut from the eq.(IV-20).

Setting the cut on eq.(IV-20), we obtained

$$(IV-21) \quad F_k(t) = e^{-\alpha_k(t-T_0) + \beta_k}, \quad k = A, B, C, JR$$

and minimized

$$(IV-22) \quad \text{Min}(\chi^2) = \sum_{i=1}^n (y_i^{(k)} - f_i)^2 / \sigma_i^2$$

where $y_i^{(k)}$ is one of the data sets obtained with the k-th detector (A, B, C, JR), The estimates of parameters α^k, β^k , by using the cut leading edge method with respect to each detector, were done by using "MINUIT". For the different time cuts, the estimates of parameters α^k, β^k are listed in tables as below.

TABLE IV

	DETECTOR A				
$t_i - T_0$	5 ns	10 ns	20 ns	30 ns	40 ns
α (ns^{-1})	0.14358E-1	0.14400E-1	0.14403E-1	0.14443E-1	0.14500E-1
error	0.76295E-4	0.78570E-4	0.85519E-4	0.94710E-4	0.86239E-4
β	6.5151	6.5208	6.5213	6.5274	6.5386
error	0.73092E-2	0.78733E-2	0.91673E-2	0.11058E-1	0.63141E-2
τ (ns)	69.65	69.44	69.43	69.24	68.97
error	0.30	0.37	0.42	0.45	0.45
χ^2	328.0	320.0	308.0	296.0	277.0
ν	323	318	308	298	288
χ^2_ν	1.01	1.01	1.00	0.99	0.96
$F(\chi^2_\alpha; \nu)$	0.59	0.54	0.51	0.48	0.33

* In the table, T_0 is relative zero time, t_i the starting point, $t_i - T_0$ the time cuts, $\nu = n - m$, $\chi^2_\nu = \chi^2 / \nu$, and $F(\chi^2_\alpha; \nu)$ is percentage points of chi-square distribution .

TABLE V

DETECTOR :B

$t_i - T_0$	5 ns	10 ns	20 ns	30 ns	40 ns
α (ns ⁻¹)	0.14350E-1	0.14400E-1	0.14412E-1	0.14404E-1	0.14348E-1
error	0.75764E-4	0.79617E-4	0.87179E-4	0.95400E-4	0.10392E-3
β	6.6902	6.6965	6.6979	6.6967	6.6885
error	0.69298E-2	0.74991E-2	0.88002E-2	0.10347E-1	0.12101E-1
τ (ns)	69.68	69.44	69.386	69.425	69.696
error	0.36	0.38	0.42	0.45	0.48
χ^2	287.0	278.0	274.0	266.0	253.0
ν	281	276	266	256	246
χ^2_ν	1.02	1.01	1.03	1.04	1.03
$F(\chi^2_\alpha; \nu)$	0.61	0.55	0.65	0.68	0.65

* In the table, T_0 is relative zero time, t_i the starting point, $t_i - T_0$ the time cuts, $\nu = n - m$, $\chi^2_\nu = \chi^2 / \nu$, and $F(\chi^2_\alpha; \nu)$ is percentage points of chi-square distribution .

TABLE VI

DETECTOR : C

$t_i - T_0$	5 ns	10 ns	20 ns	30 ns	40 ns
α (ns^{-1})	0.14242E-1	0.14338E-1	0.14413E-1	0.14397E-1	0.14411E-1
error	0.84619E-4	0.89121E-4	0.97418E-4	0.10636E-3	0.11625E-3
β	6.3869	6.3991	6.4089	6.4069	6.4087
error	0.78268E-2	0.84566E-2	0.99011E-2	0.11588E-1	0.13545E-1
τ (ns)	70.214	69.744	69.381	69.459	69.391
error	0.41	0.42	0.46	0.50	0.55
χ^2	343.0	328.0	318.0	302.0	283.0
ν	307	302	292	282	272
χ^2_ν	1.12	1.09	1.09	1.07	1.04
$F(\chi^2_\alpha; \nu)$	0.92	0.85	0.86	0.80	0.69

* In the table, T_0 is relative zero time, t_i the starting point, $t_i - T_0$ the time cuts, $\nu = n - m$, $\chi^2_\nu = \chi^2 / \nu$, and $F(\chi^2_\alpha; \nu)$ is percentage points of chi-square distribution .

TABLE VII

DETECTOR :JR

$t_i - T_0$	5 ns	10 ns	20 ns	30 ns	40 ns
α (ns^{-1})	0.14256E-1	0.14196E-1	0.14327E-1	0.14280E-1	0.14314E-1
error	0.72178E-4	0.68817E-4	0.78792E-4	0.86878E-1	0.95695E-4
β	6.9344	6.9272	6.9434	6.9371	6.9418
error	0.66284E-2	0.61250E-2	0.78048E-2	0.92083E-2	0.10860E-1
τ (ns)	70.145	70.44	69.79	70.02	69.86
error	0.35	0.34	0.37	0.41	0.48
χ^2	286.0	306.0	276.0	252.0	244.0
ν	283	278	268	258	248
χ^2_ν	1.01	1.10	1.03	0.98	0.98
$F(\chi^2_\alpha; \nu)$	0.56	0.88	0.65	0.41	0.44

* In the table, T_0 is relative zero time, t_i the starting point, $t_i - T_0$ the time cuts, $\nu = n - m$, $\chi^2_\nu = \chi^2 / \nu$, and $F(\chi^2_\alpha; \nu)$ is percentage points of chi-square distribution .

The optimum parameters were estimated respectively for each detector, and are listed in table VIII

TABLE VIII

detector	A	B	C	JR
τ (ns)	69.444	69.444	69.744	70.146
σ (ns)	0.379	0.383	0.433	0.355
χ^2	320.0	278.0	328.0	286.0
ν	318	276	302	283
χ^2_ν	1.01	1.01	1.09	1.01
$F(\chi^2; \nu)$	0.54	0.55	0.85	0.56

We thus obtained four independent mean life measurements τ_i and σ_i from Ge detectors (A,B,C,JR). According to the maximum - likelihood method, the estimate for the mean-life τ becomes, in this situation,

$$(IV-23) \quad \bar{\tau} = \frac{\sum_{i=1}^4 \tau_i / \sigma_i^2}{\sum_{i=1}^4 1 / \sigma_i^2} ,$$

namely the weighted mean of the observations.

The measurements are weighted in inverse proportion to the square of their errors and the variance on this estimate $\bar{\sigma}$ is given by

$$(IV-24) \quad \bar{\sigma} = \frac{1}{\sqrt{\sum_{i=1}^4 1/\sigma_i^2}}$$

Finally, substituting the τ_i and σ_i from table VIII into eq. (IV-23) and (IV-24), the muon mean-life in gold was obtained through the cut leading edge method:

$$(IV-25) \quad \tau = 69.709 \pm 0.192 \text{ (ns)}$$

IV. 2

(C) Method (II) : Full Curve Fitting Method

Method (I) is defective in two respects. First, if the resolution σ of the detector is large, the D region will dominate all observed curves, as shown in Fig.13, with dotted curve for σ_2 . In this case method (I) is obviously faulty. Second, when the leading edge of the observed curve is removed, the starting point on the curve will be missed and the information on the resolution (σ) of the detector also will be lost. Hence, for the above reasons, method (II) (full curve fitting) was developed.

We assume that the each Ge detector's Gaussian variance was respectively σ^k and rewrite the eq.(IV-20) [19]

$$(IV-26) \quad F(t; \sigma^k, \tau^k, A^k) = A^k \exp(-t/\tau + (\sigma^k)^2/2(\tau^k)^2) \Psi(t/\sigma^k - \sigma^k/\tau)$$

and

$$k = A, B, C, JR, TU$$

The tabulated function $\psi(x)$ is known as the cumulative normal standard distribution[18] [19] [43].

There are several ways to approximate the cumulative normal standard distribution $\Psi(x)$. Some polynomial and rational approximations based on C.Hastings, Jr.'s approximation for digital computers are provided as follows [34] [36]:

$$(IV-27) \quad \Psi(x) = 1/\sqrt{2\pi} \int_{-\infty}^x e^{-t^2/2} dt$$

$$1. \Psi(x) = 1 - \frac{\exp(-x^2/2)}{\sqrt{2\pi}} (a_1 t + a_2 t^2 + a_3 t^3) + \epsilon(x), \quad t = \frac{1}{1+px}$$

For $0 \leq x < \infty$, $\|\epsilon(x)\| < 1 \times 10^{-5}$.

$$p=0.33267 \quad a_1=0.4361846 \quad a_2=-0.1201676 \quad a_3=0.9372980$$

$$2. \Psi(x) = 1 - \frac{\exp(-x^2/2)}{\sqrt{2\pi}} (b_1 t + b_2 t^2 + b_3 t^3 + b_4 t^4 + b_5 t^5) + \epsilon(x),$$

For $0 \leq x < \infty$, $\|\epsilon(x)\| < 7.5 \times 10^{-8}$. $t = \frac{1}{1+px}$

$$p=0.2316419 \quad b_1=0.319381530 \quad b_2=-0.356563782 \quad b_3=1.781477937$$

$$b_4=-1.821255978 \quad b_5=1.330274429$$

$$3. \Psi(x) = 1 - \frac{1}{2} (1 + c_1 t + c_2 t^2 + c_3 t^3 + c_4 t^4) + \epsilon(x),$$

For $0 \leq x < \infty$, $\|\epsilon(x)\| < 2.5 \times 10^{-4}$. $t = \frac{1}{1+px}$

$$c_1=0.0196854 \quad c_2=0.115194 \quad c_3=0.000344 \quad c_4=0.019527$$

4.

$$\Psi(x) = \frac{1}{2} + \frac{1}{2} (1 - e^{-2x^2/\pi}) \frac{1}{2} \quad x > 0$$

$$1 - \frac{\frac{1}{2}}{(4+x^2) - x} (2\pi)^{-1/2} e^{-x^2/2} \quad x > 1.4$$

We choose expression 2 to meet our purposes because of the small $\| \epsilon(x) \|$.

In the summer of 1988 there were five Ge detectors on the experiment. We therefore obtained nine data sets of muon life time measurement in gold. Now we applied "MUNUIT" directly to eq.(IV-26) for minimization of χ^2 . The parameters fitted by "MINUIT" for the varied detectors are displayed in Table IX.

TABLE IX

***** Data from the run of 1988 Summer *****										
	τ (ns)	error	A	error	σ	error	χ^2	ν	χ^2_ν	$F(\chi^2_\alpha; \nu)$
Det.A	69.571	0.5087	465.6	4.3	4.39	0.14	336	311	1.08	0.842
Det.B	69.393	0.4999	377.2	3.7	4.50	0.58	418	354	1.18	0.989
Det.C	69.111	0.8158	200.3	1.5	4.85	0.35	296	282	1.04	0.728
Det.Jr	69.361	0.3884	703.6	5.1	4.50	0.31	342	343	0.99	0.495
Det.Tu	69.035	0.7496	223.4	3.1	4.80	0.32	359	283	1.26	0.998
***** Data from the run of 1987 Summer *****										
Det.A	69.738	0.357	770.5	6.0	4.57	0.16	365	360	1.01	0.583
Det.B	69.411	0.366	844.7	6.0	4.81	0.17	334	317	1.05	0.755
Det.C	70.119	0.407	668.5	5.0	4.49	0.21	397	329	1.20	0.994
Det.Jr	70.370	0.330	1093.2	6.0	4.18	0.04	323	307	1.05	0.746

In the TABLE IX the $\nu, \chi^2_\nu, F(\chi^2_\alpha; \nu)$'s definitions are the same as given before.

The nine independent mean - times τ_i and errors σ_i from table IX are compared with the values of τ_i and σ_i obtained by method (I). The values of pairs of τ_i and σ_i are absolutely consistent. Furthermore, we mixed τ_i and σ_i with weight w_i based on maximum - likelihood theory (the same way as indicated on previous page). The muon mean life in Au obtained by the full curve fitting method was as follows :

$$(IV-28) \quad \tau = 69.716 \pm 0.144 \text{ (ns)}$$

Comparing this mean-life (IV-28) to that from method (I), we see that the results are consistent with each other. The σ of method (II) is smaller than that for method (I). An advantage to method (II) is that the resolution σ of detectors at Pt energy was also determined at same time.

The resolution σ of the detector A at an energy 346.7 keV level, from table III (by using FITA program which was provided from the collaborators in PSI), is

$$\sigma(347 \text{ keV }) = 4.19 \pm 0.09 \text{ (ns)}$$

Compared to the fitting resolution σ of the detector A from table IX

$$\sigma(356 \text{ keV }) = 4.39 \pm 0.14 \text{ (ns)}$$

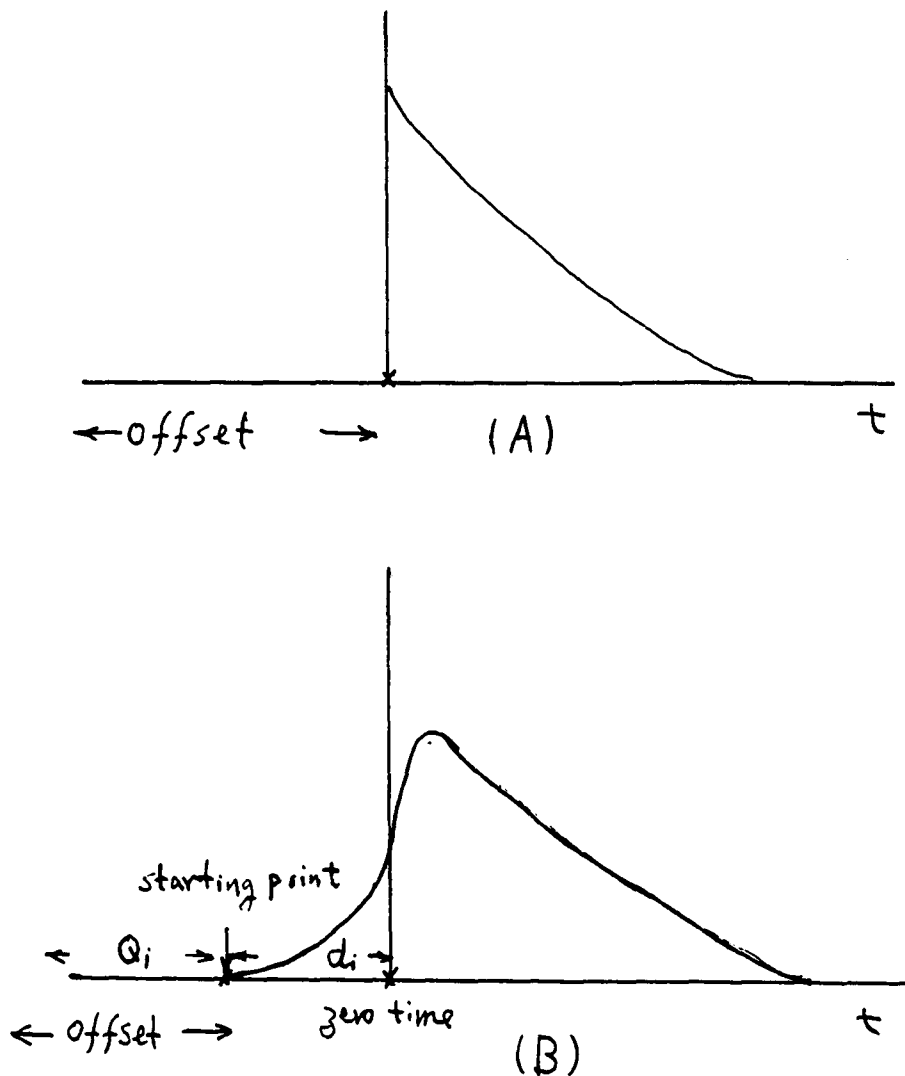
These are consistent and are good enough for fitting the detector resolution as well.

IV. 2

(D) "Starting Point", "Zero time" and "Offset Time" about Observed Curve.

We now concentrate on the "starting time", "zero time" and "offset time". It was important for precise time measurements that systematic time errors could be avoided. It is interesting that the method (II) affords a way to determine these parameters.

We redraw the Fig. 12 and Fig. 13 below.



For the theoretical curve (A), we compare Fig. 12 and 13. The starting point of time and the zero time are the same. But in the observed curve (B) they were in fact separated by a distance d . We can measure d by using method (II).

Suppose the distance d_i for the i -th detector was

$$(IV-29) \quad d_i = c_i \sigma_i + \sigma_i^2 / r_i ,$$

where $i = A, B, C, JR$ or TU and d_i was assumed a constant for each detector. It is clear that if

$$t \geq Q_i \quad Q_i = \text{offset}$$

then

$$(IV-30) \quad F(t; \sigma_i, r_i, A_i) \geq 0.$$

where $F(t; \sigma_i, r_i, A_i)$ was defined with eg. (IV-26) .

Using condition (IV-30), we fitted the c_i , d_i and Q_i by using " MINUIT ". The results are listed in Table X.

TABLE X

*****	The data from the summer of 1988					*****
Detector	A	B	C	JR	TU	
c (ns)	3.433	3.922	3.044	3.887	3.496	
error (ns)	0.121	0.049	0.194	0.035	0.075	
d (ns)	15.35	17.94	15.08	17.78	17.12	
error (ns)	0.716	2.285	1.421	1.215	1.175	
T0 ^(R) (ns)	15.358	17.944	15.100	17.780	17.110	
error (ns)	0.716	2.285	1.421	1.215	1.175	
Q _i (ns)	185.93	182.9	186.34	213.82	174.0	
error (ns)	0.032	0.011	0.12	0.026	0.07	
T0 ^(a) (ns)	201.0	200.8	201.4	231.5	191.1	
error (ns)	0.72	2.29	1.43	1.22	1.18	

TABLE XI

***** The data from the summer of 1987 *****

Detector	A	B	C	JR
c (ns)	2.875	4.070	3.650	3.310
error (ns)	0.087	0.126	0.158	0.027
d (ns)	13.46	19.89	16.67	14.08
error (ns)	0.61	0.92	1.04	0.17
T0 ^(R) (ns)	13.46	19.89	16.67	14.08
error (ns)	0.61	0.92	1.04	0.17
Q _i (ns)	37.00	79.83	68.63	91.41
error (ns)	0.013	0.028	0.059	0.054
T0 ^(a) (ns)	50.46	99.89	83.67	105.08
error (ns)	0.61	0.92	1.04	0.18

On other hand, from eq.(IV-20) we acquired knowledge of the value of $F(t)$ at the zero time,

$$\begin{aligned}
 \text{(IV-31)} \quad F^{(k)}(t=0) &= A^{(k)} e^{(\sigma^k)^2/2(\tau^k)^2} \Psi(0) \\
 &= \frac{A^k}{2} e^{(\sigma^k)^2/2(\tau^k)^2}
 \end{aligned}$$

where $k = A, B, C, JR$, or A, B, C, JR, TU . Thus zero time was the inverse function of eq.(IV-31)

$$\text{(IV-32)} \quad (t=0) = F^{-1} \left(\frac{A^k}{2} e^{(\sigma^k)^2/2(\tau^k)^2} \right)$$

where $k = A, B, C, JR$, or A, B, C, JR, TU .

By substituting $A^{(k)}$, $\tau^{(k)}$, $\sigma^{(k)}$ from table IX (A) into eq. (IV-31), the values of $F^{(k)}(t="0")$ were obtained and are listed in Table XII :

TABLE XII

***** The data comes from the summer of 1988 *****					
Detectors	A	B	C	JR	TU
$F(t="0")$	233.26	188.99	100.40	352.54	111.97
***** The data comes from the summer of 1987 *****					
Detectors	A	B	C	JR	
$F(t="0")$	386.45	423.37	334.94	547.57	

Generally it was difficult to solve the eq.(IV-32). But since we already had the data sets from the detectors, we could scan the data sets and thus find out zero time approximately for each detector. In this way, all " zero times " with respect to an individual detector were found. We list each valid part of data sets below :

***** The data comes from the summer of 1987 *****

T ^(a)	F("0")	error	
47.000000210	.500000	22.967369	
48.000000297	.000000	25.903667	
49.000000409	.000000	29.308702	Detector A
50.000000436	.500000	29.521179	
51.000000456	.000000	30.265491	
52.000000584	.500000	30.323259	

From the data from detector A, T^(a) (absolute zero time) $\approx 49 \pm 0.4$ ns was found for F("0") = 386.45. As a result it agrees with the predicted value of 50.46 (ns) ± 0.61 (ns) in Table XI.

T ^(a)	F("0")	error	
97.000000305	.500000	27.865749	
98.000000376	.500000	29.351320	
99.000000390	.500000	30.651264	
100.000000509	.500000	31.312937	Detector B
101.000000612	.000000	31.527765	
102.000000712	.000000	31.176914	

From the data from detector B, T^(a) (absolute zero time) $\approx 99 \pm 0.45$ ns was found for F("0") = 423.37. As a result it agrees with the predicted value of 99.89 (ns) ± 0.92 (ns) in Table XI.

T ^(a)	F("0")	error	
81.000000138.000000		21.587032	
82.000000178.500000		23.355942	
83.000000216.000000		24.899799	
84.000000305.000000		27.694765	Detector C
85.000000374.000000		28.879059	
86.000000435.000000		29.816103	

From the data from detector C, T^(a) (absolute zero time) $\approx 84 \pm 0.34$ ns was found for F("0") = 334.94. As a result it agrees with the predicted value of 83.67 (ns) ± 1.04 (ns) in Table XI.

T ^(a)	F("0")	error	
102.000000309.000000		31.192947	
103.000000328.500000		33.637775	
104.000000473.500000		36.338684	Detector JR
105.000000546.500000		37.463314	
106.000000665.500000		37.503334	
107.000000738.500000		37.141621	

From the data from detector JR, T^(a) (absolute zero time) $\approx 105 \pm 0.38$ ns was found for F("0") = 547.57. As a result it agrees with the predicted value of 105.08 (ns) ± 0.18 (ns) in Table XI.

***** The data comes from the summer of 1988 *****

T ^(a)	F("0")	error	
198.000000129.000000		21.470911	
199.000000196.500000		23.097618	
200.000000199.500000		24.300205	DEtector A
201.000000278.000000		25.922962	
202.000000315.000000		25.592968	
203.000000327.500000		24.829418	

From the data from detector A, T^(a) (absolute zero time) $\approx 201 \pm 0.43$ ns was found for F("0") = 233.26. As a result it agrees with the predicted value of 201.0 (ns) ± 0.72 (ns) in Table X.

$T^{(a)}$	F("0")	error	
197.000000	90.000000	18.384777	
198.000000	99.000000	20.371550	
199.000000	128.000000	21.540659	
200.000000	198.500000	23.653753	Detector B
201.000000	202.500000	22.748627	
202.000000	256.500000	22.792543	

From the data from detector B, $T^{(a)}$ (absolute zero time) \approx 200 ± 0.62 ns was found for $F("0") = 188.99$. As a result it agrees with the predicted value of 200.8 (ns) \pm 2.29 (ns) in Table X.

$T^{(a)}$	F("0")	error	
198.000000	53.500000	15.572412	
199.000000	60.000000	16.492422	
200.000000	83.000000	17.175564	
201.000000	104.500000	18.096962	Detector C
202.000000	125.000000	18.083141	
203.000000	152.000000	18.439089	

From the data from detector C, $T^{(a)}$ (absolute zero time) \approx 201 ± 0.85 ns was found for $F("0") = 100.40$. As a result it agrees with the predicted value of 201.4 (ns) \pm 1.43 (ns) in Table X.

$T^{(a)}$	F("0")	error	
228.000000	207.500000	24.052027	
229.000000	271.000000	26.589472	
230.000000	333.500000	28.679260	Detector JR
231.000000	332.500000	29.248932	
232.000000	402.000000	30.822069	
233.000000	470.000000	30.331501	

From the data from detector JR, $T^{(a)}$ (absolute zero time) \approx 231 ± 0.83 ns was found for $F("0") = 352.54$. As a result it agrees with the predicted value of 231.5 (ns) \pm 1.22 (ns) in Table X.

T ^(a)	F("0")	error	
187.000000	32.000000	12.649111	
188.000000	73.000000	14.317822	
189.000000	74.500000	17.073372	Detector TU
190.000000	133.500000	17.449928	
191.000000	127.500000	19.039433	
192.000000	121.000000	18.193405	

From the data from detector TU, T^(a) (absolute zero time) \approx
 191 \pm 1.5 ns was found for F("0") = 111.97. As a result it agrees
 with the predicted value of 191.1 (ns) \pm 1.18 (ns) in Table X.

IV 2-C.

(E) The Systematic Error Correction for the Time Distributions of the μ P Atom Diffusion in H₂ Gas.

According to Method (II) above, we obtained the "effective zero time" for each detector from Table X. Because there was a 300 ns offset in the control file for the run of the summer of 1988 and a 900 ns offset in the control file for the run of the summer of 1987, we should add 300 ns and 900 ns respectively to the values in Table X. We list them in the Table XIII.

TABLE XIII

***** The data come from the summer of 1987 *****

DETECTOR	EFFECTIVE	ZERO	TIME
A	950.46 ±	0.61	(ns)
B	999.89 ±	0.92	(ns)
C	983.67 ±	1.04	(ns)
JR	1005.8 ±	0.18	(ns)

***** The data come from the summer of 1988 *****

A	501.0 ±	0.72	(ns)
B	500.8 ±	2.29	(ns)
C	501.4 ±	1.43	(ns)
JR	531.5 ±	1.22	(ns)
TU	491.1 ±	1.18	(ns)

Production of the data sets of transfer related time distributions depended on the determination of the effective zero times. Previously, we determined the zero times in this way: (1) find a prompt peak near the Pt 356 peak; (2) fit the time peak using the program FITA[41]; (3) then define the centroid of the peak as the effective zero time.

We list them below in Table X IV :

TABLE X IV

***** The data come from the summer of 1988 *****

DETECTOR	EFFECTIVE	ZERO TIME
	(compression factor 8)	(conversion factor 8 to 1)
A	63 ch	504 ns
B	63 ch	504 ns
C	63 ch	504 ns
JR	67 ch	536 ns
TU	62 ch	496 ns

Comparing these values with those in Table X III, we get the systematic error for each detector and list them below in Table X V :

TABLE X V

***** The data come from the summer of 1988 *****

DETECTOR	SYSTEMATIC ERRORS
A	3.00 ± 0.72 (ns)
B	3.02 ± 2.29 (ns)
C	2.60 ± 1.43 (ns)
JR	4.50 ± 1.22 (ns)
TU	4.90 ± 1.18 (ns)

Thus, we are able to correct the systematic errors for each detector by shifting the data set of time distributions a time interval Δt from the Table X V with respect to each detector. Since the time distributions from the five Ge detectors have already been combined into a single time distribution for each condition, we simply combine the systematic error of all five detectors, with the following result for the mean error :

$$\overline{\text{error}} = 3.4 \text{ ns}$$

We then shift the data set of the single time distribution backwards a time $\Delta t = 3.4 \text{ ns}$. Since in our experiment time ranges up to $2 \mu\text{s}$, the 3.4 ns systematic error does not play a significant role.

IV 2-c.

(F) Response Function [18] [19] [43]

We should rewrite eq.(IV-20) as follows :

$$(IV-33) \quad F(t; \sigma^k, \tau^k, A^k) = A^k \exp(-t/\tau^k + (\sigma^k/\tau^k)^2/2) \Psi(t/\sigma^k - \sigma^k/\tau^k)$$

Then integrating from $-\infty$ to ∞

$$(IV-34) \quad \int_{-\infty}^{\infty} F(t; \sigma^k, \tau^k, A^k) dt = A^k \tau^k$$

Thus the normalized response function was obtained :

$$(IV-35) \quad F^{(n)} = 1/\tau^k \exp(-t/\tau^k + (\sigma^k/\tau^k)^2/2) \Psi(t/\sigma^k - \sigma^k/\tau^k)$$

This function (IV-35) has been defined as a response function of a Ge detector for transfer events from the the 356 keV Pt γ -ray from the Au foil. Among the k-th detectors, in the measurement of each of the parameters τ^k and σ^k , there were only slight differences in the experiment. For instance, when we ran the experiment in the summer of 1987, the parameters below were obtained :

Detector	A	B	C	JR
σ^k	4.57 ± 0.16	4.81 ± 0.17	4.49 ± 0.2	4.18 ± 0.4
τ^k	69.74 ± 0.36	69.41 ± 0.37	70.12 ± 0.41	70.37 ± 0.33

For this reason, we ignore the differences of σ^k and τ^k among the detectors' measurements. As a result, we omit the superscript (k) and rewrite the unique response function as follows:

$$(IV-36) \quad F^{(res)}(t, \sigma, \tau) = 1/\tau \exp(-t/\tau + (\sigma/\tau)^2/2) \Psi(t/\sigma - \sigma/\tau)$$

where σ and τ are averages of $\sigma^{(k)}$ and $\tau^{(k)}$ with weights in inverse proportion to the square of the errors. We have already

obtained the $\tau = 69.716$ (ns) from eq. (IV-28). Thus, the average standard deviation is :

$$\sigma = \frac{\sum_{k=1}^9 \frac{\sigma^{(k)}}{(\text{error})^2}}{\sum_{k=1}^9 \frac{1}{(\text{error})^2}} = 4.267 \text{ (ns)}$$

Substituting σ and τ into eq. (IV-36), the unique response function is obtained for this experiment.

The purposes of this experiment are to measure the time distribution of μd or μp atoms which initially form in the gas H_2 or D_2 and then drift to the Au foils.

There are some general properties about the response function that are shown below (See Fig.14):

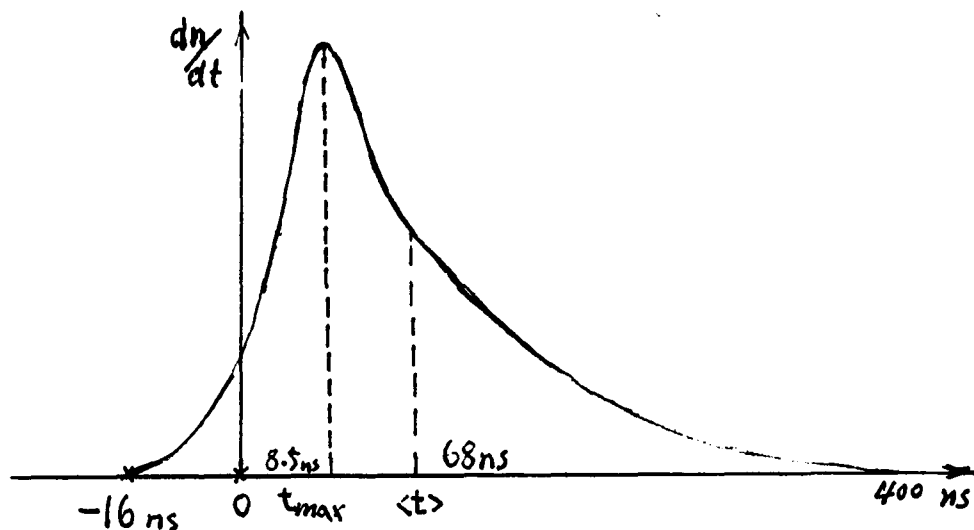


Fig. 14

The average time

$$\langle t \rangle = \int_{-\infty}^{\infty} t F^{\text{res}}(t) dt = 68.199 \text{ (ns)}$$

and the maximum probability was located at

$$T_{\max} = 8.57802.$$

Further,

$$F^{\text{res}}(t=t_{\max}) = 0.0123812$$

and at zero time the value of the response function was

$$F^{\text{res}}(t=0) = 0.00718$$

The response time t_r ranged significantly from -16ns to 400ns, due to $F^{\text{res}}(-16) = 1.25 \cdot 10^{-6}$, $F^{\text{res}}(400\text{ns}) = 4.6 \cdot 10^{-5}$ and the integral from -16ns to 400ns gives

$$\int_{-16\text{ns}}^{400\text{ns}} F^{\text{res}} dt = 0.998$$

Finally below we plot the actual response function in this experiment :(see Fig. 15)

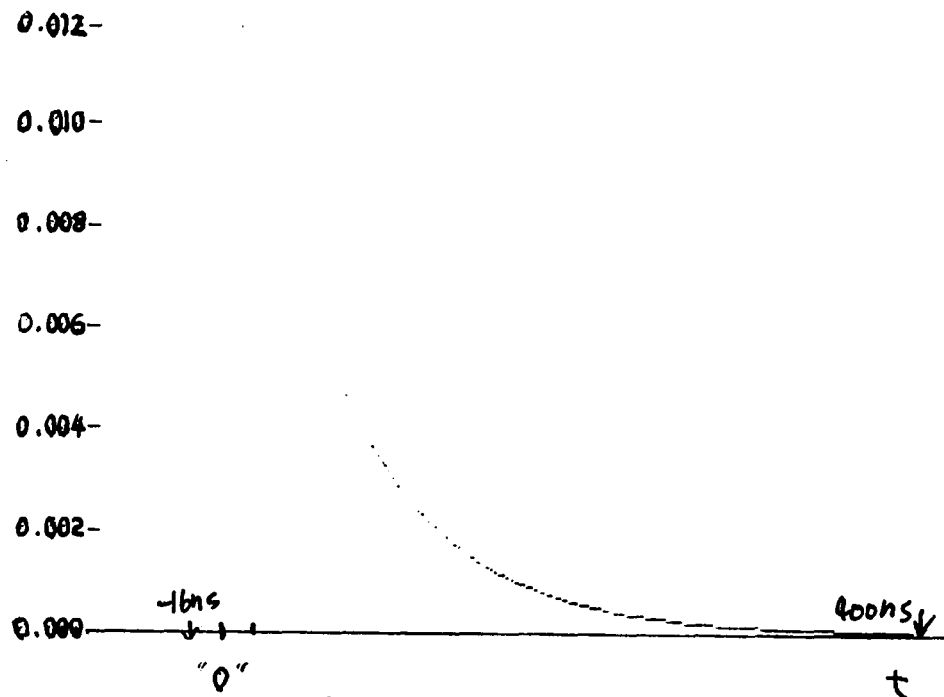


Fig. 15

IV 2.

(G) A use for the short mean life measurements of the Method (II)

In section IV.1 we investigated mean life measurements in the case where the mean life time τ was much greater than the time resolution σ of a Ge detector. If the mean life time which is to be measured is much shorter than the time resolution σ of a Ge detector (see Fig.13 the dotted line), Method (II) provides a possible way to do this. We note that, when the mean life time τ is less than the time resolution σ of a detector, the shape of the observed curve will not be a simple exponential decay curve. However, the observed curve still contains the information of the mean life time. We can apply Method (II) to this case, and demonstrate it by a data set generated by the Monte Carlo method (see Appendix B for more details.)

In the following examples, we have assumed that (1) the mean life time was 2ns;(2) the Ge detector had the time FWHM 9.4 ns ($\sigma=4$ ns); and (3)the TDC was 0.054 ns per channel. We generated a data set with the 2×10^5 decay events that had 2 ns mean life time and was measured by a Ge detector with time FWHM 9.4 ns. We draw the data set below which was generated by the Monte Carlo Method : (See Fig. 16)

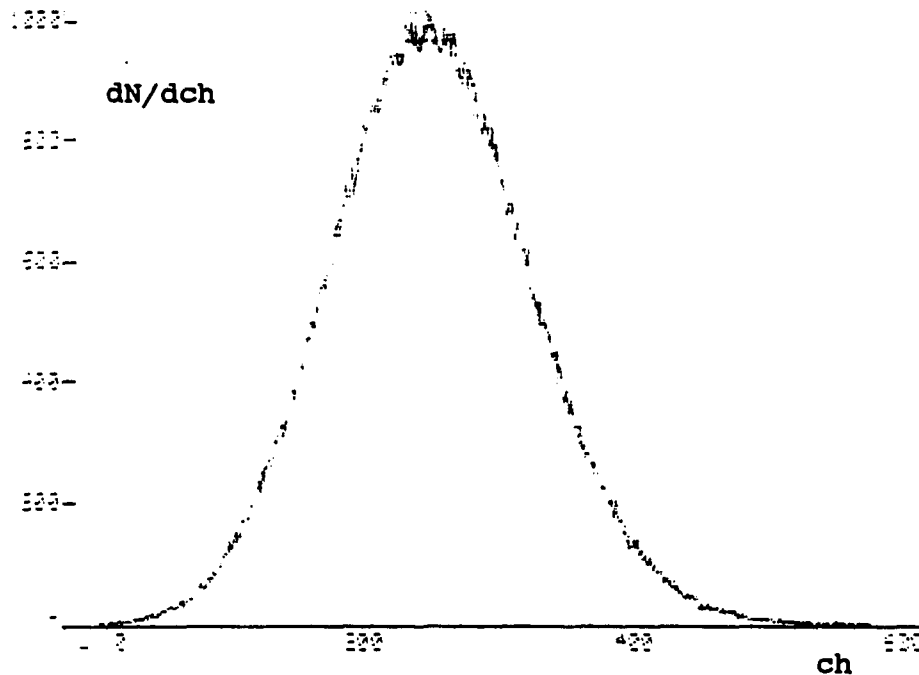


Fig. 16

In Fig. 16, the X--coordinate was the number of the channels, where each channel was 0.054 ns wide.

Now we directly apply Method (II) eq. (IV-26), to fit the curve generated by the Monte Carlo method. The parameters fitted by "Minuit" are displayed below :

<u>TDC 0.054 ns/ch</u>									
τ (ch)	error	A	error	σ (ch)	error	χ^2	ν	χ^2_ν	$F(\chi^2_\alpha; \nu)$
40.622	0.044	8.82	0.36	72.229	0.16	526	638	0.82	$4.5 \cdot 10^{-4}$

Converting the channel to ns, we obtain

$$(IV-37) \quad \begin{aligned} \tau &= 40.622 * 0.054 \text{ ch} = 2.198 \pm 0.003 \text{ ns} \\ \sigma &= 72.229 * 0.054 \text{ ch} = 3.90 \pm 0.008 \text{ ns} \end{aligned}$$

In comparison with the Monte Carlo method, the results are good. This agreement implies that Method (II) works well for the case in which the mean life time is much shorter than the time resolution σ of a Ge detector.

Secondly, we assumed that the mean life time τ and the resolution σ of the Ge detector are kept the same, but that the TDC is changed to 0.108 ns for each channel. The purpose of this option is to verify the validity of using Method (II).

As we did above, we first generate a data set with 2×10^5 decay events with mean life time 2 ns, 4 ns resolution of the Ge detector and TDC 0.108 ns/ch. We draw the data set below (See Fig. 17) :

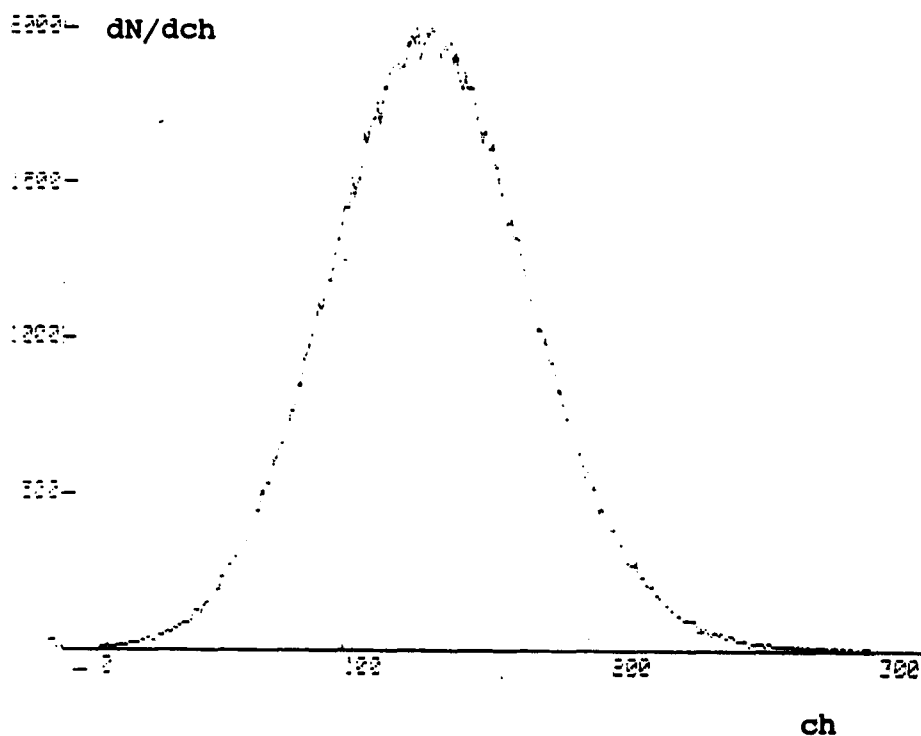


Fig. 17

In Fig. 17, the X--coordinate is the number of TDC channels and each channel is 0.108 ns.

Again we use Method (II) to fit the curve generated by Monte Carlo method. The parameters which are obtained are listed below:

TDC 0.108 ns/ch

r (ch)	error	A	error	σ (ch)	error	χ^2	ν	χ^2_ν	$F(\chi^2_\alpha; \nu)$
18.060	0.022	2.37	0.001	37.113	0.04	189	317	0.60	$1.2 \cdot 10^{-4}$

Converting the channel to ns, we obtain

$$r = 18.060 * 0.108 \text{ ch} = 1.951 \text{ ns}$$

and

$$\sigma = 37.113 * 0.108 \text{ ch} = 4.008 \text{ ns}$$

Finally

$$r = 1.951 \pm 0.002 \text{ ns}$$

$$\sigma = 4.008 \pm 0.004 \text{ ns}$$

Again for the same purpose, we change the TDC to 0.54 ns/ch. We represent the data set below which is obtained with the Monte Carlo method (See Fig. 18):

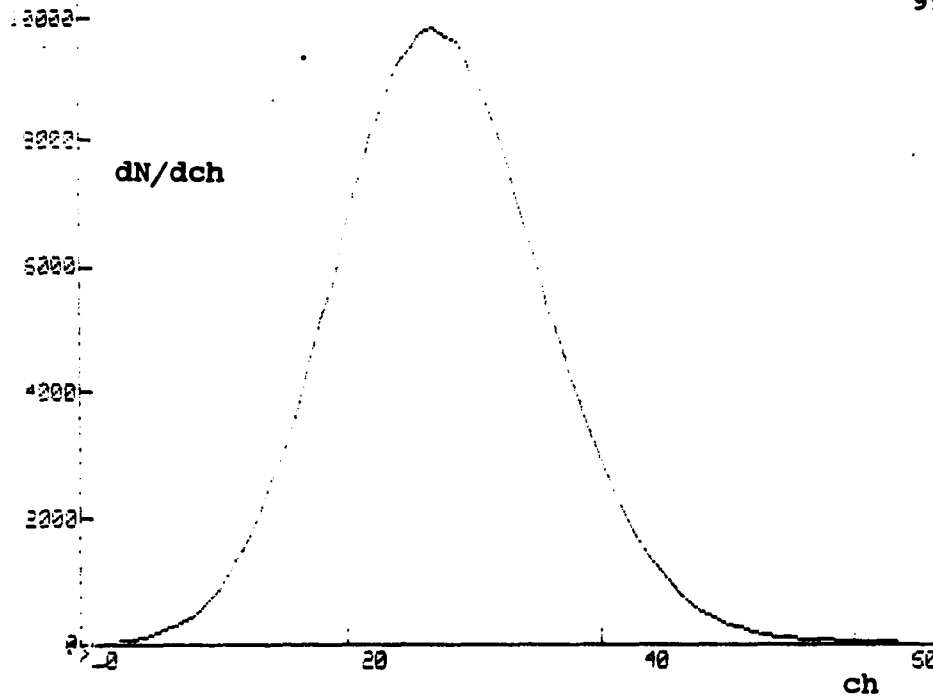


Fig. 18

In Fig. 18, the X--coordinate is the number of the TDC channels and each channel is 0.54 ns.

We then use Method (II) to fit the curve generated by the Monte Carlo method. The parameters which are obtained are listed below:

TDC 0.54 ns/ch

r (ch)	error	A	error	σ (ch)	error	χ^2	ν	χ^2_ν	$F(\chi^2_\alpha; \nu)$
3.5401	0.049	2.03	0.2	7.4729	0.002	34.2	60	0.57	$3.0 \cdot 10^{-3}$

Converting the channel to ns, we obtain

$$\tau = 3.5401 * 0.54 \text{ ch} = 1.912 \text{ ns}$$

and

$$\sigma = 7.4729 * 0.54 \text{ ch} = 4.035 \text{ ns}$$

Finally

$$\tau = 1.912 \pm 0.003 \text{ ns}$$

$$(IV-38) \quad \sigma = 4.008 \pm 0.001 \text{ ns}$$

Comparing (IV-37) and (IV-38) (parameters $\sigma=2 \text{ ns}$ and $\tau = 4 \text{ ns}$), it is clear that good fits are obtained for the $\tau < \sigma$ case by using method (II) . Thus, the reliability of method (II) for the shorter time measurement has been proved.

IV 2-C.

(G) Discussion of Results

We have thus obtained for μ^- lifetime in Au :

$$(IV-39) \quad \tau = 69.716 \pm 0.144 \text{ (ns)}$$

This value is in disagreement with the values quoted in the literature :

$$\tau = 72.77 \pm 0.47 \text{ (ns) [38]}$$

$$\tau = 74.3 \pm 1.5 \text{ (ns) [37]}$$

However, since in our experiment we did not set out to make a precision lifetime measurement, we consider our results to be adequate confirmation of the time scale used for the μp diffusion studies.

Chapter V

Experimental Data

V. 1 Data Analysis Routines

A. Consistency Checks of the Experimental Data

The first step was to check the consistency of the experimental data . At regular intervals, we performed routine checks of drifts of the energy and time spectra both on-line or off-line (See Fig. V-1). We chose the centroids of the $\mu\text{C2-1}$ and $\mu\text{F2-1}$ as monitor lines for the energy scale and determined the drifts of these lines between writing tapes. If there were significant electronic drifts between tapes, a degradation of the FWHM of the energy peaks would be observed when histograms were summed together. We continued checks on drifts of the electronics and insured that the magnitudes of these drifts were small enough to have negligible effect on the FWHM of the transfer peaks. However, if there were bad drifts of photopeaks in the spectra, then we could not sum their histograms together, and an additional ' off-line ' treatment was required.

NO.	CH	AREA	ENERGY ± ERROR	FWHM	NOMINAL ENERGY
1	0.4334339E+04	3021.0	510.954± 0.073	3.12	511.004 E+E-
2	0.3022730E+04	2389.0	355.680± 0.043	1.60	355.650 PT196
3	0.1868048E+04	4028.0	219.004± 0.056	1.56	218.903 F 6-1
4	0.1843807E+04	11619.0	216.135± 0.043	1.58	216.129 F 5-1
5	0.1800623E+04	18862.0	211.024± 0.030	1.56	211.028 F 4-1
6	0.1707387E+04	22860.0	199.988± 0.028	1.56	199.988 F 3-1
7	0.1441015E+04	104738.0	188.462± 0.012	1.59	188.463 F 2-1
8	0.8130830E+03	7070.0	94.148± 0.062	1.51	94.090 C 4-1
9	0.7718260E+03	11634.0	89.230± 0.042	1.51	89.295 C 3-1
10	0.6535340E+03	28791.0	75.288± 0.022	1.51	75.258 C 2-1
11	0.4203710E+03	1188.0	47.674± 0.136	1.42	47.716 F 5-2
12	0.3768120E+03	3463.0	42.519± 0.054	1.42	42.618 F 4-2

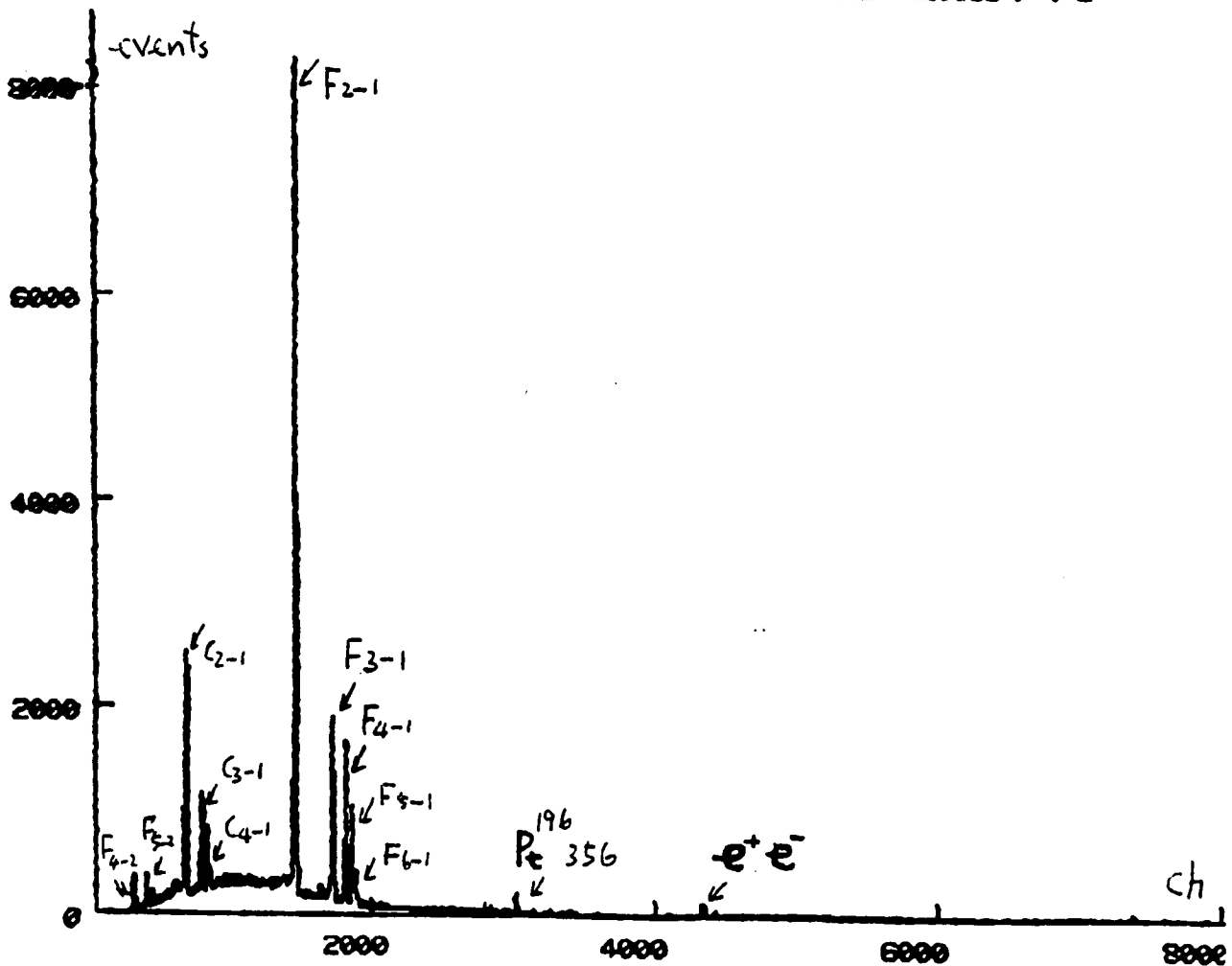


Fig. V-1

During the June 1988 run under the 750mbar condition, we observed significant electronic drifts of the Ge detectors (A, B, C), such that the photopeaks in the spectra of these detectors could not be summed together(See Table V-1).

Table V-1

<u>Tape</u>	<u>Detector</u>					
	A		B		C	
	Al2-1	FWHM	Al2-1	FWHM	Al2-1	FWHM
	(ch)		(ch)		(ch)	
244	3796.4	16.7	3678.4	15.6	3867.9	13.9
245	3793.5	14.4	3680.6	13.5	3846.3	14.4
246	3805.6	14.2	3700.2	15.6	3831.3	23.2
247	3818.1	18.2	3695.3	14.3	3831.3	28.3
248	3822.5	14.4	3688.9	17.1	3822.9	14.9
249	3823.6	15.3	3700.1	14.0	3818.8	14.2
250	3815.3	21.4	3690.4	19.1	3830.9	24.9
251	3814.4	14.0	3681.9	12.7	3829.8	17.3

The maximum drifts of the Al2-1 lines were 30 ch, 22ch, and 49 ch for Ge detectors A, B, and C, respectively. Obviously, these were significant drifts (when compared with their FWHM) and the histograms could not be summed together. In this case, we developed

an off-line 'gain shift' program to shift the drifted peaks back to their original positions. Clearly, we could apply this 'gain shift' program to those drifted data sets, and then sum them together (refer to Fig. V-2, V-3 and V-4).

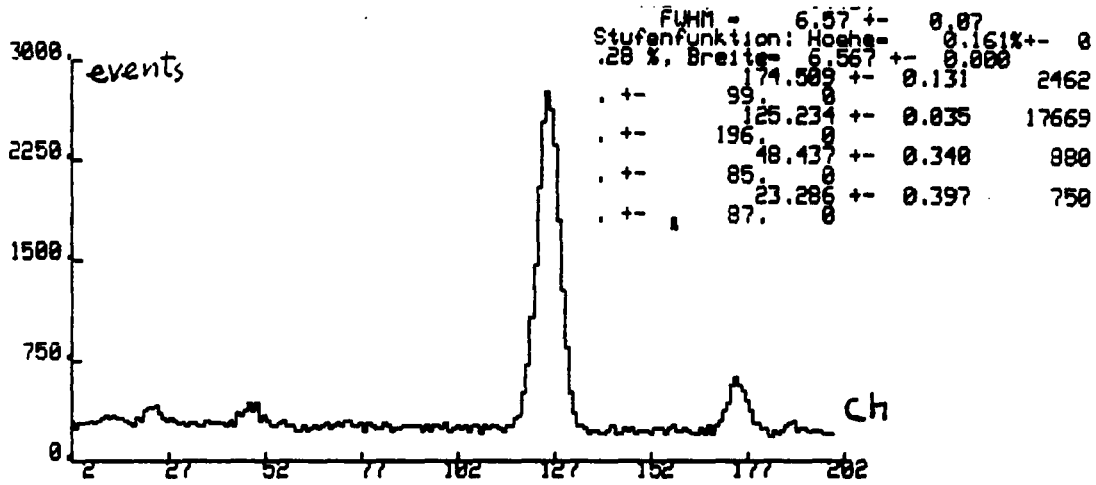


Fig. V-2

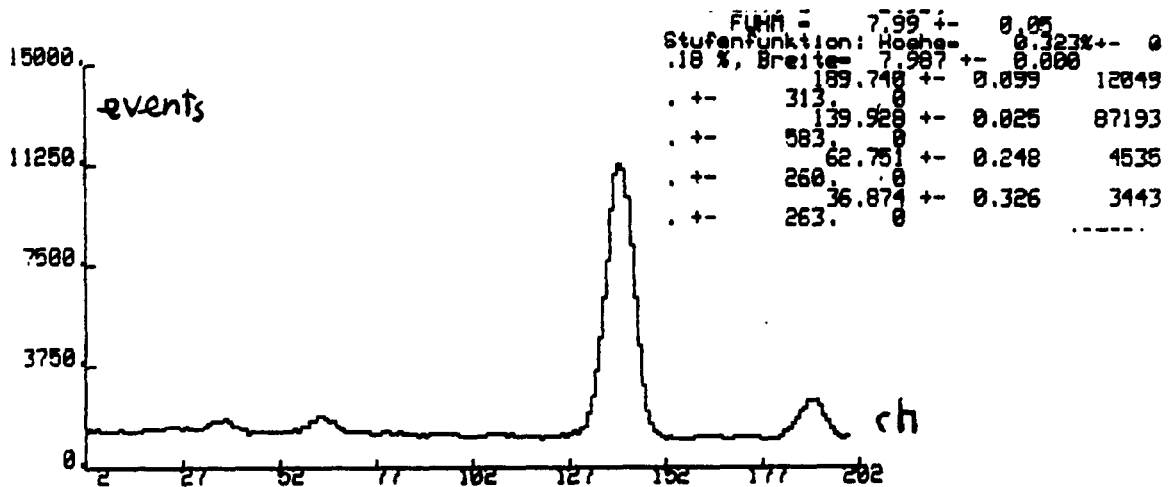


Fig. V-3

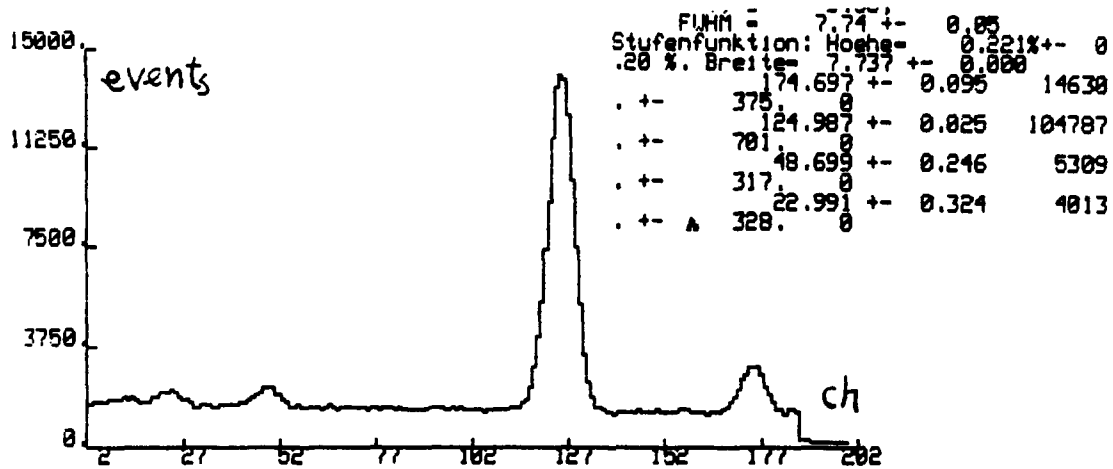


Fig. V-4

In addition, we continuously checked the ratios of μ_{C2-1}/μ_{real} , μ_{F2-1}/μ_{real} and μ_{C2-1}/μ_{F2-1} . If the ratios of μ_{C2-1}/μ_{real} , μ_{F2-1}/μ_{real} or μ_{C2-1}/μ_{F2-1} were determined to be the same within their errors, we were confident that the experimental data were consistent and stable (See Table. V-2 below).

Table V-2

Tape	Detector								
	A			B			C		
	$\mu\text{C2-1}$	$\mu\text{F2-1}$	Ratio	$\mu\text{C2-1}$	$\mu\text{F2-1}$	Ratio	$\mu\text{C2-1}$	$\mu\text{F2-1}$	Ratio
(Area)			(Area)			(Area)			
244	50898	100135	0.508	42224	87427	0.482	50169	107624	0.466
245	123884	244593	0.506	102922	214843	0.479	123626	265925	0.465
246	110699	208984	0.529	92765	193362	0.479	111453	238907	0.466
247	45374	89554	0.506	37513	78459	0.478	45343	96641	0.469
248	87834	171905	0.510	72353	151929	0.476	87047	186664	0.466
249	85412	167090	0.511	70785	146300	0.483	84410	180345	0.468
250	60431	118610	0.509	49819	104336	0.477	60177	127614	0.471
251	28422	55432	0.512	23443	48453	0.483	28248	60378	0.467

The maximum fluctuations of the ratio are 0.023, 0.007 and 0.006 for Ge detectors A, B, and C respectively from the Table V-2.

The presence of a permanent 5Å layer of carbon residue on the surface of the Au foil may have affected the time distribution of the μp atoms by intercepting the slower μp atoms before they reached the Au layer. Therefore, we had to determine whether any carbon (C3-1, C4-1, C5-1) lines were in the delayed spectrum. We concentrated on C3-1, C4-1 and C5-1 lines to determine the delay time spectra. We did not find any significant delayed muonic carbon x-rays, and thus no evidence that the 5Å layer of carbon prevent the (μP) from penetrating the target foils. The carbon data which were obtained at 750 mbar, 375 mbar

and 188 mbar, are illustrated in Table V - 3 below :

Table V-3

Detector B

Time	C3-1		C4-1		C5-1		(750 mbar)
	Error		Error		Error		
760	160.5	163.8	285.0	158.0	94.9	181.6	
1000	348.0	109.0	253.0	132.0	109.9	156.8	
1240	142.6	90.2	202.0	90.0	----	-----	
1480	130.9	102.8	42.0	106.0	-----	-----	
1720	47.4	77.2	----	----	-----	-----	
1960	90.6	83.6	130.0	64.0	137.0	76.0	

Time	C3-1		C4-1		C5-1		(375mbar)
	Error		Error		Error		
760	----	-----	79.0	74.0	126.9	91.3	
1000	92.0	50.0	133.0	53.0	----	-----	
1240	171.7	84.4	102.0	77.0	----	-----	
1480	----	-----	127.0	54.0	-----	-----	
1720	22.4	54.7	1.2	54.0	----	-----	
1960	----	-----	120.0	48.0	-----	----	

Time	C3-1		C4-1		C5-1		(188mbar)
	Error		Error		Error		
760	69.8	105.3	200.0	83.0	124.9	109.0	
1000	277.0	96.0	288.0	103.0	-----	-----	
1240	82.5	75.3	117.0	57.0	62.0	77.3	
1480	----	-----	----	-----	----	---	
1720	30.6	67.5	----	-----	70.0	51.0	
1960	----	-----	60.0	46.0	71.0	47.0	

Each time bin was 240 ns in Table V-3. As we expected, there was no direct evidence in this data that the 5Å carbon layer was involved in the delayed time distribution of (μp) atom transfer signals. It is reasonable to assume that the delayed data in Table V-3 came from a second muon incident by random coincidence, since the time distributions are consistent with such an interpretation.

We also checked the probability that the μp atoms punched through the Au layer into the Kynar substrate. If this were to happen, we should observe the μF_2-1 line appearing in the delayed spectrum as well as carbon. We checked the delayed time data sets of the μF_2-1 line and did not find any significant rate of delayed μF_2-1 signals. Thus no evidence was found of μp atoms punching through the Au layers.

The on-line routine checks also include checks of the impurities of the working(H_2 or D_2) gas. The presence of impurities in the gas was monitored by using a quadrupole mass spectrometer. In addition, we searched for the N2-1 (102 kev) line in the spectrum and thereby estimated the contamination of nitrogen gas . Because we had the advantage of a Pd filter in this experiment, we are confident that there was no significant contamination by nitrogen under any condition of the experiment.

B. Routine Treatment of the Experimental Data

In order to produce data sets of transfer-related time distributions from raw experimental data, the following routine steps were taken in sequence :

- 1) We concentrated on the γ rays ^{196}Pt 356, ^{196}Pt 332, and ^{196}Pt 328
- 2) We created two-dimensional energy versus time histograms for each Ge detector and covered the γ rays in the region of selected energy in the histograms of each detector.
- 3) We summed the histograms of data taken together under the same conditions.
- 4) We used the ' gain shift ' program if there were drifts of ^{196}Pt γ rays photopeaks in the spectrum.
- 5) We used the program FITA, which implements a method of non - linear least χ^2 fitting, to obtain the raw data of each of three γ - ray peaks for each Ge detector.
- 6) We subtracted the vacuum data from the raw data of each of three peaks, respectively, using the formula below :

$$(V-1) \quad (\text{data})_{\text{net}} = (\text{data})_{\text{raw}} - \alpha (\text{vacuum})$$

where α is a ratio of the $(C4-1)_{\text{raw}} / (C4-1)_{\text{vacuum}}$

- 7) We scaled each of the two weaker Pt γ rays with the stronger Pt 356 γ ray signal. The scale factors are defined respectively as the ratios of the total signal areas.

8) We combined the scaled three Pt γ ray time distributions by using the weighted mean, namely,

$$(V-2) \quad \overline{X} = \frac{\sum_{j=1}^n x^j / \sigma_j^2}{\sum_{j=1}^n 1/\sigma_j^2}$$

and

$$(V-3) \quad \overline{\sigma^2} = \left(\sum_{j=1}^n 1/\sigma_j^2 \right)^{-1}$$

where x^j is j th data set and σ_j is j th error set.

9) We scaled the time distribution from each of the A, B, C and TU detectors to the GMX detector using the method mentioned above.

10) We combined the scaled time distributions of five detectors into the unique final time distribution using formulas (V-2) and (V-3)

11) We corrected the time distributions for muon decay effects.
(See last two columns of Tables V-4 to V-8)

12) We normalized the 140 ns in response to 655 events (normalization). (See Tables V-9 to V-10)

V. 2. The Final Data Sets of The Time Distributions Under Five Conditions

A) The Time Distributions of Each Detector

After following the routine steps detailed above, we obtained the data sets of the time distribution for each detector. They are shown in Table V-4 , V-5, V-6, V-7, and V-8 below (" MIX" is the weighted averages from all detectors):

Table V-4 (H2 DG 750 mbar)

Tns	A	ERROR	B	ERROR	C	ERROR	TU	ERROR	MIX	ERROR
100	902.5	42.8	1152.1	40.8	989.3	48.4	2521.5	54.6	2301.3	37.6
140	766.1	41.2	996.8	39.8	991.6	42.9	2058.7	54.8	1965.5	36.5
180	676.7	31.9	751.7	37.4	707.2	37.5	1575.7	44.0	1516.7	30.4
220	499.7	28.0	595.3	31.0	616.9	32.7	1126.0	40.0	1147.6	26.8
260	471.6	28.2	501.7	27.8	484.4	25.9	967.1	37.1	984.7	24.4
300	411.1	25.3	429.7	26.3	391.4	24.9	743.2	32.8	797.2	22.2
340	369.1	24.5	340.8	24.0	310.8	21.4	645.3	30.3	670.7	20.3
380	343.7	22.9	323.4	23.5	302.9	21.7	602.5	28.2	633.7	19.5
440	523.2	23.6	570.6	30.4	531.4	29.4	1023.1	39.6	538.8	12.6
520	511.5	31.3	479.2	31.2	537.7	31.2	965.3	40.2	504.4	13.6
600	434.0	27.2	414.4	27.3	432.5	27.5	841.9	36.5	430.6	12.1
680	412.8	25.6	371.8	29.7	387.2	28.4	773.7	36.3	396.4	12.2
760	341.2	24.5	344.3	25.6	339.3	24.1	721.9	41.1	354.4	11.9
840	303.0	21.8	320.1	25.7	322.3	26.3	672.3	39.3	328.2	11.7
920	292.7	23.3	346.6	28.2	307.3	22.3	600.2	33.3	312.5	10.9
1000	299.7	21.9	313.3	24.4	316.8	23.3	572.6	31.0	304.5	10.3
1080	243.8	21.4	295.6	24.0	208.8	19.2	494.3	30.7	249.1	9.8
1160	223.5	21.3	262.4	23.1	220.8	19.7	432.6	27.2	229.2	9.2
1240	221.3	20.7	171.6	18.1	246.2	20.3	453.2	35.7	217.8	9.7
1320	201.7	20.3	204.0	24.0	215.5	22.1	395.7	26.9	205.9	9.4
1400	212.1	20.8	204.0	26.0	201.7	19.8	346.7	27.5	194.0	9.4
1480	141.9	22.1	151.0	21.0	189.8	18.8	283.6	24.8	155.2	8.7
1560	118.4	15.4	139.0	21.0	183.0	22.0	341.4	26.0	156.1	8.5
1640	123.4	16.4	132.0	19.0	143.0	20.0	293.0	23.4	140.8	8.0
1720	162.9	17.3	164.0	25.0	108.0	17.0	258.2	25.4	137.9	8.4
1800	128.0	19.0	87.0	18.0	108.0	17.0	248.7	24.8	115.6	8.1
1880	105.0	21.0	86.0	17.0	101.0	16.0	253.0	27.0	108.9	8.2
1960	80.0	16.0	113.0	20.0	120.0	18.0	208.0	25.0	104.9	8.1

Table V-5 (H2 DG 375 mbar)

Tns	A	ERROR	B	ERROR	C	ERROR	GM	ERROR	TU	ERROR	MIX	ERROR
100	346.9	33.9	472.9	33.6	588.9	34.5	840.5	40.3	1286.4	42.1	1118.3	25.5
140	409.6	29.5	442.4	27.8	617.3	30.3	817.1	40.1	1057.9	40.4	1040.0	23.5
180	372.3	25.3	407.0	23.8	522.9	27.6	665.1	31.7	881.5	34.1	885.6	19.9
220	291.2	21.6	284.7	23.9	371.8	25.0	522.9	29.3	656.6	31.1	660.9	18.3
260	253.4	20.3	268.6	20.4	313.3	22.0	407.6	26.9	546.3	28.6	555.6	16.6
300	200.4	18.6	221.7	18.7	259.6	18.7	283.0	29.6	442.9	27.2	443.3	15.7
340	179.6	17.3	141.0	14.4	205.2	17.4	258.3	22.3	344.7	23.6	349.0	13.3
380	145.2	33.0	128.4	14.2	162.9	16.1	217.8	21.3	295.9	22.5	291.9	13.3
440	257.5	26.0	213.8	19.8	277.0	21.5	357.2	26.1	513.2	31.0	249.2	8.6
520	201.2	22.0	201.8	20.3	243.0	19.3	322.4	26.0	376.7	26.7	207.5	7.9
600	208.5	25.0	130.4	25.0	217.4	18.9	261.4	23.6	361.6	28.1	182.8	8.1
680	181.0	25.0	191.0	23.0	152.0	15.9	238.5	25.3	330.3	27.2	161.5	7.7
760	141.0	22.0	99.0	18.0	153.2	17.2	208.8	22.5	304.2	24.9	140.3	7.2
840	137.0	18.0	144.0	19.0	140.0	19.0	214.0	26.0	236.5	25.2	133.8	7.5
920	136.0	19.0	113.0	17.0	186.0	20.0	163.0	22.0	280.0	29.0	135.1	7.5
1000	130.0	25.0	115.0	18.0	145.0	18.0	238.0	24.0	238.0	25.0	132.6	7.4
1080	111.0	17.0	127.0	18.0	153.0	19.0	184.0	23.0	196.0	22.0	117.4	6.8
1160	132.0	19.0	82.0	14.0	127.0	18.0	139.0	21.0	180.0	23.0	100.1	6.6
1240	75.0	16.0	75.0	21.0	162.0	20.0	147.0	21.0	204.0	25.0	102.8	7.1
1320	125.0	21.0	103.0	18.0	88.0	16.0	153.0	27.0	165.0	22.0	93.1	7.0
1400	64.0	15.0	69.0	12.0	69.0	13.0	152.0	24.0	212.0	26.0	81.6	6.1
1480	57.0	12.0	102.0	19.0	82.0	15.0	128.0	28.0	147.0	24.0	76.0	6.5
1560	71.0	21.0	80.0	16.0	79.0	15.0	81.0	16.0	124.0	24.0	65.3	6.1
1640	54.0	15.0	52.0	12.0	57.0	14.0	132.0	21.0	104.0	25.0	60.6	6.1
1720	0.0	0.0	47.0	13.0	79.0	13.0	87.0	16.0	124.0	20.0	61.2	5.7
1800	0.0	0.0	37.0	11.0	36.0	15.0	92.0	16.0	75.0	18.0	43.5	5.5
1880	0.0	0.0	30.0	11.0	38.0	16.0	64.0	15.0	94.0	19.0	40.8	5.5

Table V-6 (H2 DG 188 mbar)

Tns	A	ERROR	B	ERROR	C	ERROR	GM	ERROR	TU	ERROR	MIX	ERROR
100	110.1	55.2	728.5	47.2	695.4	71.7	1093.8	57.5	2188.2	58.5	1784.9	40.5
140	495.7	53.4	683.2	41.4	803.7	50.8	1189.5	53.4	1868.3	64.5	1714.5	39.1
180	551.6	44.7	638.1	38.6	852.8	48.6	1123.6	50.8	1737.2	50.7	1658.2	34.0
220	482.7	37.6	593.7	33.6	655.6	44.4	916.7	44.3	1309.2	46.1	1327.6	30.2
260	494.7	36.6	466.8	29.4	512.7	37.6	762.2	37.4	1109.1	40.5	1114.0	26.4
300	369.4	27.8	431.0	28.0	494.6	36.5	541.7	35.9	812.6	38.7	878.0	24.8
340	392.4	30.7	370.5	27.7	343.0	33.7	550.2	33.0	708.7	39.1	784.5	24.4
380	295.7	26.3	315.0	25.6	276.0	29.8	380.5	30.0	520.7	34.9	591.1	21.9
440	388.1	33.4	492.2	31.1	558.3	46.0	646.1	42.3	889.4	42.4	489.1	14.1
520	356.4	31.2	309.2	26.9	380.0	39.4	450.9	37.4	674.4	38.5	356.6	12.6
600	280.0	29.4	329.4	31.5	358.0	39.0	369.2	32.4	607.2	36.4	317.4	12.1
680	272.1	29.2	239.9	26.2	268.0	34.0	346.0	33.4	430.5	34.3	251.6	11.4
760	174.2	25.0	233.0	30.0	218.0	37.0	296.4	31.5	373.5	32.4	211.2	11.1
840	161.3	30.4	171.0	29.0	188.0	52.0	242.7	29.7	327.2	29.7	176.1	10.9
920	89.0	19.0	135.0	33.0	217.0	39.0	289.8	32.7	326.0	29.8	168.9	10.5
1000	112.0	22.0	161.0	28.0	208.0	38.0	181.9	34.9	342.2	37.4	166.0	11.8
1080	185.0	35.0	178.0	30.0	129.0	27.0	206.0	31.7	268.0	31.2	150.7	10.8
1160	88.0	22.0	133.0	28.0	59.0	24.0	232.0	41.0	242.9	26.5	119.3	9.7
1240	110.0	23.0	79.0	18.0	97.0	35.0	156.0	31.0	222.7	27.7	109.6	9.4
1320	103.0	31.0	138.0	24.0	132.0	28.0	120.0	26.0	233.8	27.9	118.4	9.6
1400	131.0	24.0	96.0	24.0	123.0	34.0	114.0	26.0	202.3	26.6	106.4	9.3
1480	94.0	21.0	99.0	25.0	104.0	62.0	100.0	30.0	211.8	26.5	103.2	9.8
1560	41.0	10.0	46.0	20.0	98.0	29.0	94.0	28.0	160.2	27.2	68.3	7.8
1640	104.0	25.0	85.0	20.0	56.0	17.0	122.0	34.0	177.3	24.5	85.6	8.3
1720	53.0	25.0	59.0	23.0	0.0	0.0	97.0	34.0	138.0	29.0	69.3	10.7
1800	43.0	18.0	46.0	17.0	0.0	0.0	79.0	26.0	95.0	25.0	51.9	8.6
1880	26.0	55.0	69.0	22.0	0.0	0.0	91.0	24.0	69.0	22.0	47.8	8.7

Table V-7 (H2 DG 94 mbar)

Tns	A ERROR		B ERROR		C ERROR		TU ERROR		GM ERROR		MIX ERROR	
100	0.0	0.0	575.3	61.6	589.0	60.4	2166.8	67.2	893.4	62.7	1185.9	32.4
140	0.0	0.0	609.1	51.7	716.7	46.6	2044.0	61.6	1041.0	56.1	1199.7	28.5
180	335.4	49.3	684.4	52.8	776.4	43.7	1662.2	55.4	1057.5	50.3	1064.8	24.9
220	433.3	40.9	584.1	46.2	667.9	38.2	1426.5	49.8	962.5	47.3	945.7	22.3
260	462.2	34.5	530.3	42.8	613.0	39.0	1069.1	46.7	809.5	42.3	789.9	20.7
300	436.9	31.5	376.7	36.8	479.5	33.9	1036.5	46.1	662.9	39.5	690.4	19.3
340	429.7	31.6	346.5	44.0	456.5	31.1	762.2	39.1	606.6	43.2	588.7	18.4
380	399.7	28.1	256.7	29.8	422.5	30.0	613.8	42.5	559.5	42.4	513.4	17.9
440	311.8	25.2	497.3	55.2	522.5	35.1	1018.1	51.5	807.1	53.0	344.5	10.6
520	532.0	36.0	409.0	49.0	387.2	30.6	733.4	42.2	577.6	48.0	290.2	9.9
600	397.5	33.0	324.1	45.6	310.6	30.7	633.3	48.3	472.8	44.1	242.5	10.1
680	274.5	33.9	195.5	31.6	229.8	25.0	471.7	44.7	364.3	36.3	174.0	8.8
760	169.0	21.9	169.2	40.6	205.6	26.9	392.1	43.6	324.4	33.8	145.7	8.3
840	192.3	25.8	172.8	39.3	156.3	24.5	325.0	34.7	271.7	34.8	125.1	7.8
920	175.0	42.0	222.0	77.0	174.0	24.1	275.0	44.0	219.7	30.4	112.7	8.8
1000	178.0	30.0	123.0	40.0	160.6	25.0	175.0	32.0	123.2	23.2	77.2	6.9
1080	93.0	23.0	119.0	42.0	130.0	29.0	232.0	38.0	170.2	33.4	83.9	8.1
1160	109.0	28.0	75.0	25.0	135.0	31.0	222.0	42.0	220.0	64.0	81.7	9.1
1240	98.0	18.0	174.0	86.0	93.0	22.0	192.0	32.0	192.0	40.0	74.8	7.2
1320	112.0	26.0	27.0	22.0	77.0	30.0	141.0	29.0	139.0	28.0	54.4	6.7
1400	77.0	28.0	150.0	169.0	91.0	23.0	131.0	27.0	127.0	33.0	54.0	7.0
1480	73.0	27.0	139.0	133.0	62.0	24.0	120.0	28.0	105.0	33.0	46.3	7.1
1560	74.0	31.0	71.0	35.0	74.0	19.0	105.0	28.0	163.0	57.0	46.9	7.1
1640	57.0	21.0	76.0	31.0	41.0	16.0	183.0	32.0	140.0	39.0	51.0	6.6
1720	0.0	0.0	91.0	41.0	78.0	20.0	134.0	37.0	160.0	57.0	55.2	8.8
1800	0.0	0.0	12.0	10.0	0.0	0.0	40.0	15.0	82.0	32.0	14.5	4.2
1880	0.0	0.0	0.0	0.0	0.0	0.0	100.0	33.0	49.0	28.0	30.5	8.8
1960	0.0	0.0	0.0	0.0	0.0	0.0	49.0	17.0	0.0	0.0	16.9	5.3

Table V-8 (H2 DG 47 mbar)

Tns	A ERROR		B ERROR		C ERROR		TU ERROR		GM ERROR		MIX ERROR	
100	0.0	0.0	200.3	43.1	165.0	32.7	0.0	0.0	335.2	45.3	254.4	26.0
140	0.0	0.0	203.5	35.2	276.5	28.0	342.3	50.0	351.0	40.4	293.9	18.7
180	118.1	32.6	221.5	31.7	311.1	27.7	417.1	41.7	342.0	33.4	295.5	15.3
220	197.0	33.0	188.9	26.0	257.7	23.3	347.6	35.7	262.5	28.6	260.4	13.2
260	173.0	27.9	208.6	26.1	242.8	22.8	373.8	33.1	266.2	31.0	260.9	12.8
300	197.9	26.8	206.5	28.7	209.4	20.4	345.5	31.8	188.5	24.9	232.1	11.9
340	166.2	23.2	157.1	21.0	134.6	16.4	273.4	28.0	172.0	24.2	181.0	10.2
380	129.8	24.8	144.3	39.0	80.4	11.9	265.1	28.7	128.6	22.3	129.8	9.4
440	178.3	32.1	175.7	34.0	239.3	24.4	362.0	46.6	225.2	28.0	122.2	7.4
520	205.1	34.0	135.0	29.0	191.1	21.5	324.5	37.8	179.1	29.1	105.5	6.7
600	104.0	36.0	113.7	25.0	98.0	20.0	238.0	29.3	149.2	37.0	71.6	6.2
680	161.0	32.0	92.0	32.0	93.0	26.0	170.4	28.9	122.0	26.0	62.7	6.3
760	79.0	23.0	41.0	16.0	65.0	20.0	87.0	30.0	68.0	24.0	34.0	5.2
840	0.0	0.0	84.0	33.0	55.0	21.0	107.0	27.0	92.0	45.0	37.9	6.7
920	0.0	0.0	68.0	28.0	90.0	29.0	120.0	39.0	56.0	23.0	38.7	7.1
1000	0.0	0.0	28.0	19.0	58.0	20.0	102.0	37.0	57.0	17.0	29.0	5.4
1080	0.0	0.0	0.0	0.0	0.0	0.0	113.0	42.0	0.0	0.0	38.8	14.4
1160	0.0	0.0	0.0	0.0	0.0	0.0	78.0	26.0	0.0	0.0	26.8	8.9
1240	0.0	0.0	0.0	0.0	0.0	0.0	94.0	30.0	0.0	0.0	32.3	10.3

B. The Final Data Sets of the Time Distribution With Decay
Correction and normalization to 140 ns in Response to 655 events
Under the Five Conditions

We mixed the time distributions of five detectors under the same conditions with respective weights. Finally, the unique time distributions with decay correction and normalization under each condition were obtained. They are listed in Tables V-9 and V-10 below :

Table V-9

T (ns)	HD750	Error	HD375	Error
100	753.1	12.3		
140	655.0	12.2	655.0	14.8
180	514.7	10.3	568.0	12.7
220	396.7	9.3	431.7	12.0
260	346.5	8.6	369.5	11.1
300	285.8	8.0	300.3	10.7
340	244.9	7.4	240.8	9.2
380	235.6	7.2	205.0	9.4
440	205.8	4.8	179.9	6.2
520	199.8	5.4	155.3	5.9
600	177.0	4.9	142.0	6.3
680	168.9	5.2	130.1	6.2
760	156.6	5.3	117.2	6.0
840	150.4	5.4	115.8	6.4
920	148.6	5.2	121.4	6.7
1000	150.1	5.1	123.5	6.9
1080	127.3	4.9	113.3	6.6
1160	121.6	4.9	100.3	6.6
1240	119.7	5.4	106.8	7.4
1320	117.4	5.4	100.3	7.5
1400	114.7	5.6	91.3	6.9
1480	95.2	5.3	88.1	7.6
1560	99.3	5.4	78.5	7.4
1640	92.8	5.3	75.6	7.5
1720	94.4	5.8	79.1	7.3
1800	82.0	5.7	58.3	7.3
1880	80.2	6.0	56.8	7.6
1960	80.0	6.1		

Table V-10

T (ns)	HD188	Error	HD94	Error	HD47	Error
100	669.5	15.2	635.8	17.4	556.7	56.9
140	655.0	14.9	655.0	15.5	655.0	41.7
180	645.1	13.2	592.0	13.8	670.7	34.7
220	526.0	12.0	535.5	12.6	601.8	30.5
260	449.5	10.6	455.5	12.0	614.1	30.1
300	360.8	10.2	405.4	11.3	556.3	28.5
340	328.3	10.2	352.0	11.0	441.8	24.9
380	251.8	9.4	312.6	10.9	322.7	23.4
440	214.2	6.2	215.7	6.6	312.2	18.8
520	161.9	5.7	188.4	6.5	279.6	17.9
600	149.5	5.7	163.2	6.8	196.6	17.1
680	122.9	5.5	121.5	6.1	178.7	17.9
760	106.9	5.6	105.5	6.0	100.5	15.2
840	92.5	5.7	93.9	5.8	116.2	20.5
920	92.0	5.7	87.8	6.8	122.8	22.7
1000	93.7	6.7	62.3	5.5	95.4	18.0
1080	88.3	6.3	70.3	6.8	132.5	49.2
1160	72.5	5.9	70.9	7.9	94.8	31.5
1240	69.1	5.9	67.4	6.5	118.6	37.8
1320	77.4	6.2	50.8	6.2		
1400	72.1	6.3	52.3	6.7		
1480	72.5	6.9	46.6	7.1		
1560	49.8	5.7	48.8	7.4		
1640	64.8	6.3	55.1	7.1		
1720	54.4	8.4	61.9	9.8		
1800	42.2	7.0	16.8	4.9		
1880	40.3	7.4	36.8	10.6		
1960			21.1	7.3		

Chapter VI

DISCUSSIONS AND CONCLUSIONS

The goal of the experiment was to extract the initial velocity distribution of a μp (or μd) atom formed in H_2 (or D_2) gas from the time distribution data sets. Due to the difficulties of theoretical calculations, we cannot obtain directly the initial velocity distribution from the experimental data sets because of scattering. But we can indirectly infer the initial velocity distribution by using the Monte Carlo Method.

We assumed a reasonable initial velocity distribution and nuclear cross section set for μp elastic scattering from H atoms which was provided by theory [7]. We also assumed that the molecular scattering cross-section will be 2.5 (2.0) times the nuclear $\mu p + p$ cross-section below (above) a hyperfine energy E of 0.3 eV, in accord with previous results for $\mu d + d$ scattering [44]. We input those ' parameters ' into the Monte Carlo program (provided by a colleague [44]). The Monte Carlo program generates the theoretical time distribution sets for each pressure.

As a first assumption, we chose the Maxwellian distribution and the preliminary result obtained is that the mean energy is $E=3.4$ eV. The Monte Carlo time distribution data sets and experimental data sets are illustrated in Fig. VI -1 to Fig. VI-10.

According to the usual model, a negative muon formed muonic hydrogen in highly excited states (μp^* or μd^*) when negative muons are stopped in H_2 or D_2 gas. Assume that the μp^* (μd^*) are the results of the initial formation process, i.e. do not result from the deexcitation of (μppe) molecular states which were themselves the actual initial formation products. Then conservation of momentum in the initial formation will dictate that the μd atom's speed will be approximately half (0.52) of the speed of μH atom and the kinetic energy of μd atom is approximately half (0.52) that of μp atom as well. We note that this is totally consistent with the results for D_2 and H_2 data -- the mean kinetic energy of a μD atom is 1.8 ± 0.1 eV compared to 3.4 eV for μp .

If the μp was initially formed directly as described above, we then get the mean kinetic energy of the muon at its capture time by H atom or H_2 molecule from (II-27) as follows :

$$E_c = 34 \text{ eV for H atom and } E_c = 68 \text{ eV for } H_2 \text{ molecule.}$$

The muon capture energy distribution is given below :

$$P(E_c) = (3f/4\pi \overline{E_c})^{3/2} \exp(-3E_c/2 \overline{E_c})$$

where E_c is the capture energy of the muon and $\overline{E_c}$ is the mean energy of muons. The f has two values $f=10$ or 20 for μH atom or μH_2 molecule respectively.

In addition, the lifetime of negative muons has been measured in Au. A significant improvement over most previous measurements [38] [37] is obtained in this experiment. The mean lifetime of negative muon in Au is :

$$\tau = 69.716 \pm 0.144 \text{ ns}$$

compared to previous measurements :

$$\tau = 72.77 \pm 0.47 \text{ ns [38]}$$

and

$$\tau = 74.3 \pm 1.5 \text{ ns [37]}$$

750 mbar

Events/ 40ns

1000

100

10

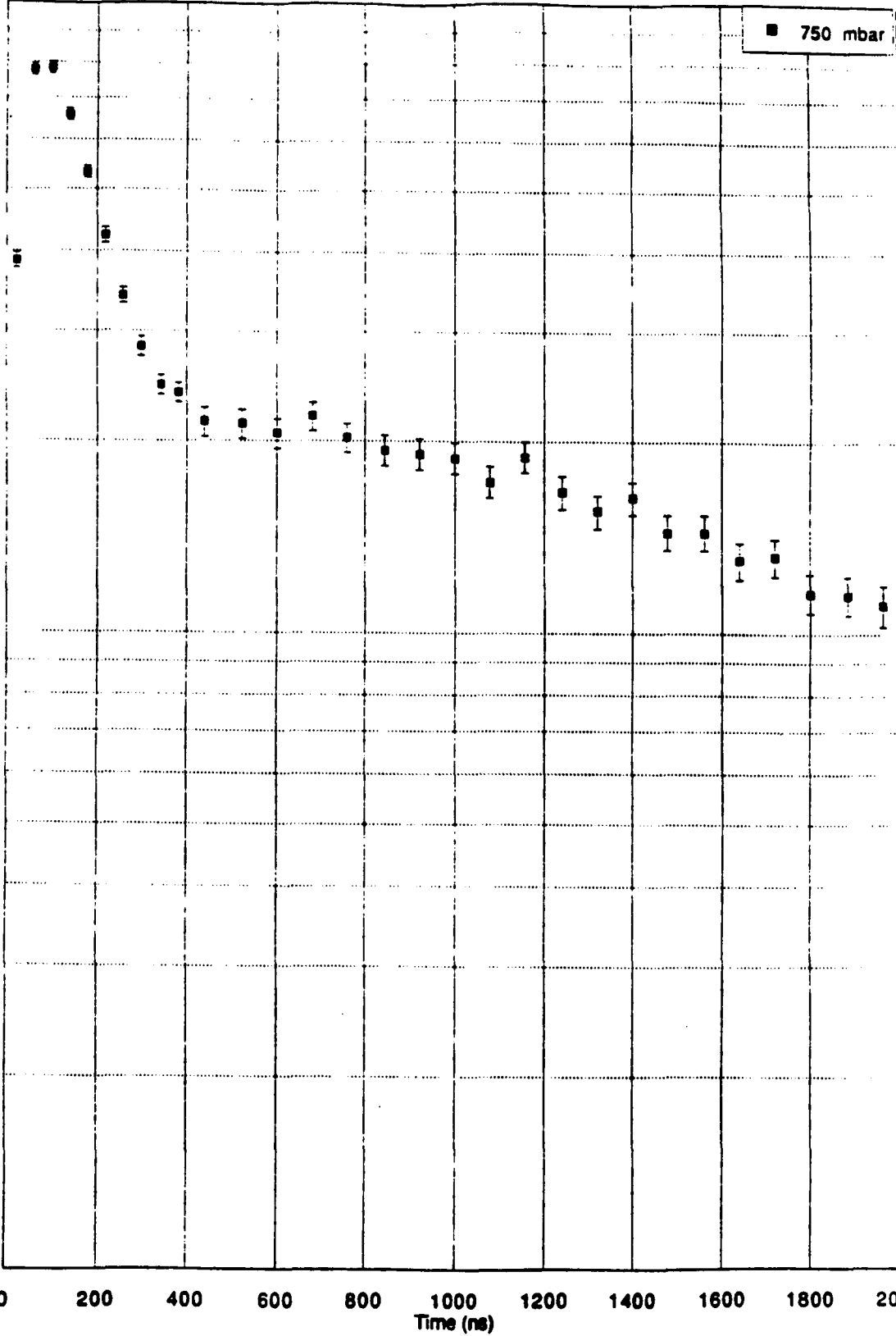


Fig. VI-1

Monte Carlo Time Distribution [E = 3.4 eV 2.5 (2.0)]
375mbar

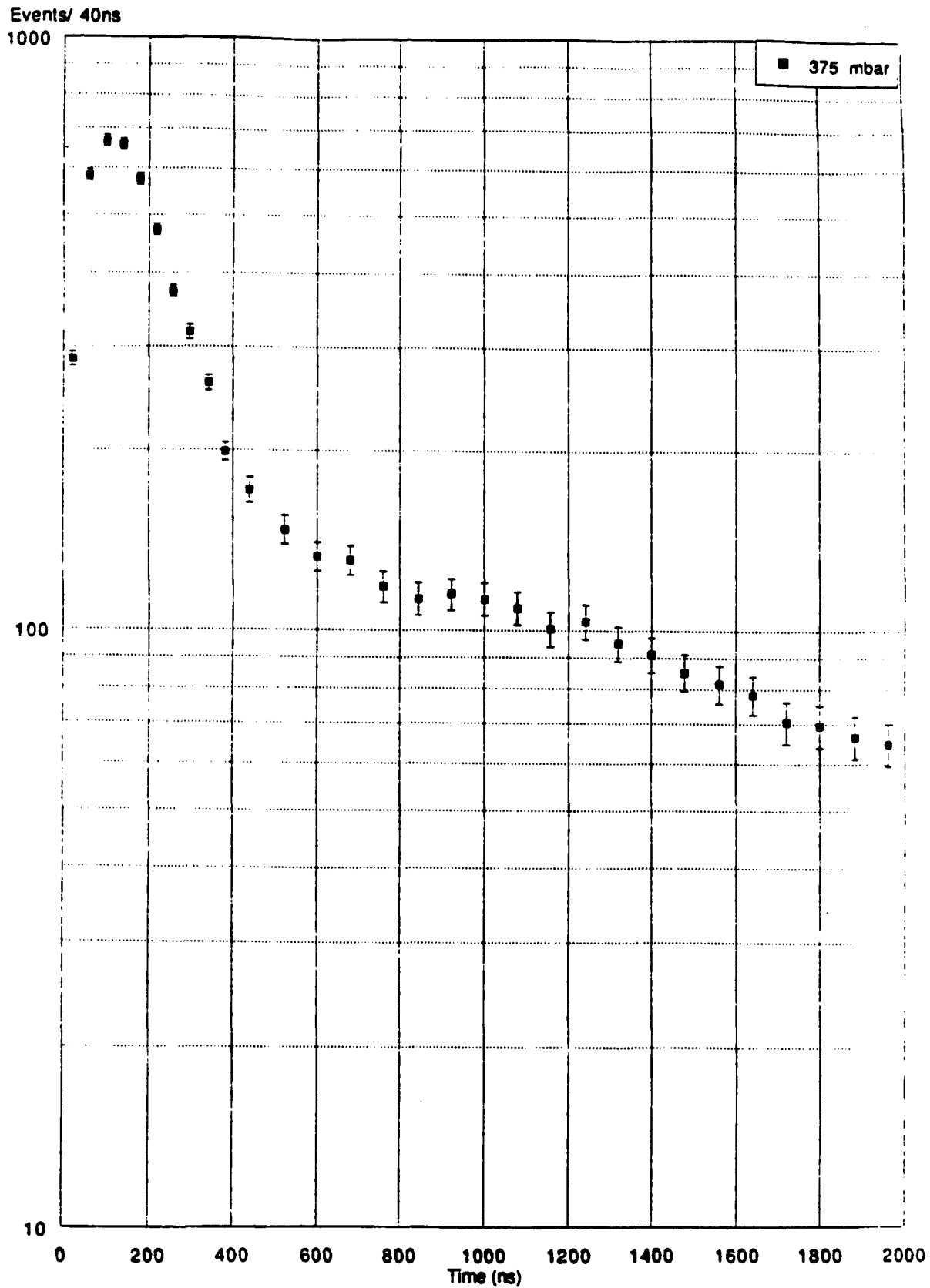


Fig. VI-2

188mbar

Events/ 40ns

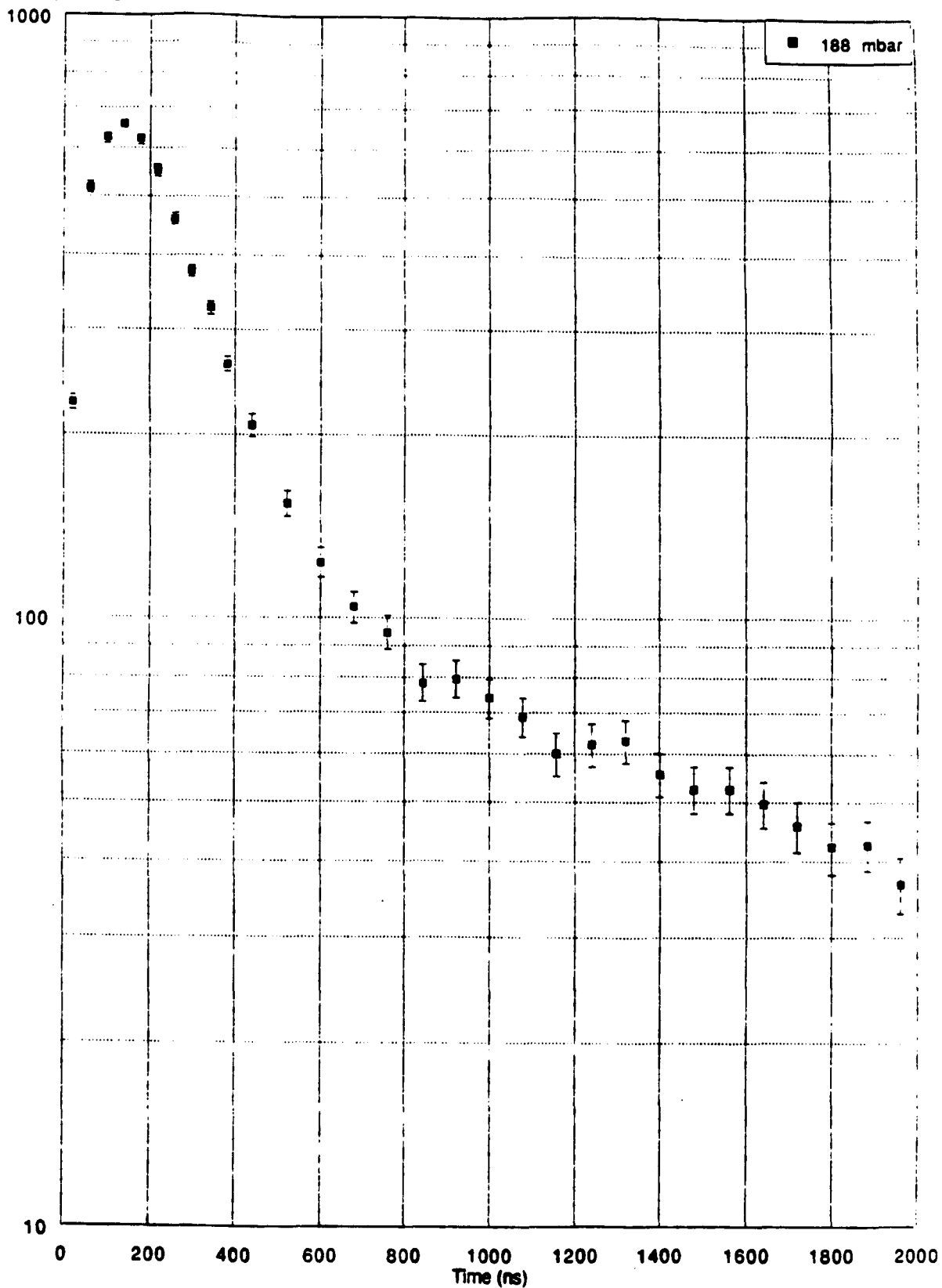


Fig. VI-3

94 mbar

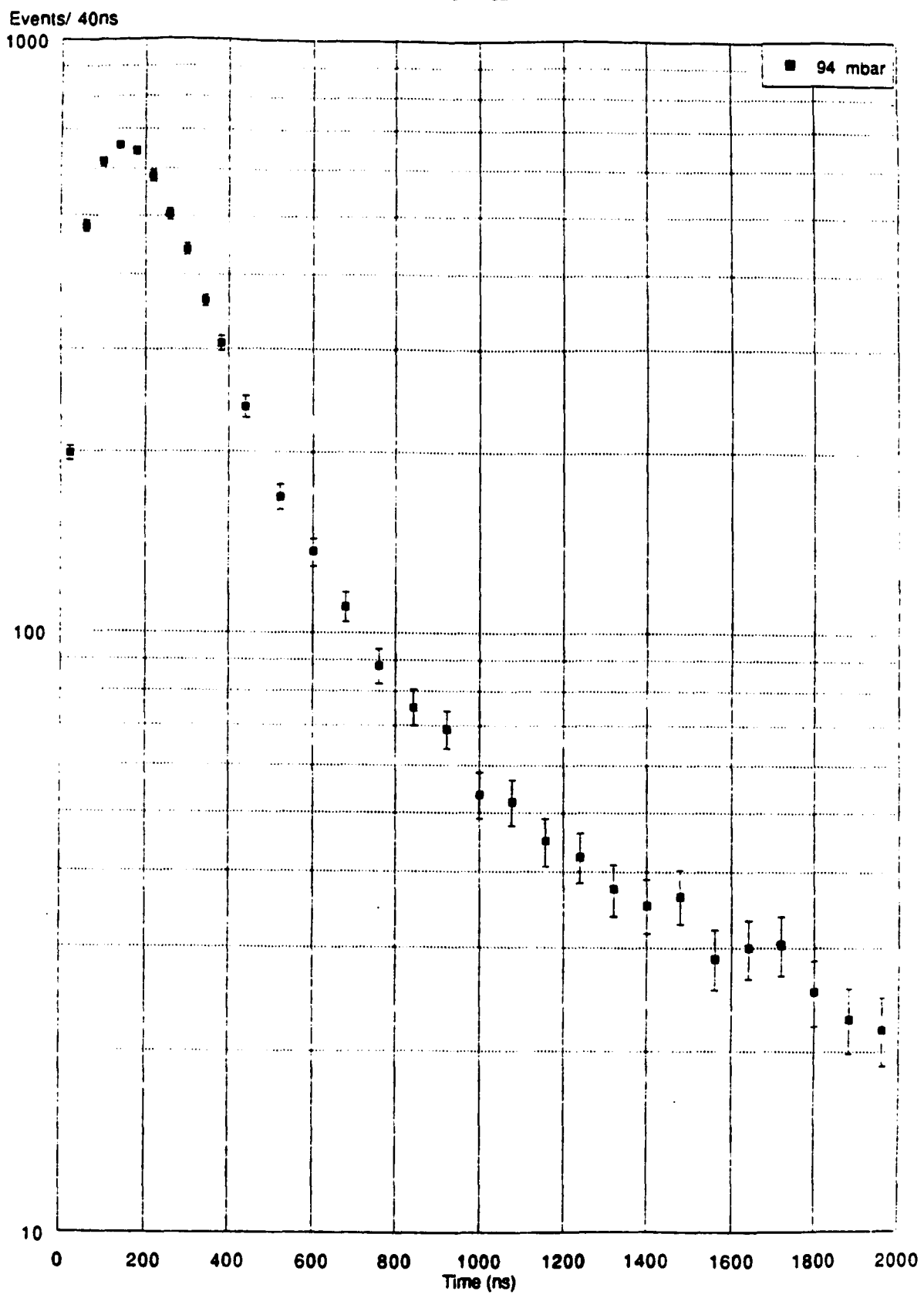


Fig. VI-4

Monte Carlo Time Distribution [E = 3.4 eV 2.5 (2.0)]
47 mbar

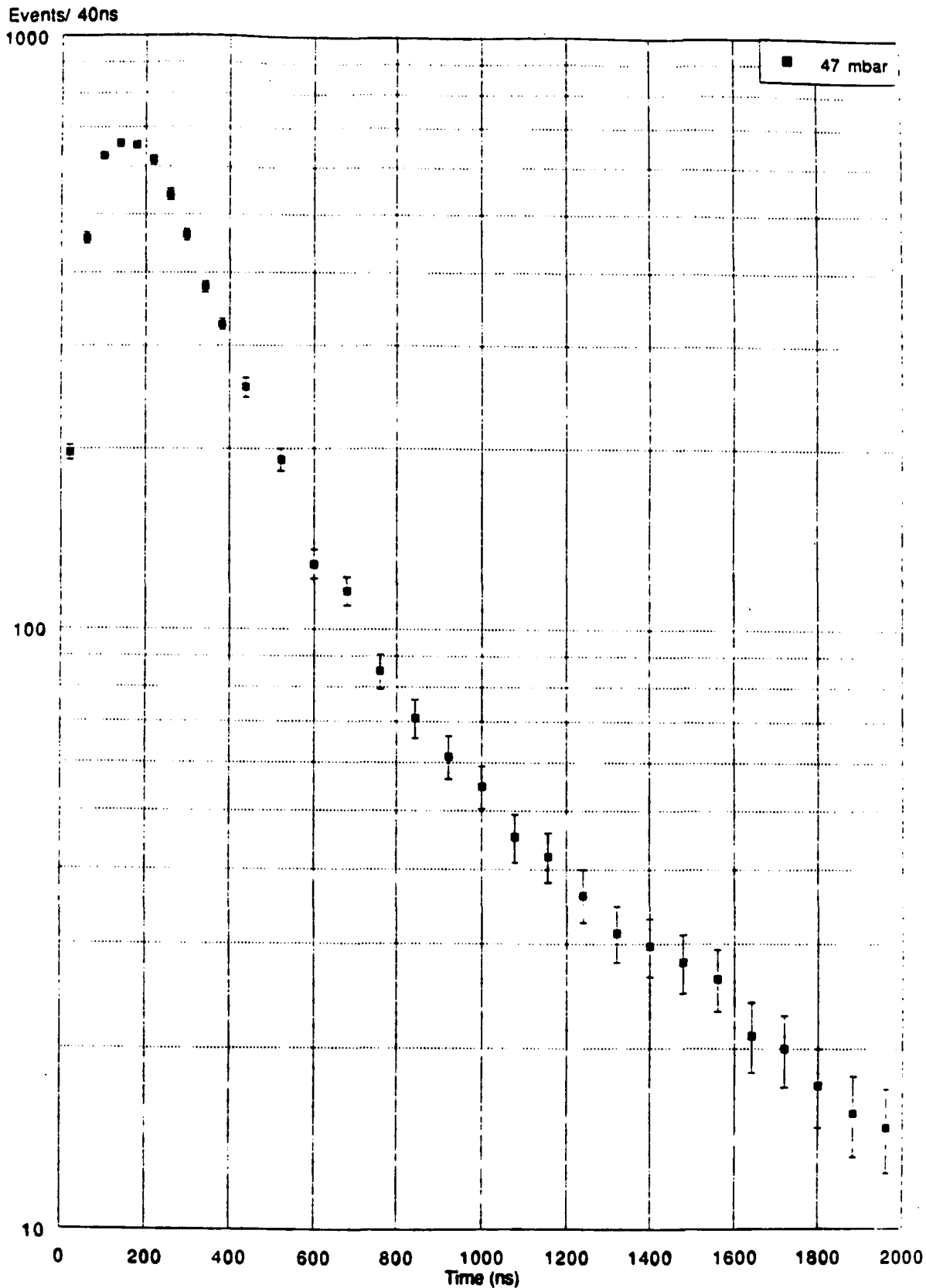


Fig. VI-5

Experimental Time Distribution 750 mbar

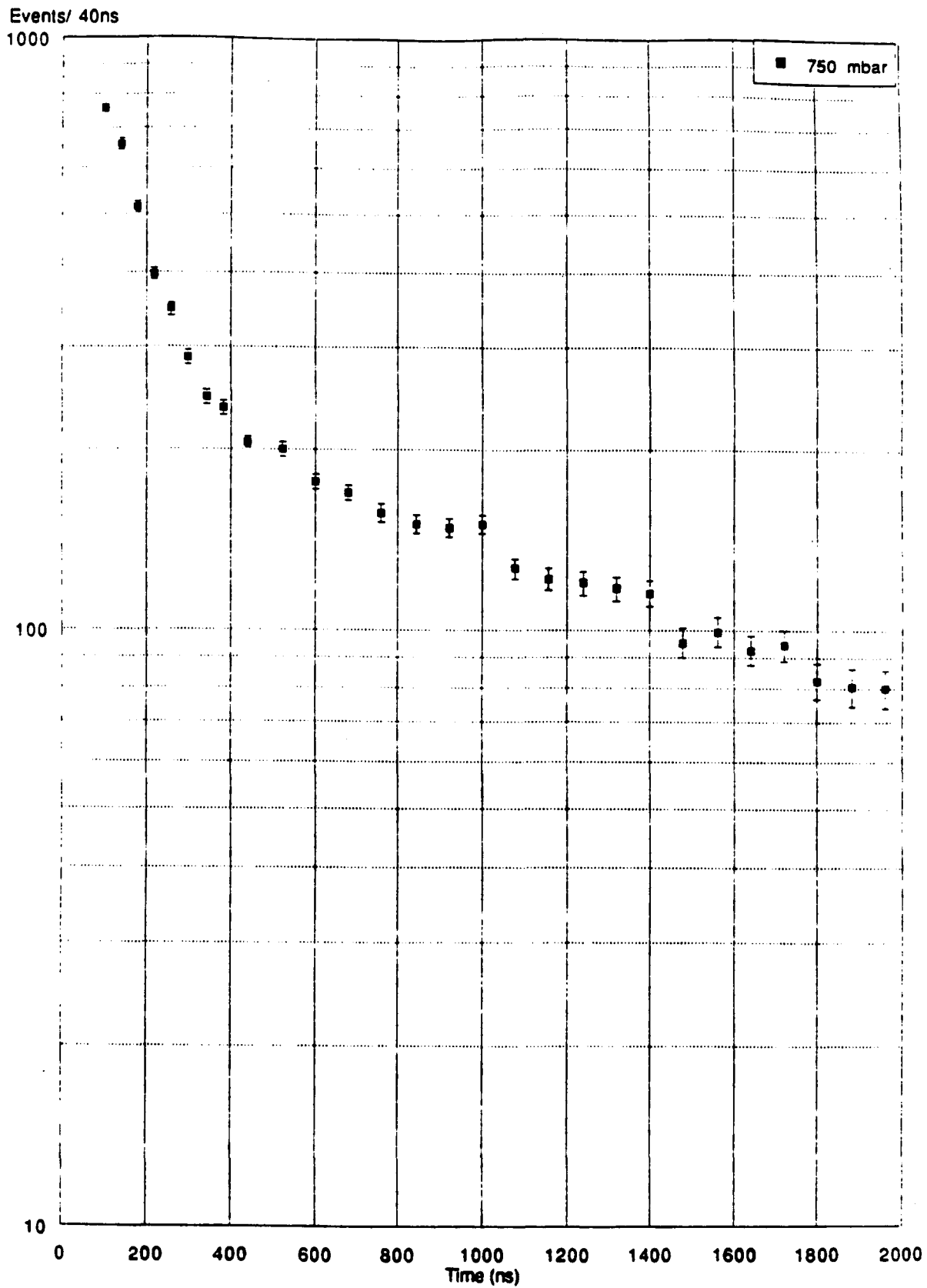


Fig. VI-6

Experimental Time Distribution

375 mbar

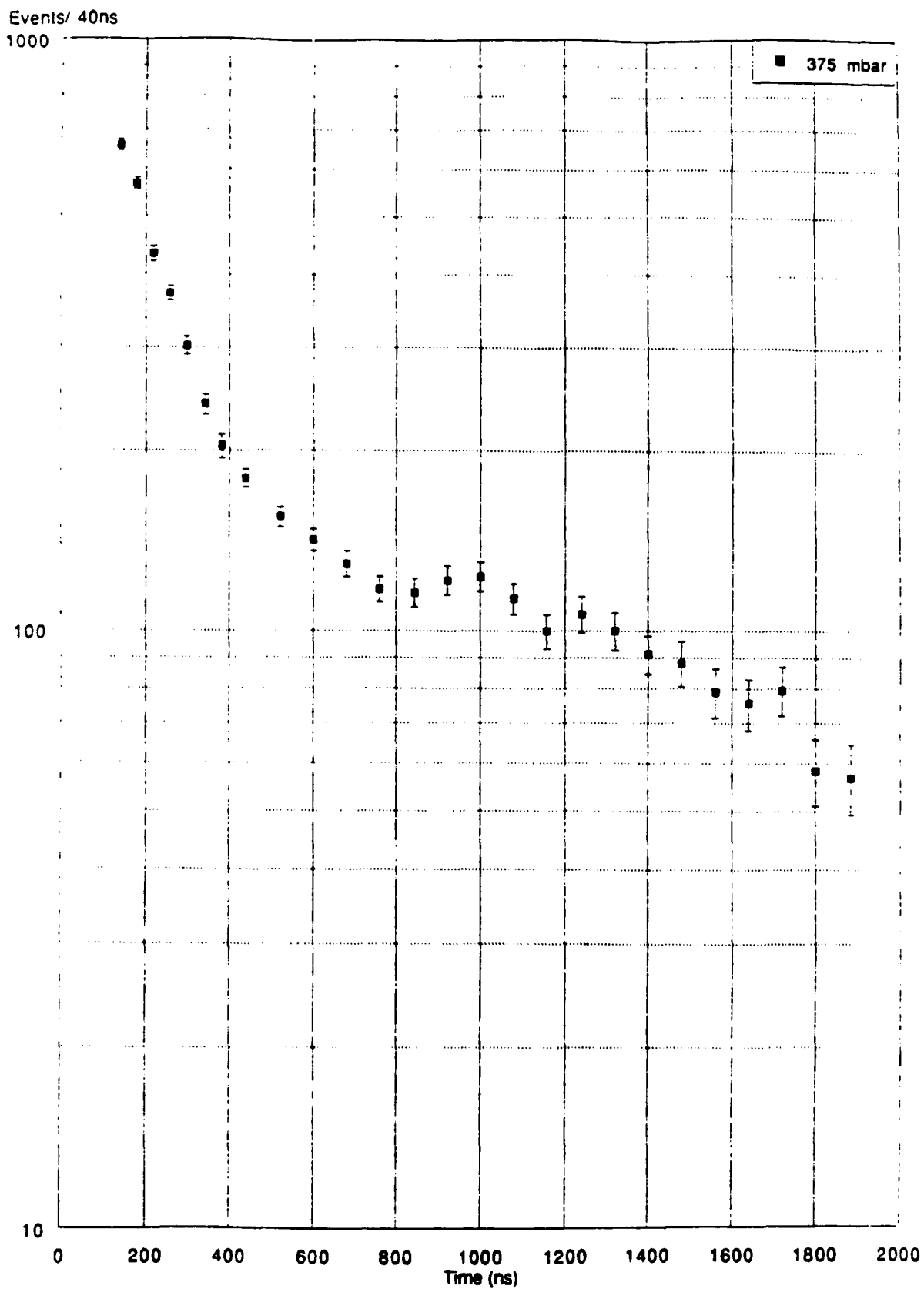


Fig. VI-7

Experimental Time Distribution

47 mbar

Events/ 40ns

1000

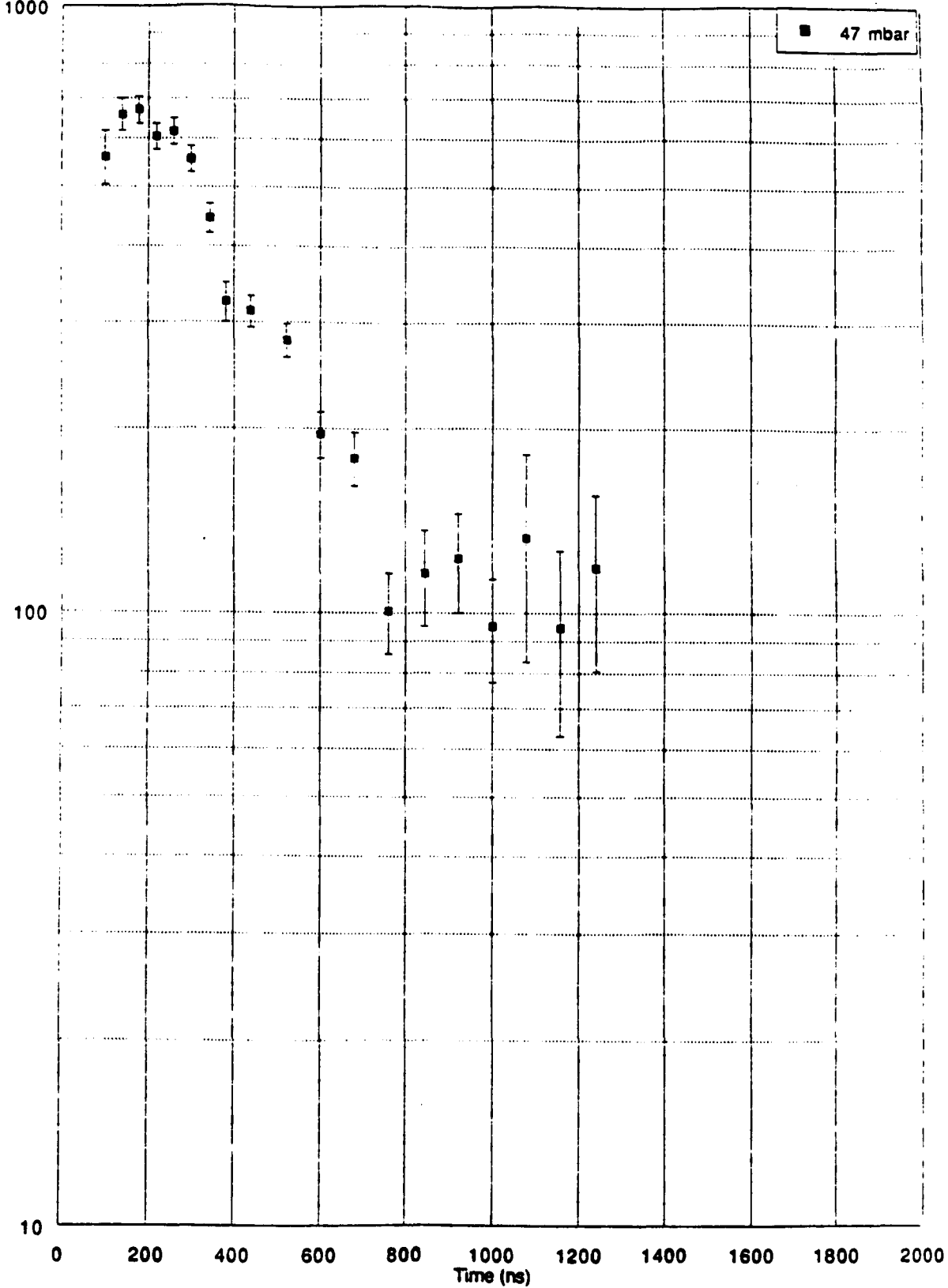


Fig. VI-10

Experimental Time Distribution
188 mbar H2

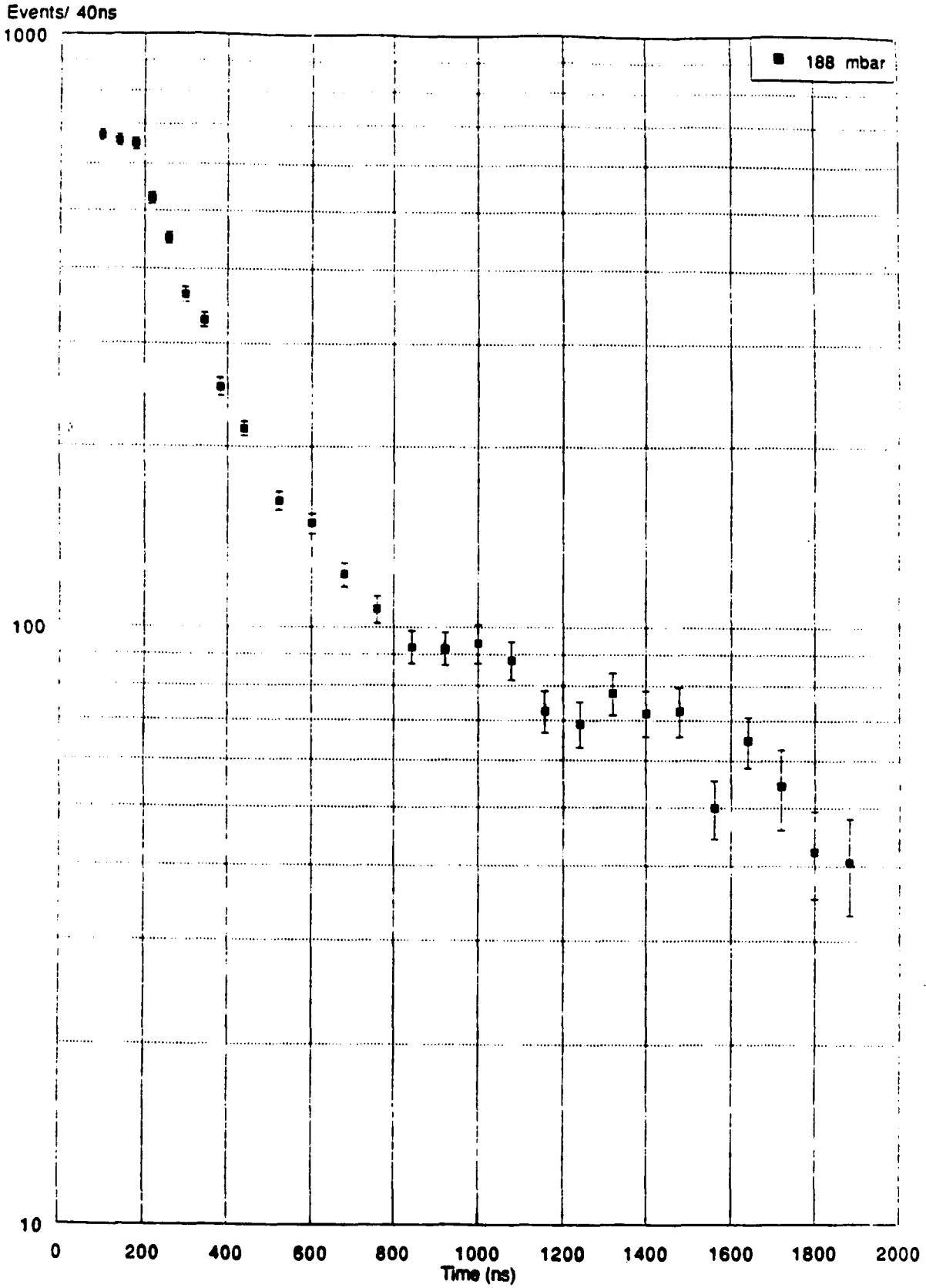


Fig. VI-8

Experimental Time Distribution

94 mbar

Events/ 40ns
1000

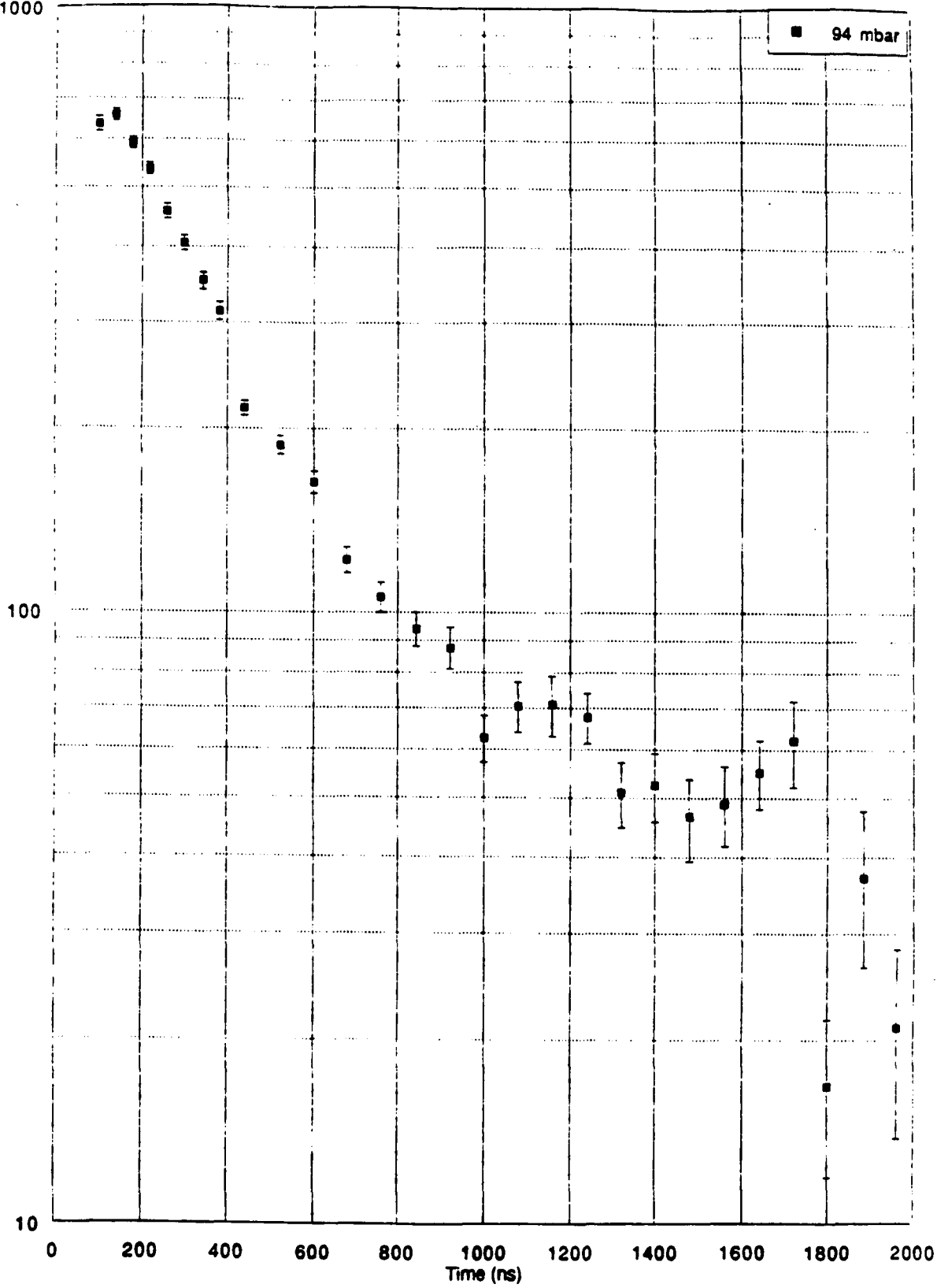


Fig. VI-9

47 mbar

Events/ 40ns

1000

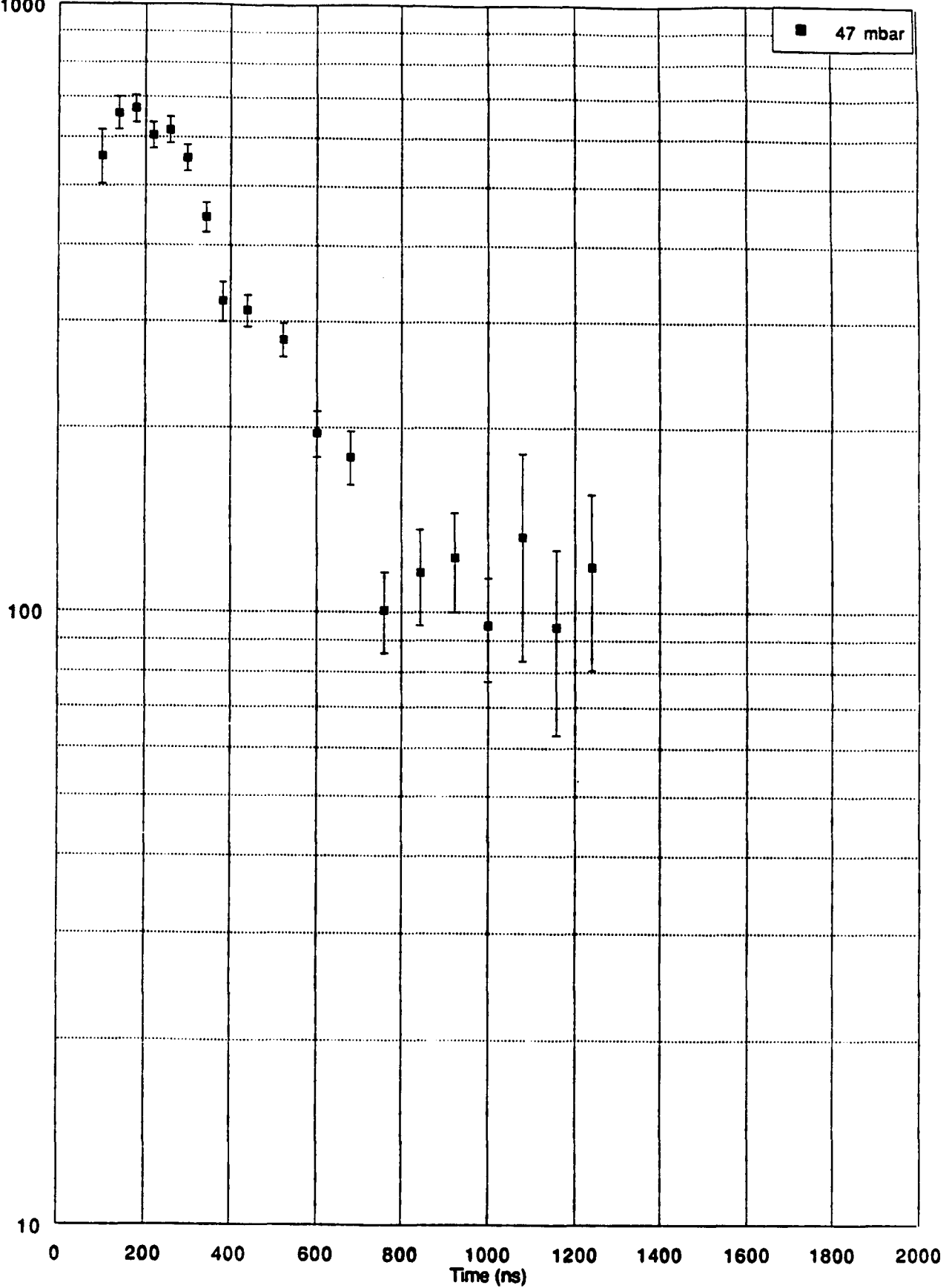
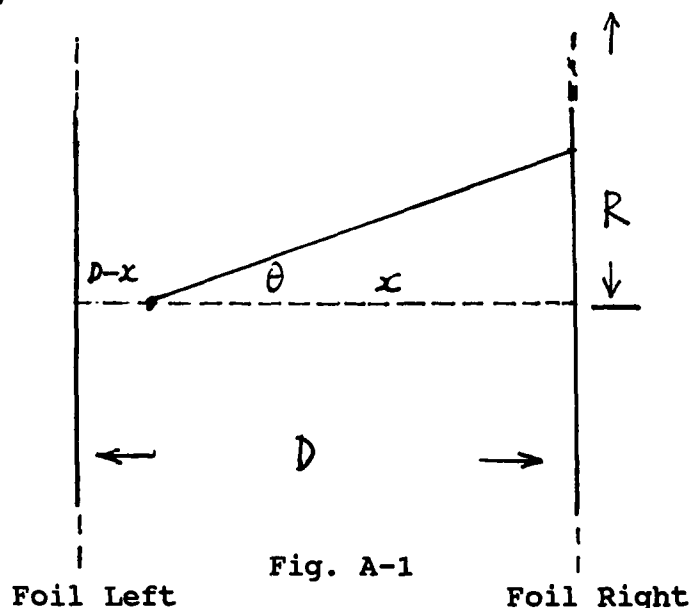


Fig. VI-10

Appendix A

In the $\mu p + p$ scattering experiment the μp atoms are assumed to form uniformly in the H₂ (or D₂) gas gap between two foils separated by a distance D with $R/D \gg 1$ (with reference to Fig. A-1 below)



where R is the radius of a foil and D is a distance between two foils.

One of goals of the experiment is to determine the time distribution of μp atoms arriving at a foil and then to determine the initial velocity distribution of μp atoms.

Here, we answer this question-if we know the initial velocity distribution $f(\mathbf{x}, \mathbf{v})$, then what kind of time distribution will be determined in the experiment ? [44]

Experimental Time Distribution

47 mbar

Events/ 40ns

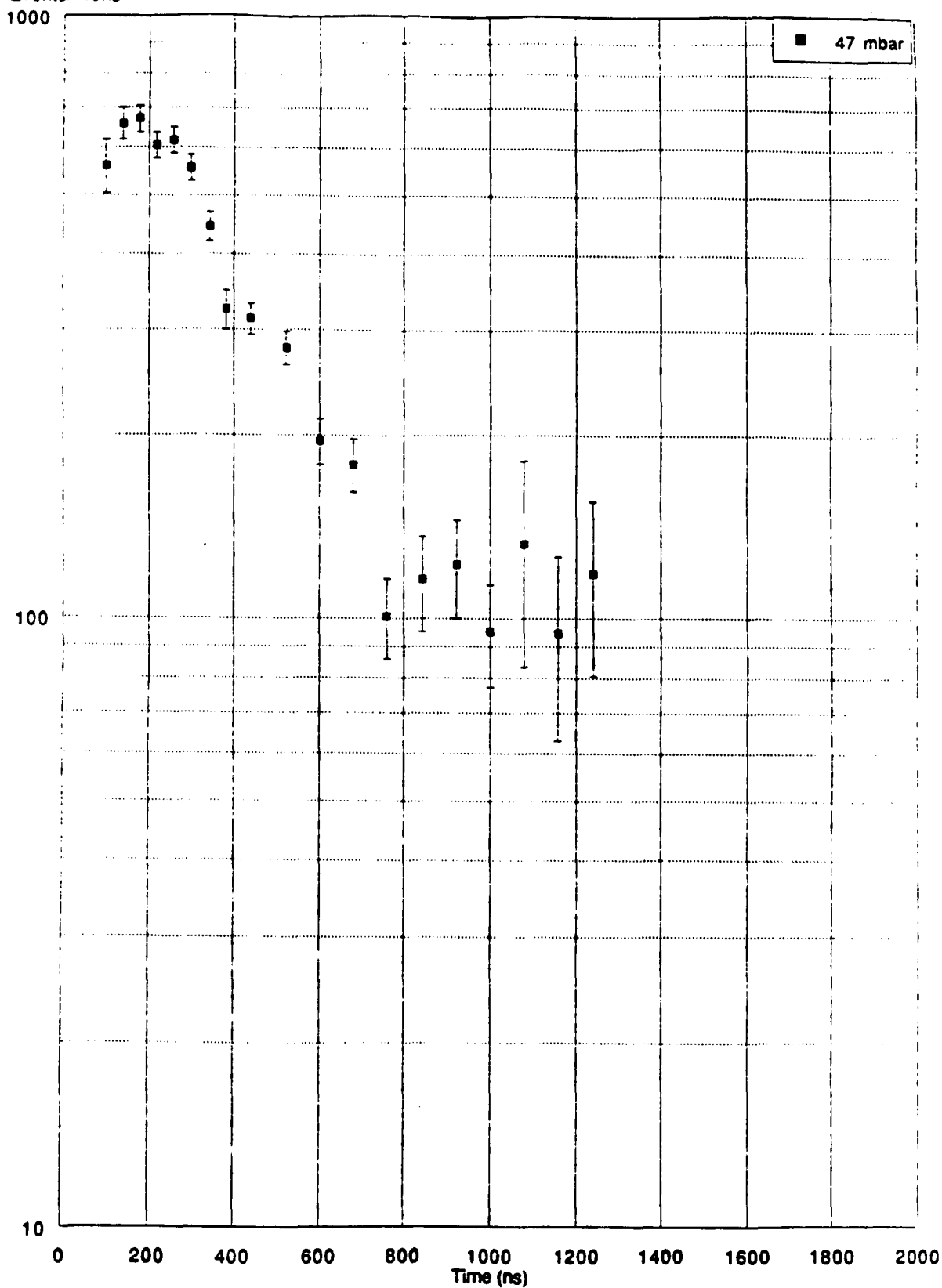


Fig. VI-10

Appendix A

In the $\mu p + p$ scattering experiment the μp atoms are assumed to form uniformly in the H₂ (or D₂) gas gap between two foils separated by a distance D with $R/D \gg 1$ (with reference to Fig. A-1 below)

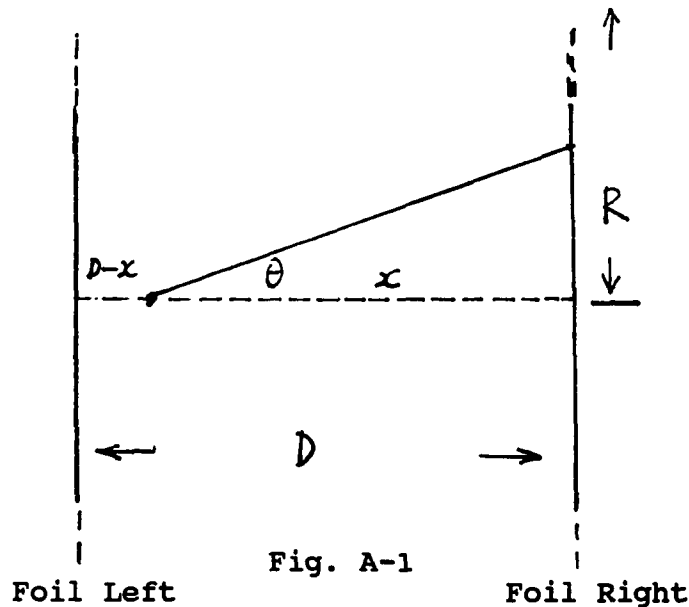


Fig. A-1

where R is the radius of a foil and D is a distance between two foils.

One of goals of the experiment is to determine the time distribution of μp atoms arriving at a foil and then to determine the initial velocity distribution of μp atoms.

Here, we answer this question-if we know the initial velocity distribution $f(\mathbf{x}, \mathbf{v})$, then what kind of time distribution will be determined in the experiment ? [44]

Initially, we assume the μp atoms formed at point (\mathbf{x}, \mathbf{v}) in phase space with density

$$\Pi = \Pi(\mathbf{x}, \mathbf{v}) \quad (\text{A-1})$$

The initial velocity distribution (in \mathbf{v} space) and density (in \mathbf{x} space) are independent each other. Thus, we can separate the variables in eq. (A-1) and rewrite the expression as follows

$$\Pi = \rho(x, y, z) f(\mathbf{v}) \quad (\text{A-2})$$

where \mathbf{v} is a vector. Furthermore, we assume the initial velocity distribution of μp atoms is spherically symmetrical. So eq. (A-2) becomes :

$$\Pi = \rho(x, y, z) f(v) \quad (\text{A-3})$$

where $v = \|\mathbf{v}\|$ is a scalar.

Physically the μp atoms can only be formed in the gap; namely, the x -coordinates are limited in the intervals $0 < x < D$ and $y^2 + z^2 \leq R^2$. So the density of the probability of μp atoms can be written as follows :

$$\rho = \omega(x, y, z) \theta(x) \theta(D-x) \quad (\text{A-4})$$

Because $R/D \gg 1$, we ignore the limits of y and z coordinates.

We consider the case of a μp atom not scattering after its formation in the gap.

Suppose during the T time N μp atoms formed in the gas gap. The number of μp atoms which formed in the interval $x \rightarrow x + dx$ is

$$dn = N \rho(x, y, z) dx dy dz \quad (\text{A-5})$$

$$= N \omega(x, y, z) \theta(x) \theta(D-x) dx dy dz \quad (\text{A-6})$$

The foils collect those μp atoms which drift to the surfaces of foils with initial velocity distribution $f(\mathbf{v})$. We consider only those μp atoms in $x + dx$ interval through various directions (γ_1) and with various velocities v_1 arriving at the surface of the foils (foil₁ and foil₂) at the same time (with reference to Fig. A-2). That is, we impose a restriction on μp atoms which are collected by foil₁ as follows :

$$v_1 \cos \theta_1 t = x \quad (\text{A-7})$$

and collected by foil₂

$$v_{i+1} \cos \theta_{i+1} t = -(D-x) \quad (\text{A-8})$$

where x and t are fixed and v_1, v_{i+1}, θ_1 and θ_{i+1} are variables.

These restrictions are illustrated in Fig. A-2 below :

hint :

$$v_1 \cos \theta_1 = v_2 \cos \theta_2$$

$$= v_3 \cos \theta_3$$

.

.

.

$$= v_i \cos \theta_i$$

$$= x/t$$

for foil₁ and

$$v_{i+1} \cos \theta_{i+1} = v_{i+2} \cos \theta_{i+2}$$

$$= v_{i+3} \cos \theta_{i+3}$$

$$= -(D-x)/t$$

for foil₂ .

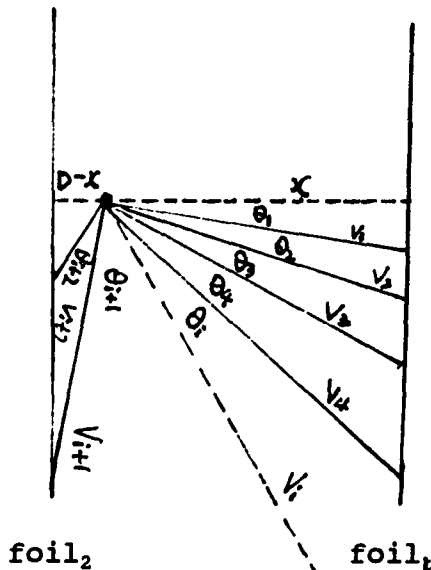


Fig. A-2

In the absence of scattering, the μp atoms travel to the surface of the foil with the velocity v equal to their initial velocity. Therefore, the number of μp atoms within $v_i + dv_i$ and solid angle $\Omega_i + d\Omega_i$ which arrived at the surface of foils per unit time will be :

$$\begin{aligned} dm &= N v_x \Pi(\mathbf{x}, \mathbf{v}) dx dy dz dv_x dv_y dv_z \\ &= N v_x \omega(x, y, z) \theta(x) \theta(D-x) f(v) dx dy dz v^2 dv d\Omega \quad (A-9) \end{aligned}$$

As a result, the number of μp atoms which collect at the foils at the same time t equals the sum over the velocities v_i and the solid angles Ω_i under the restriction (A-7, A-8), i.e.,

$$\begin{aligned} m(\mathbf{x}, t) dx dy dz &= (m_{foi11} + m_{foi12}) dx dy dz \\ &= \sum_{v_i} \sum_{\Omega_i} dm_i \\ &\quad (\text{under the condition } v_i \cos \theta_i = x/t = \text{constant}) \\ &+ \sum_{v_{i+1}} \sum_{\Omega_{i+1}} dm_i \\ &\quad (\text{under the condition } v_{i+1} \cos \theta_{i+1} = -(D-x)/t = \text{constant}), \end{aligned}$$

where $m_{foi11} dx dy dz$ is the number of μp atoms collected by foil₁ and $m_{foi12} dx dy dz$ is the number of μp atoms collected by foil₂ .

Using the integral over v space instead of the sum $\sum_{v_i} \sum_{\Omega_i}$ and

$$\sum_{v_{i+1}} \sum_{\Omega_{i+1}} \quad \text{and } \delta(x - v t \cos \theta) \quad \text{and } \delta(D - x + v t \cos \theta)$$

instead of the restriction (A-7 , A-8), we obtain

$$m(\mathbf{x}, t) \, dx dy dz = N \rho(\mathbf{x}, y, z) \, dx dy dz \int_0^\infty \int_0^{2\pi} \left\{ \int_{\pi/2}^0 \delta(vt \cos \theta - x) f(\mathbf{v}) v \, dv d\Omega \right. \\ \left. + \int_{\pi/2}^\pi \delta(D - x + vt \cos \theta) f(\mathbf{v}) v^2 \, dv d\Omega \right\}, \quad (\text{A-10})$$

where the \mathbf{x} and t are still fixed, the $N \rho(\mathbf{x}, y, z) \, dx dy dz$ is the number of μp atoms which formed in gas gap at the point (\mathbf{x}, y, z) within the volume $dx dy dz$, and $m(\mathbf{x}, t) \, dx dy dz$ is the number of the μp atoms which were collected at time t per unit time at a distance x (Refer to Fig. A-2).

Now we fix only t and integrate expression (A-10) over the whole gap. Thus, we obtain the total number which were collected by foils at t time :

$$M(t) = N \int_{\text{gap}} \rho(\mathbf{x}, y, z) \, dx dy dz \left\{ \int_{\text{v-space (right-semisphere)}} \delta(x - vt \cos \theta) v^2 f(\mathbf{v}) \, dv d\Omega \right. \\ \left. + \int_{\text{v-space (left-semisphere)}} \delta(D - x + vt \cos \theta) v^2 f(\mathbf{v}) \, dv d\Omega \right\} \quad (\text{A-11})$$

The probability of μp atoms arriving at the foils at time t is

$$P(t) = P_1(t) + P_2(t) \\ = M(t)/N \\ = \int_{\text{gap}} \rho(\mathbf{x}, y, z) \, dx dy dz \left\{ \int_{\text{v-space (right-semisphere)}} \delta(x - vt \cos \theta) v^2 f(\mathbf{v}) \, dv d\Omega \right. \\ \left. + \int_{\text{v-space (left-semisphere)}} \delta(D - x + vt \cos \theta) v^2 f(\mathbf{v}) \, dv d\Omega \right\},$$

$$(\text{A-12})$$

where $P_1(t)$ is a time distribution of the μp atoms collected by foil₁ and $P_2(t)$ is a time distribution of the μp atoms collected by foil₂. $P(t)$ is the total time distribution.

Eventually, the time distribution $P(t)$ of μp atoms is obtained, for μp atom forming in the gas gap with the initial velocity distribution $f(\mathbf{v})$ and the density $\rho(x, y, z)$.

Expression (A-12) for the time distribution satisfies most cases except when the initial velocity distribution depends on the density $\rho(x, y, z)$. In that case, we cannot separate the variables \mathbf{x} and \mathbf{v} from $\Pi(\mathbf{x}, \mathbf{v})$; namely, $\Pi(\mathbf{x}, \mathbf{v})$ is not equal to $\rho(x, y, z) f(v_x, v_y, v_z)$.

By substituting eq. (A-3) into (A-12), we obtain

$$\begin{aligned}
 P_1(t) &= 2\pi S \int_0^D dx \int_0^\infty f(v) v^3 dv \int_0^{-1} \omega(x) \theta(x) \theta(D-x) \delta(D-x+vt\cos\theta) \cos\theta d\cos\theta \\
 &= 2\pi S \int_0^\infty f(v) v^3 dv \int_0^{-1} \omega(D+vt\cos\theta) \theta(D+vt\cos\theta) \theta(vt\cos\theta) \cos\theta d\cos\theta \\
 &\quad (\pi \geq \theta \geq \pi/2)
 \end{aligned}$$

We change the variable θ to α , $\alpha = \theta + \pi$; thus

$$\begin{aligned}
 P_1(t) &= 2\pi S \int_0^\infty f(v) v^3 dv \int_0^1 \omega(D-vt\cos\alpha) \theta(D-vt\cos\alpha) \theta(vt\cos\alpha) \cos\alpha d\cos\alpha \\
 &\quad (\pi/2 \geq \alpha \geq 0)
 \end{aligned}$$

and

$$\begin{aligned}
P_2(t) &= 2\pi S \int_0^D dx \int_0^\infty f(v) v^3 dv \int_0^1 \omega(x) \theta(x) \theta(D-x) \delta(D-x-vt \cos \theta) \cos \theta d \cos \theta \\
&= 2\pi S \int_0^\infty f(v) v^3 dv \int_0^1 \omega(vt \cos \theta) \theta(vt \cos \theta) \theta(D-vt \cos \theta) \cos \theta d \cos \theta \\
&\quad (\pi/2 \geq \theta \geq 0)
\end{aligned}$$

The definition of the θ function is as follows :

$$\begin{aligned}
\theta(x) &= 1, \quad \text{if } x \geq 0 \\
\theta(x) &= 0, \quad x < 0
\end{aligned}$$

Therefore, the integral $P_1(t)$ and $P_2(t)$ become :

$$\begin{aligned}
P_1(t) &= 2\pi S \int_0^\infty f(v) v^3 dv \int_0^1 \omega(D-vt \cos \alpha) \theta(D-vt \cos \alpha) \cos \alpha d \cos \alpha \\
&\quad (\pi/2 \geq \alpha \geq 0) \quad (A-14)
\end{aligned}$$

and

$$\begin{aligned}
P_2(t) &= 2\pi S \int_0^\infty f(v) v^3 dv \int_0^1 \omega(vt \cos \theta) \theta(D-vt \cos \theta) \cos \theta d \cos \theta \\
&\quad (\pi/2 \geq \theta \geq 0) \quad (A-15)
\end{aligned}$$

Before we integrated eqs. (A-14, A-15), the following cases were treated :

1) $v \leq D/t$; then

$$\theta(D-vt \cos \theta) \equiv 1, \quad \cos \theta \text{ from } 0 \text{ to } 1 ; \quad (A-16)$$

2) $v > D/t$; if

$$vt \cos \theta < D;$$

then

$$\Theta(D-vt\cos\theta) \equiv 1, \cos\theta \text{ from } 0 \text{ to } D/vt \quad (\text{A-17})$$

3) when $v > D/t$, or if

$$vt\cos\theta > D;$$

then

$$\Theta(D-vt\cos\theta) \equiv 0, \cos\theta \text{ from } D/vt \text{ to } 1 \quad (\text{A-18})$$

Now we substitute (A-16), (A-17) and (A-18) into integral (A-14), and then the integrals become as follows :

$$P_1(t) = 2\pi S \left\{ \int_0^{D/t} v^3 f(v) dv \int_0^1 \omega(D-vt\cos\theta) \cos\theta d\cos\theta \right. \\ \left. + \int_{D/t}^{\infty} v^3 f(v) dv \int_0^{D/vt} \omega(D-vt\cos\theta) \cos\theta d\cos\theta \right\} \quad (\text{A-19})$$

and

$$P_2(t) = 2\pi S \left\{ \int_0^{D/t} v^3 f(v) dv \int_0^1 \omega(vt\cos\theta) \cos\theta d\cos\theta \right. \\ \left. + \int_{D/t}^{\infty} v^3 f(v) dv \int_0^{D/vt} \omega(vt\cos\theta) \cos\theta d\cos\theta \right\} \quad (\text{A-20})$$

The expressions (A-19) and (A-20) satisfy condition (A-13); that is, we can calculate the time distribution $P_1(t)$ and $P_2(t)$, respectively, for foil₁ and foil₂ when the μp atoms are formed in gas the gap ununiformly along the x coordinate ($\rho = \omega(x)$).

Finally, we obtain the total time distribution :

$$P(t) = P_1(t) + P_2(t) \quad (\text{A-21})$$

For simplicity, we assume the density $\rho(x)$ is left - right symmetric along x coordinate :

$$\rho(x) = \rho(D-x) \quad (A-22)$$

Then $P_1(t)$ is equal to $P_2(t)$; that is, the time distribution of foil₁ is as same as the time distribution of foil₂ and the total time distribution $P(t)$ is as follows :

$$\begin{aligned} P(t) &= P_1(t) + P_2(t) \\ &= 4\pi S \left\{ \int_0^{D/t} v^3 f(v) dv \int_0^1 \omega(vt \cos \theta) \cos \theta d\cos \theta \right. \\ &\quad \left. + \int_{D/t}^{\infty} v^3 f(v) dv \int_0^{D/vt} \omega(vt \cos \theta) \cos \theta d\cos \theta \right\} \quad (A-23) \end{aligned}$$

Furthermore, in this experiment we assume that μp atoms form uniformly in the whole gap. So, the density of probability

$$\begin{aligned} \omega(x) &= \text{constant} \\ &= 1/SD, \quad (A-24) \end{aligned}$$

where S is an area of a foil.

In this particular case, substituting (A-24) into (A-23), the time distribution $P(t)$ becomes as follows :

$$\begin{aligned} P(t) &= 4\pi/D \left\{ \int_0^{D/t} v^3 f(v) dv \int_0^1 \cos \theta d\cos \theta + \int_{D/t}^{\infty} v^3 f(v) dv \int_0^{D/vt} \cos \theta d\cos \theta \right\} \\ &= 2\pi/D \left\{ \int_0^{D/t} v^3 f(v) dv + \int_{D/t}^{\infty} D^2 v F(v)/t^2 dv \right\} \quad (A-25) \end{aligned}$$

Thus, in principle, it is possible to determine the time distribution of the μp atoms when they hit the foil by knowing the initial velocity distribution $f(v)$ from eq. (A-25). Here, three examples are given as follows :

1) The initial velocity distribution is a Maxwell distribution

$$\begin{aligned} f(v) &= \left(\frac{m}{2\pi kT} \right)^{3/2} \exp\left(-\frac{mv^2}{2kT} \right) \\ &= (\beta/\pi)^{3/2} \exp(-\beta v^2) \end{aligned} \quad (A-26)$$

where $\beta = m/2kT$.

So, the integral (A-25) becomes

$$P(t) = 2\pi/D \left\{ \int_0^{D/t} v^3 (\beta/\pi)^{3/2} \exp(-\beta v^2) dv + \int_{D/t}^{\infty} \frac{D^2}{t^2} v/t^2 (\beta/\pi)^{3/2} \exp(-\beta v^2) dv \right\}.$$

Setting $\chi = v^2$ and $d\chi = 2v dv$, We then obtain the time distribution (with reference to Table (A-1)) :

$$P(t) = 2/D (2kT/\pi m)^{1/2} (1 - \exp(- mD^2/2kTt^2)) \quad (A-27)$$

2) The initial velocity distribution is exponential :

$$f(v) = \beta \exp(-\beta v) \quad (A-28)$$

So, the integral (A-25) becomes (refer to Table A-1)

$$P(t) = 2\pi/D \left\{ \int_0^{D/t} v^3 \beta \exp(-\beta v) dv + \int_{D/t}^{\infty} \frac{D^2}{t^2} v \beta \exp(-\beta v) dv \right\}$$

$$= 12\pi/D\beta^3 \{ 1 - \exp(-\beta D/t) [\beta^2 D^2 / 3t^2 + \beta D/t + 1] \}$$

(A-29)

3) The initial velocity distribution is a delta function

$$f(v) = \frac{\delta(v-v_0)}{4\pi v_0^2}$$

(A-30)

We substitute (A-30) into the integral (A-25) and obtain the following :

$$P(t) = 2\pi/D \left\{ \int_0^{D/t} v^3 \frac{\delta(v-v_0)}{4\pi v_0^2} dv + \int_{D/t}^{\infty} D^2 v \frac{\delta(v-v_0)}{4\pi v_0^2} / t^2 dv \right\} \quad (A-31)$$

In this case, obviously, the integral (A-31) is broken up into two integrals because if $v_0 < D/t$, the second part of the integral (A-31) vanishes. If $v_0 > D/t$, the first part of the integral (A-31) vanishes. Therefore, we obtain the time distribution as follows :

$$P_1(t) = \frac{1}{2Dv_0^2} \int_0^{D/t} v^3 \delta(v-v_0) dv$$

$$= v_0/2D, \quad t < D/v_0 \quad (A-32)$$

and

$$P_2(t) = \frac{\pi}{D} \int_{D/t}^{\infty} \frac{D^2 v \delta(v-v_0)}{D/t t^2 4\pi v_0^2} dv$$

$$= D/2v_0 t^2 \quad t > D/v_0 \quad (A-33)$$

Finally, we note the following : the foil is not actually infinite in size and thus the angle θ cannot reach $\pi/2$. Thus we set the maximum angle θ_m , $h_m = \cos\theta_m$ ($h_m \approx 0$) and the maximum velocity $v_m = x/th_m$. Thus, in the real experimental case, we obtain the time distribution as follows :

$$P(t) = 4\pi/D \left(\int_0^{D/t} v^3 f(v) dv \int_{h_m}^1 \cos\theta d\cos\theta + \int_{D/t}^{v_m} v^3 f(v) dv \int_{h_m}^{D/vt} \cos\theta d\cos\theta \right)$$

(A-34)

Table A-1

- 1) $\int x \exp(ax) dx = \exp(ax) [x/a - 1/a^2]$
- 2) $\int x^2 \exp(ax) dx = \exp(ax) [x^2/a - 2x/a^2 + 2/a^3]$
- 3) $\int x^3 \exp(ax) dx = \exp(ax) [x^3/a - 3x^2/a^2 + 6x/a^3 - 6/a^4]$

Appendix B

The purpose of this appendix is to describe the standard method used to generate the various pseudo-random distributions which are needed for many applications. We start by assuming that we have a " good " pseudo-random generator which produces the random number U within a specified range (0 to 1) [34], [35].

A) Transformation Method [34] [35]

1) Exponential Deviate

$$y = \lambda e^{-\lambda x} \quad (\text{B-1})$$

and

$$U = \int_0^{\infty} y dx = 1 - e^{-\lambda x} \quad (\text{B-2})$$

So, we simply obtain the exponential deviate

$$x = -1/\lambda \ln(1-U)$$

or

$$x = -1/\lambda \ln(U) \quad (\text{B-3})$$

2) Lorentzian Deviate

$$y = 1/\pi (1 + x^2) \quad (\text{B-4})$$

and as above :

$$U = \int_{-\infty}^{\infty} dx / \pi(1+x^2) \quad (\text{B-5})$$

$$= 1/\pi (\tan^{-1}x + \pi/2) \quad (\text{B-6})$$

We obtain the Lorentzian deviate

$$x = \tan(\pi U - \pi/2) \quad (\text{B-7})$$

3) Normal Deviate

$$y = 1/\sqrt{2\pi} \exp(-x^2/2) \quad (\text{B-8})$$

Suppose U and V are two uniform deviates. The two independent normal distributions are obtained by computing

$$x_1 = \sqrt{-2 \ln U \cos(2\pi V)} \quad (\text{B-9})$$

$$x_2 = \sqrt{-2 \ln U \sin(2\pi V)} \quad (\text{B-10})$$

We consider the joint probability density function of x_1 and x_2 :

$$f(x, y) = \int_0^1 \int_0^1 \delta(x - \sqrt{-2 \ln U \cos(2\pi V)}) \delta(y - \sqrt{-2 \ln U \sin(2\pi V)}) dU dV \quad (\text{B-11})$$

Making a change of variables to

$$\begin{aligned} \alpha &= \sqrt{-2 \ln U \cos(2\pi V)} \\ \beta &= \sqrt{-2 \ln U \sin(2\pi V)}, \end{aligned} \quad (\text{B-12})$$

We then have

$$\begin{aligned}
 f(x,y) &= \frac{1}{\sqrt{2\pi}} \int_{-\infty}^{\infty} \int_{-\infty}^{\infty} \delta(x-\alpha) \delta(y-\beta) \exp[-(\alpha^2 + \beta^2)/2] d\alpha d\beta \\
 &= \frac{1}{\sqrt{2\pi}} \exp(-x^2/2) \cdot \frac{1}{\sqrt{2\pi}} \exp(-y^2/2)
 \end{aligned}$$

(B-13)

Thus, we have proved that x_1 and x_2 are independent normal distributions

4) Gaussian Deviate

$$y = \frac{1}{\sqrt{2\pi}} e^{-\left(\frac{x-\mu}{\sigma}\right)^2}$$

(B-14)

If Z a normal random distribution then the Gaussian distribution is

$$x = \sigma Z + \mu$$

(B-15)

B. Rejection Method [34]

1) Normal deviate

We first generate two uniform randoms, $U \in [-1,1]$ and $V \in [-1,1]$, Then we compute the radius $R^2 = U^2 + V^2$; if $R^2 < 1$, we continue, If not, we reject this choice of U and V , then try again. We obtain two independent normal deviates by computing

$$\begin{aligned}
 x_1 &= U/R \sqrt{-4\ln R} \\
 x_2 &= V/R \sqrt{-4\ln R}
 \end{aligned}$$

(B-16)

We consider the joint probability density function

$$f(x,y) = \frac{\int_{-1}^1 \int_{-1}^1 \theta(1-R^2) \delta(x-x_1) \delta(y-x_2) dUdV}{\int_{-1}^1 \int_{-1}^1 \theta(1-R^2) dUdV} \quad (\text{B-17})$$

with a change of variables to

$$\begin{aligned} U &= R \cos\phi \\ V &= R \sin\phi \end{aligned} \quad (\text{B-18})$$

$f(x,y)$ becomes

$$\frac{\int_{-1}^1 \int_{-1}^1 \theta(1-R^2) \delta(x-\cos\phi/\sqrt{-2\ln R^2}) \delta(y-\sin\phi/\sqrt{-2\ln R^2}) R dr d\phi}{\int_0^{2\pi} \int_0^2 \theta(1-R^2) R dR d\phi} \quad (\text{B-19})$$

By means of the substitution $Z=R^2$, we obtain

$$f(x,y) = 1/2\pi \int \int \delta(x-\cos\phi/\sqrt{-2\ln Z}) \delta(y-\sin\phi/\sqrt{-2\ln Z}) dz d\phi \quad (\text{B-20})$$

Now, by transforming to $r=\sqrt{-2\ln Z}$, we get

$$f(x,y) = 1/2\pi \int_0^{2\pi} \int_0^{\infty} \exp(-r^2/2) \delta(x-r\cos\phi) \delta(y-r\sin\phi) r dr d\phi \quad (\text{B-21})$$

Finally, using variables

$$\begin{aligned}\alpha &= r \cos \phi \\ \beta &= r \sin \phi\end{aligned}\quad (\text{B-22})$$

we get

$$\begin{aligned}f(x, y) &= \frac{1}{2\pi} \int_{-\infty}^{\infty} \int_{-\infty}^{\infty} \exp\left(-\frac{\alpha^2 + \beta^2}{2}\right) \delta(x-\alpha) \delta(y-\beta) d\alpha d\beta \\ &= \frac{1}{\sqrt{2\pi}} \exp(-x^2/2) \frac{1}{\sqrt{2\pi}} \exp(-y^2/2)\end{aligned}\quad (\text{B-23})$$

Therefore, x_1 and x_2 are normal distributions and are independent of each other.

2) A Volume of the Unit n-sphere

We compute a volume of a unit n-sphere using the formula :

$$V_n = \int \int \dots \int_{\sum_{i=1}^n x_i^2 \leq 1} \prod_{i=1}^n dx_i \quad (\text{B-24})$$

where R is a radius of a n-dimension sphere (for unit n-sphere $R = 1$) and $V_n(R)$ is the volume.

According to the rejection method, we generate N uniform randoms U_n , then compute the $S = \sum U_n^2$. If $S < 1$, we continue; otherwise, we reject this choice of U_n and try again. Suppose the rejected times to be M , The volume of the unit n-sphere is then :

$$V_n = \frac{N-M}{N} 2^n \quad (\text{B-25})$$

Then we can compare this with the analytic calculation :

$$V_n(R) = \frac{\pi^{n/2}}{(n/2)!} R^n ; \quad (\text{B-26})$$

for instance, when $n=2$, $R=1$, $V_2 = \pi$, $n=3$, $R=1$, $V_3 = 4\pi/3$ and $n=4$, $R=1$, $V_4 = \pi^2/2$, etc.

REFERENCES

1. Eugene D. Commins and Philip H. Bucksbaum, Weak Interactions of Leptons and Quarks, (Cambridge University Press, Cambridge 1983)
2. J.D. Bjorken and S.D. Drell, Relativeistic Quantum Mechanics, (MC Graw-Hill Book Company, 1964)
3. Francis Halzen and Alan D. Martin, Quarks and Leptons : An Introductory Course in Modern Particle Physics, (John Wiley & Sons. 1984)
4. Masato Morita, Beta Decay and Muon Capture, (Osaka University, Japan, 1973)
5. R.J. Blin-Stoyle, Fundamental Interactions and the Nucleus (North-Holland Publishing Company 1973)
6. A. Bertin, M. Cappon, et al , NUOV. CIM. 86A 125 (1985)
7. M. Bubck and M. P. Faifman, JINR Preprint E, -87-464. Dubna (1987)
8. A. Adamczak and V.S. Melezhik, Muon Catalyzed Fusion 2 (1988)
9. A. Adamezak, V.S. Melezhik and L. Z. Menshikov, Atoms Molecules and Clusters (1986)
10. V.I. Fomichev and A.I. Mikhalol, Muon Catalyzed Fusion 2 (1988)
11. A. Adamczak and V.S. Melezhik, Physics Letter A VOL 118 (1986)
12. G. Bardin, J. Duclos, A. Magnon, J. Martino and A. Richter, Physics Letters, 104B, 320 (1981)
13. G. Ya Koremman and S. I. Rogovaya, J. Phys. B13, 641 (1980)
14. Ta-Tu Wu and Takashi Ohmura, Quantum Theory of Scattering, (Prentice-Hall, Inc. Englewood Cliffs, New Jersey 1962)
15. T.D. Lee, Weak Interactions and High-Energy Neutrino Physics, (Academic Press New York and London 1966)

16. E.H.S. Burhop, High Energy Physics, (Academic Press New York and London 1966)
17. Herwing F. Schopper, Weak Interactions and Nuclear Beta Decay, (North-Holland Publishing Company Amsterdam 1966)
18. A.G. Frodesen, O. Skjeggstad and H. Toffe, Probability and Statistics In Particle Physics, (Universitytsforlaget 1979)
19. Siegmund Brandt, Statistical and Computational Methods in Data Analysis (North-Holland Publishing Company 1970)
20. Matvenko A.V., Ponomorev L.I., TMF, 1972, 12, P64.
21. Emilio Segre, Nucei and Particles, an Introduction to Nuclear and Subnuclear Physics, (W.A. Bemjamin, INC. New York 1964 Amsterdam)
22. G.A. Baber, Phys. Rev. 117, 1130 (1960)
23. R.A. Mann and M.E. Rose, Phys. Rev. 121, 293 (1961)
24. P.K. Haff and T.A. Tombrello, Ann. of Phys. 86, 178 (1974)
25. G. Ya. Korenman and S.I. Rogovaya, J. Phys. 86, 178 (1974)
26. J.S. Cohen, R.L. Martin, and W.L. Wadt, Phys. Rev. A24, 33 (1981)
27. M.Y. Au-Yang and M.L. Cohen, Phys. Rev. 174, 468 (1968)
28. SIN User's Handbook (1981)
29. Rich and R. H. Pehl, Physics Today, 50 (November/1977)
30. Ozer Ciftcioglu, Nuclear Instruments and Methods, 174, 209 (1980)
31. Ozer Ciftcioglu, Nuclear Instruments and Methods, 198, 391 (1980)
32. Fred S. Goulding and Richard H. Pehl, Lawrence Berkeley Laboratory, 289.
33. H.H. Jorch and J.L. Compbell, Nucl. Instr. and Meth. 143 551 (1977)
34. Press, William H, Numerical Recipes ; The Art Of Scientific Computing, Cambridge University Press (1986)

35. S.C. Black, Computers in Physic, 59(Sep/Oct 1989)
36. Milton Abramowitz and Irene A. Stezun, Handbook of Mathematical Functions, Dover Publications, Inc., New York(1965)
37. T. A. Filippas, P. Palit, R. T. Siegel and R. E. Welsh, Physics Letters, V. 8, 118 (1963)
38. T. Suzuki, D. F. Measday and J. P. Roalsig, Phys. Rev. C 35, 2212 (1987)
39. F. J. Hartmann, etal. Zeit, Physik, A305, 1089 (1982)
40. MINUIT, F. James and M. Roos, CERN Program Library D506
41. FITA, Technical University of Munich
42. C. M. Lederer and V. S. Shirley, ed., Table of Isotopes , 7th Ed. (John Wiley and Sons, Inc., New York, 1978)
43. Philip R. Bevington, Data Reduction and Error Analysis for the Physical Sciences.
44. James B. Kraiman, Thesis ' The Diffusion of Muonic Deuterium Atoms in Deuterium Gas ', WMHEG-89-2. See also J. B. Kraiman, et al, Phys. Rev. Lett. B3, 1942 (1989)
45. F. J. Hartmann, Private Communication
46. R. Engfer, H. Schneuwly, J. L. Villeumier, H. K. Walter and A. Zehnder, At. Dat and Nucl. Dat. Tab. 14, 509 (1974)

GUO FU CHEN

Dept. Of Physics
College of William and Mary
Williamsburg, Virginia 23185
USA
(804) 221-3571

Job Objective : Post-Doctoral Research Position

Education

May 1 1990 Ph.D., Physics
College of William and Mary, Williamsburg, VA
Thesis: Diffusion Of Muonic Hydrogen Atoms
in Hydrogen Gas

May 1986 M.S., Physics
College of William and Mary

Jan., 1984 M.S., Physics
Graduate School, University of Science and
Technology of China

Dec., 1981 to 1983 Completed courses in Physics
Graduate School, University of Science and
Technology of China

EMPLOYMENT

Sept., 1985 to present Research Assistant
Dept., of Physics, College of William and Mary
Williamsburg, Virginia, USA
Developed computer software packages. Gained
experience in data reduction and analysis and
familiarity with Ge detector, fast electronics
Micro VAX, VAX, IBM PC XT AT.

Jan., 1982 to Sept., 1984 Research Assistant at Institute of High Energy
Physics, Chinese Academy of Science, Peking, China

May 1980 to Nov. 1981 Research Assistant in MARK-J, F13, DESY,
West Germany
Gained experience in fast electronics
(CAMAC, NIM, MBD) and PDP 11/55, IBM 360/168, JCL.

Publications

"Experimental Study of Electroweak Parameters
at PETRA Energies" ($12 \leq E_{c.m.} \leq 36.7$ GeV)
D. P. Barber, et. al., Phys. Rev. Lett. 46, 1663
(1981)
"Diffusion of Muonic Hydrogen Atoms,"
W. Breunlich, et. al. News Letter, SIN, NL58
(1988)
"Diffusion of Muonic Deuterium in D₂ Gas"
J. B. Kraiman, et. al., Phys. Rev. Lett. 63,
1942 (1989)

Reference

Available upon request.